



**Biological effects of herbal molecules
in ocular neovascularization
in vitro and *in vivo***

LIU, Huanming

A Thesis Submitted in Partial Fulfillment of the Requirements for the Degree

of

Doctor of Philosophy

in

Ophthalmology & Visual Sciences

The Chinese University of Hong Kong

August 2010

UMI Number: 3483856

All rights reserved

INFORMATION TO ALL USERS

The quality of this reproduction is dependent upon the quality of the copy submitted.

In the unlikely event that the author did not send a complete manuscript and there are missing pages, these will be noted. Also, if material had to be removed, a note will indicate the deletion.



UMI 3483856

Copyright 2011 by ProQuest LLC.

All rights reserved. This edition of the work is protected against unauthorized copying under Title 17, United States Code.



ProQuest LLC
789 East Eisenhower Parkway
P.O. Box 1346
Ann Arbor, MI 48106-1346

Thesis/Assessment Committee

Professor Chi Pui PANG (Chair)

Professor Dennis Shun Chiu LAM (Thesis Supervisor)

Professor Gary Hin Fai YAM (Supervisor)

Professor Ronald Chi Chiu WANG (Committee Member)

Professor Kwok Pui FUNG (Committee Member)

Professor Hannah Hong XUE (External Examiner)

ABSTRACT

Abstract of the thesis entitled:

Biological effects of herbal molecules in ocular neovascularization: in vitro and in vivo studies

Submitted by Huan Ming LIU

For the degree of Doctor of Philosophy

At The Chinese University of Hong Kong in August 2010

Angiogenesis is a process of new blood vessels sprouting from the pre-existing vasculature, and mediated by multiple angiogenic and anti-angiogenic factors. Disturbance of the balance often leads to development of neovascular diseases. Neovascularization affecting the eye is a common cause of visual impairment and even blindness, particularly when corneal or choroidal neovascularization (NV) is involved. While there are effective treatment modes for ocular neovascularization, they are expensive and only inhibit disease progress. Since herbal medicine has been applied for anti-angiogenesis and anti-carcinogenesis therapies, we investigate the anti-angiogenic effect of selected herbal molecules: isoliquiritigenin (ISL), a flavonoid from licorice; epigallocatechin gallate (EGCG), a polyphenol from green tea; and resveratrol (Rst), a polyphenol phytoalexin derived from grapes.

This thesis contains two major parts. The first *in vitro* cell-based analysis investigated the toxicity of these herbal chemicals and their effect on endothelial cell growth and migration. The expression profile of vascular endothelial growth factor (VEGF) signaling cascade events, including Akt and focal adhesion kinase (FAK) activation, VEGF, pigment epithelium-derived factor (PEDF) and matrix metalloproteinases (MMPs) were examined by

Western blotting. Then three *in vivo* models were established to study the effect of these herbal chemicals on angiogenesis. They were (1) developmental angiogenesis in chick chorioallantoic membrane (CAM), (2) pathological angiogenesis in silver nitrate cauterization-induced corneal neovascularization in BALB/c mice and, (3) laser photocoagulation-induced choroidal neovascularization in C57BL/6 mice. Changes of vascularization were determined by qualification of vessel number changes on the edge of gelatin sponge in 24 hours (chick CAM assay), measurement of vascularized area, live imaging of vessel leakage (fundus fluorescence angiography, FFA) and immunohistochemistry using antibodies specific for endothelial cells (corneal & choroidal NV assays) respectively.

Results showed that sub-toxic levels of ISL (10 μM), EGCG (50 μM) and Rst (10 μM) effectively suppressed endothelial cell proliferation and migration in the scratch-wound assay. Treatment with ISL was found to significantly up-regulate PEDF, which is known as a potent angiostatic factor. EGCG and Rst downregulate VEGF signaling cascade by suppressing Akt and FAK activation and affecting MMP-2, MMP-9 expression. *In vivo* angiogenesis assays further showed the suppressive effect of ISL, EGCG and Rst on neovascularization in three different animal models. Application of ISL at 1 μM showed the suppressive effect on chick CAM assay, corneal NV and choroidal NV assays consistently, the most effective dosage was close to 10 μM . EGCG at 1 μM showed the effect to reduce chick CAM vessel formation and corneal NV, and at 10 μM (the lowest tested concentration) to suppress choroidal NV in mice. Variable effects were observed in Rst treatment. Rst at 10 μM prohibited vessel growth in chick CAM, and 1 μM suppressed corneal NV formation and 2 μM deterred choroidal NV development.

In conclusion, by *in vitro* and *in vivo* studies, we showed that ISL, EGCG and Rst contributed to anti-angiogenesis via different biological mechanisms. We propose that these three herbal molecules (ISL, EGCG and Rst) are candidate anti-angiogenic agents for the

treatment of ocular angiogenesis diseases. Their distribution profiles and pharmacokinetic properties should be investigated.

摘要

此摘要取自論文題

《中藥分子對眼部新生血管生物作用的體內、體外的研究分析》

於二零一零年八月

呈交自 劉煥明

作為香港中文大學眼科及視覺科學哲學博士學位的結業所需

摘要

新生血管形成是指新的血管從已經存在的血管上發芽形成的過程，是由多種促進因子和抑制因子來調控的，並保持一種平衡的狀態，如果這個平衡被打破了，就會導致新生血管性疾病，發生於眼部就會導致視力受損，或者失明，特別是生長於角膜或脈絡膜的新生血管。當然目前有一些有效的抑制眼部新生血管的藥物，但價錢昂貴，並且只抑制疾病的進程。因為中藥已經用於抑制新生血管形成和抗腫瘤治療，我們就來探究這些一定原則選擇的中藥分子，包括從甘草中提取的異甘草素、綠茶中提取的表沒食子兒茶素，和從葡萄中提取的白藜蘆醇的抑制新生血管形成的作用。

這篇論文就包括兩個方面的主要內容。第一：以細胞為基礎的體外研究來探究這些中藥化學物的細胞毒性及其內皮細胞生長和遷移。這些中藥化學物對血管內皮生長因子的信號傳導系統的影響，包括啟動 Akt, FAK 途徑，以及對 VEGF, PEDF, 和 MMP 的表達的調節，則是通過應用 Western blotting 來分析。第二：通過建立三種體內實驗的動物模型來進一步研究這些中藥化學物對新生血管形成的作用，分別是（1）雞胚

絨毛尿囊膜模型來研究這些藥物對發展期新生血管形成的影響，(2) 以 BALB/c 鼠為基礎的硝酸銀角膜灼傷模型和 (3) 以 C57BL/6 鼠為基礎的鐳射誘發的脈絡膜視網膜病變模型來研究藥物對病理的新生血管形成的影響。血管的變化在雞胚絨毛尿囊膜模型以計數 24 小時時間間隔明膠海綿邊緣的血管數目的增減來決定，在角膜灼傷模型或者鐳射誘發脈絡膜模型，則是由測量血管化的面積或通過活體眼底螢光血管造影檢查來評估血管的滲漏情況來判斷。

實驗結果顯示，亞毒性濃度水準的 10 μ M 異甘草素、50 μ M 表沒食子兒茶素和 10 μ M 白藜蘆醇有效地抑製了臍靜脈內皮細胞的增殖與在傷口癒合模型中遷移。異甘草素能有效地上調色素上皮生長因子（新生血管抑製因子之一）的分泌，表沒食子兒茶素和白藜蘆醇則抑製 Akt 和 FAK 的啟動，影響基質金屬蛋白酶 2 和基質金屬蛋白酶 9 的表達和啟動。體內實驗模型通過雞胚絨毛尿囊膜模型，硝酸銀角膜灼傷模型，鐳射誘發的脈絡膜視網膜病變模型進一步證實了這三種中藥分子在低濃度的狀態下可以有效地抑製新生血管的形成，且抑制效果呈濃度依賴性。異甘草素在低濃度 1 μ M 狀態下，顯示出有效抑制三種動物模型中新生血管的形成。沒食子兒茶素在 1 μ M 抑製雞胚絨毛尿囊膜模型，硝酸銀角膜灼傷模型的新生血管形成，和在 10 μ M（最低測試濃度）抑制脈絡膜新生血管的形成。我們觀察到白藜蘆醇在三種動物模型與上述兩種藥物不同的抑製效果。白藜蘆醇在 10 μ M 有效抑製雞胚絨毛尿囊膜的血管形成，1 μ M 抑製角膜新生血管的形成，2 μ M 抑製脈絡膜新生血管的形成。

總而言之，通過體內和體外實驗研究，我們證實了異甘草素、表沒食子兒茶素和白藜蘆醇通過不同的生物機制有效地抑制了新生血管的形成。我們建議這三種中藥分子可以用於抑制眼部新生血管疾病的治療。它們的藥代動力學和在組織內的分佈還有待進一步的研究。

ACKNOWLEDGEMENTS

First, I thank my supervisor Professor Dennis Shun-Chiu LAM for his mentorship and inspiration. I am encouraged by his achievement in the academy and endeavor to help the others and contribution to the society.

I am also very grateful to the Division head Professor Chi-Pui PANG, for his continuous support in my PhD program. He brought me in the angiogenesis research in the first place. What I learned from him is not only the academic knowledge, but also the way to become a person who is honorable, faithful and helpful to the team and to the society and also how to lead and contribute in a team.

Special thanks goes to my third supervisor, Dr. Gary YAM, who helped me in completing the angiogenesis research, and writing PhD thesis as well as the challenging research that lies behind it. Gary has been a good friend and mentor. He was always there to listen and to give advice, instruct and guide me into every detail of scientific research and show me different ways to approach a research problem and the need to be persistent to accomplish any goal.

Thank is also given to Dr. Vishal JHANJI who helped me in the corneal assay and Dr. Vincent LEE for his support and involvements in the laser experiment, Dr Winnie LI in the managing and organizing animal work.

Besides my advisors, let me also say “ thanks” to the DOVS team members, and those who are involved in my research work in different periods; in particular Dr Liming CAO, Ms Nancy LIU, Dr Kasin LAW and Dr Shirley LIU and Yolanda Yip. I have to say that I could not finish my experiments without their contribution and selfishless support. They had to work very late in the evening and also weekends for the experiments. They have

become my good friends too. I would never forget the time I spent in DOVS in these three years, growing up mentally with enhancement of knowledge in the science research.

Last, but not least, I thank my family - my parents, LIU Shu Xian and QU Lan Hua, for giving me life in the first place, for educating me from bachelor degree to this PhD degree, for unconditional support and encouragement to pursue my career and to be a valuable person to the society. My husband and my little daughter who have to live independently without my caring and accompany. They are the spiritual pillar and love of my life. My thesis is dedicated to them for their unselfish support and teaching me things that I could never learn from book. For words like grateful, thankful and obliged are not sufficient to describe my feelings to my family.

TABLES OF CONTENTS

<i>TITLE PAGE</i>	<i>I</i>
<i>ABSTRACT</i>	<i>II</i>
<i>摘要</i>	<i>III</i>
<i>ACKNOWLEDGEMENTS</i>	<i>IV</i>
<i>TABLES OF CONTENTS</i>	<i>V</i>
<i>LIST OF TABLES</i>	<i>VI</i>
<i>LIST OF FIGURES</i>	<i>VII</i>
<i>ABBREVIATIONS</i>	<i>VIII</i>
<i>PUBLICATIONS</i>	<i>IX</i>
<i>CONFERENCE PRESENTATIONS</i>	<i>X</i>
CHAPTER 1 INTRODUCTION.....	1
1.1 Angiogenesis.....	1
1.1.1 Definition and characterization.....	1
1.1.2 Cellular and molecular mechanisms of angiogenesis	2
1.1.2.1 The cellular mechanisms of angiogenesis:.....	2

1.1.2.2	The intussusceptive mode of angiogenesis:	3
1.1.2.3	Molecular regulation of angiogenesis	4
1.1.3	Angiogenesis and its regulatory proteins	4
1.1.4	Vascular endothelial growth factor (VEGF)	5
1.1.4.1	VEGF isoforms.....	6
1.1.4.2	VEGF receptors.....	7
1.1.5	VEGF signaling pathway (Figure 1).....	8
1.1.6	Endothelial cells and role in angiogenesis	10
1.2	Deregulated angiogenesis in eye diseases - ocular neovascularization	12
1.2.1	Corneal neovascularization in corneal surface wounding	12
1.2.1.1	Epidemiology of corneal neovascularization	13
1.2.1.2	Molecular mediators of corneal neovascularization.....	14
1.2.2	Choroidal neovascularization in wet type of age-related macular degeneration.....	14
1.2.2.1	Epidemiology and classification of age-related macular degeneration.....	14
1.2.2.2	Definition of choroidal neovascularization	15
1.2.2.3	Cellular and molecular mechanism of choroidal neovascularization.....	16
1.3	<i>In vitro</i> and <i>in vivo</i> angiogenesis model for ocular neovascularization.....	18

1.3.1	<i>In vitro</i> scratch-wound HUVEC migration assay	18
1.3.2	MTT cell viability assay	19
1.3.3	<i>In vivo</i> chick chorioallantonic membrane (CAM) assay.....	20
1.3.3.1	Embryological origin and development of CAM.....	20
1.3.3.2	In ovo and ex ovo model of chick cam assay	22
1.3.3.3	Advantages and limitations of Chick CAM assay.....	23
1.3.4	<i>In vivo</i> corneal neovascularization assay	24
1.3.5	<i>In vivo</i> laser-induced choroidal neovascularization assay	26
1.4	Natural products and potential anti-angiogenic effects.....	28
1.4.1	Introduction.....	28
1.4.2	Criteria of selecting herbal molecule to study its potent angiostatic character	29
1.4.3	Isoliquiritigenin (ISL)	29
1.4.4	Epigallocatechin gallate (EGCG)	30
1.4.5	Resveratrol (Rst).....	30
CHAPTER 2 OBJECTIVES AND STUDY DESIGN.....		32
CHAPTER 3 GENERAL MATERIALS & METHODS		34
3.1	Materials	34
3.1.1	Herbal chemicals and angiogenesis controls	34

3.1.2	Antibodies.....	34
3.1.3	Chemicals for cell culture	35
3.1.4	Miscellaneous chemicals	35
3.2	Methods.....	35
3.2.1	<i>In vitro</i> cell viability assay	35
3.2.2	<i>In vitro</i> angiogenesis assay	36
3.2.2.1	Cell culture	36
3.2.2.2	Scratch wound HUVEC growth and migration assay	37
3.2.2.3	Western blot analysis.....	37
3.2.3	<i>In vivo</i> angiogenesis assay	39
3.2.3.1	Chick chorioallantonic membrane assay.....	40
3.2.3.2	Silver nitrate cauterization-induced corneal neovascularization assay	44
3.2.3.3	Laser-induced choroidal neovascularization assay	48
 CHAPTER 4 RESULTS: The effect of selected herbal molecules in ocular neovascularization: <i>in vitro</i> & <i>in vivo</i> studies		
4.1	Effect of isoliquiritigenin in ocular angiogenesis	54
4.1.1	<i>In vitro</i> studies.....	54
4.1.1.1	Cytotoxicity analysis	54

4.1.1.2	Scratch wound HUVEC migration assay	54
4.1.2	<i>In vivo</i> angiogenesis studies.....	55
4.1.2.1	Developmental angiogenesis in chick CAM assay	55
4.1.2.2	Pathological angiogenesis of silver nitrate cauterization induced corneal neovascularization assay	57
4.1.2.3	Pathological angiogenesis of laser-induced choroidal neovascularization assay	58
4.1.2.4	Choroidal neovascularization area	60
4.1.3	Protein analysis	60
4.1.3.1	VEGF expression (Figure 48)	60
4.1.3.2	PEDF expression analysis (Figure 48)	61
4.1.3.3	Akt activation assay (Figure 49)	61
4.1.3.4	Pan-Akt expression (Figure 49)	62
4.1.3.5	FAK activation assay (Figure 50).....	62
4.1.3.6	MMP-2 expression (Figure 51)	62
4.1.3.7	MMP-9 expression (Figure 51)	63
4.1.4	Discussion	63
4.1.5	Conclusion	69
4.2	Effect of epigallocatechin gallate in ocular angiogenesis.....	70
4.2.1	<i>In vitro</i> studies.....	70

4.2.1.1	Cytotoxicity by MTT Assay	70
4.2.1.2	Effect on HUVEC migration.....	70
4.2.2	<i>In vivo</i> angiogenesis studies.....	71
4.2.2.1	Suppression of developmental vessel growth in chick CAM asay	71
4.2.2.2	Suppression of silver nitrate cauterization-induced corneal neovascularization.....	72
4.2.2.3	Suppression of laser-induced choroidal neovascularization.....	74
4.2.3	Protein analysis	76
4.2.3.1	VEGF expression (Figure 48)	76
4.2.3.2	PEDF expression analysis (Figure 48).....	77
4.2.3.3	Akt activation assay (Figure 49)	77
4.2.3.4	Pan-Akt expression (Figure 49)	77
4.2.3.5	FAK activation assay (Figure 50).....	78
4.2.3.6	MMP-2 expression (Figure 51).....	78
4.2.3.7	MMP-9 expression (Figure 51).....	79
4.2.4	Discussion	79
4.2.5	Conclusion	83
4.3	Effect of resveratrol in ocular angiogenesis.....	84
4.3.1	<i>In vitro</i> studies.....	84

4.3.1.1	Cytotoxicity by MTT Assay	84
4.3.1.2	Effect on HUVEC migration.....	84
4.3.2	<i>In vivo</i> angiogenesis studies.....	84
4.3.2.1	Suppression of developmental vessel growth in chick CAM assay	84
4.3.2.2	Suppression of silver nitrate cauterization induced corneal neovascularization.....	86
4.3.2.3	Suppression of laser-induced choroidal neovascularization.....	87
4.3.3	Protein analysis	89
4.3.3.1	VEGF expression (Figure 48)	89
4.3.3.2	PEDF expression analysis (Figure 48).....	89
4.3.3.3	Akt activation assay (Figure 49)	90
4.3.3.4	Pan-Akt expression (Figure 49)	90
4.3.3.5	FAK activation assay (Figure 50).....	91
4.3.3.6	MMP-2 expression (Figure 51).....	91
4.3.3.7	MMP-9 expression (Figure 51).....	91
4.3.4	Discussion	92
4.3.5	Conclusion	97
CHAPTER 5 GENERAL CONCLUSIONS		98
CHAPTER 6 FUTURE PROSPECTS		100

TABLES	102
FIGURES	104
REFERENCES	155

LIST OF TABLES

Table 1: A summary of commonly used corneal neovascularization (NV) model	102
Table 2: A summary of commonly used Chick CAM model.....	103

LIST OF FIGURES

Figure 1: VEGF signaling pathway	104
Figure 2: Chemical structure of Isoliquiritigenin.....	105
Figure 3: Resources of isoliquiritigenin: licorice & licorice root.....	106
Figure 4: Effect of ISL on cell viability of ARPE-19 cells.	107
Figure 5: The inhibitory effect of ISL on VEGF-A-induced HUVEC migration in a scratch wound healing assay.	108
Figure 6: Morphological analysis of blood vessel changes of chick chorioallantoic membrane at 24 hours after treatments.	109
Figure 7: Representative photographs showing the effect of ISL on developmental chick chorioallantoic membrane assay at 24 hours after treatments.	110
Figure 8: ISL suppressed blood vessel development in the gelatin-sponge chick chorioallantonic membrane assay.	111
Figure 9: Effect of ISL corneal neovascularization development.....	112
Figure 10: Effect of ISL on blood vessel manifestation in corneal neovascularization assay	113
Figure 11: Suppression of neovascularized area after ISL treatment for 7 days.	114
Figure 12: Effect of ISL corneal neovascularization development.....	115
Figure 13: Effect of ISL on blood vessel manifestation in corneal neovascularization assay	116
Figure 14: Suppression of neovascularized area after ISL treatment for 14 days.	117
Figure 15: Anti-angiogenic effect of ISL on laser photocoagulation-induced choroidal NV model.....	118
Figure 16: ISL suppressed choroidal NV severity scored after fundus fluorescein angiography.....	119
Figure 17: ISL reduced the vascularized area in laser-induced choroidal NV assay.	120
Figure 18: Chemical structure of epigallocatechin-3-gallate.....	121
Figure 19: Resources of Epigallocatechin-3-gallate: green tea.	122

Figure 20: Effect of EGCG on cell viability of ARPE-19 cells.....	123
Figure 21: The inhibitory effect of EGCG on VEGF-A-induced HUVEC migration in a scratch wound healing assay.....	124
Figure 22: Representative micrographs showing the effect of EGCG on developmental chick chorioallantoic membrane assay at 24 hours.....	125
Figure 23: EGCG suppressed blood vessel development in the gelatin-sponge chick chorioallantonic membrane assay.....	126
Figure 24. Effect of EGCG corneal neovascularization development.....	127
Figure 25: Effect of EGCG on blood vessel manifestation in corneal neovascularization assay.....	128
Figure 26: Suppression of neovascularized area after EGCG treatment for 7 days.....	129
Figure 27: Effect of EGCG corneal neovascularization development.....	130
Figure 28: Effect of EGCG on blood vessel manifestation in corneal neovascularization assay.....	131
Figure 29: Suppression of neovascularized area after EGCG treatment for 14 days.....	132
Figure 30: Anti-angiogenic effect of EGCG on laser photocoagulation-induced choroidal NV model.....	133
Figure 31: EGCG suppressed choroidal NV examined by fundus fluorescein angiography.....	134
Figure 32: EGCG suppressed the vascularized area in laser-induced choroidal NV assay.....	135
Figure 33: Chemical structure of Resveratrol.....	136
Figure 34: Resources of resveratrol: grapes and red wine.....	137
Figure 35: Effect of Rst on cell viability of ARPE-19 cells.....	138
Figure 36: Inhibition of Rst on VEGF-A-induced HUVEC migration.....	139
Figure 37: Representative photographs showing chick chorioallantoic membrane changes at 24 hours after Rst treatments.....	140
Figure 38: Rst suppressed chick chorioallantonic membrane vessel development.....	141
Figure 39: Effect of Rst corneal neovascularization development.....	142

Figure 40: Effect of Rst on blood vessel manifestation in corneal neovascularization assay	143
Figure 41: Anti-angiogenic effect of Rst on mice corneal NV after treatment for 7 days.	144
Figure 42: Effect of Rst corneal neovascularization development.	145
Figure 43: Effect of Rst on blood vessel manifestation in corneal neovascularization assay	146
Figure 44: Anti-angiogenic effect of Rst on corneal NV model after treatment for 14 days.....	147
Figure 45: Anti-angiogenic effect of Rst on laser photocoagulation-induced choroidal NV model.....	148
Figure 46: Rst affected choroidal NV development by fundus fluorescein angiography.....	149
Figure 47: Rst suppressed the vascular area in laser-induced choroidal NV assay.	150
Figure 48: VEGF & PEDF expression by Western blot and quantification analysis by band densitometry.	151
Figure 49: Akt activation assay by Western blot analysis and quantification analysis by band densitometry.	152
Figure 50: FAK activation assay by Western blot and band densitometry analysis.....	153
Figure 51: MMP-2 & MMP-9 expression by Western blotting	154

ABBREVIATIONS

- Herbal molecules

ISL	isoliquiritigenin
EGCG	epigallocatechin gallate
Rst	resveratrol

- Growth factors and cytokines

VEGF	vascular endothelial growth factor
PEDF	pigment epithelial derived factor
FAK	focal adhesion kinase
TGF	transforming growth factor
TNF	tumor necrosis factor
TSP	thrombospondin
MMP	matrix metalloproteinase
PIGF	placenta-induced growth factor
RTK	receptor tyrosine kinase
Flt-1	<i>fms</i> -like tyrosine kinase-1
KDR	kinase insert domain-containing receptor
EGF	epidermal growth factor
IGF-1	insulin-like growth factor-1
IL	interleukin
ERK	extracellular signal-regulated kinase
MAPK	mitogen-activated protein kinase
bFGF	basic fibroblast growth factor

GMCSF	granulocyte-macrophage colony-stimulating factor
Robo4	Roundabout receptor protein 4
uPA	urokinase-type plasminogen activator
ICAM-1	intercellular adhesion molecule 1
siRNA	small interfering RNA
Cox-2	Cyclooxygenase-2
5-LOX	5-Lipoxygenase
PSA	prostate-specific antigen
NF- κ B	nuclear factor kappa-light-chain-enhancer of activated B cells
AP-1	activator protein 1
Egr-1	early growth response protein 1
PI3 kinase	phosphoinositide 3-kinase
HGF	hepatocyte growth factor
HO-1	heme oxygenase 1
HIF-1 α	hypoxia-inducible factor 1 α

- Cell lines

HUVEC	human umbilical vein endothelial cell
RPE cell	retinal pigment epithelium cell
ECs	endothelial cells
OVCAR-3	human ovarian carcinoma cell line
ACC	acinar cell carcinoma

- Chemical agents

MTT	3-(4,5-dimethylthiazol-2-yl)-2,5-diphenyltetrazolium bromide
-----	--

(also called as Method of Transcriptional and Translational)

DMSO	dimethyl sulfoxide
FBS	fetal bovine serum
GAPDH	glyceraldehyde-3-phosphate dehydrogenase
PBS	phosphate buffer solution
HRP	horseradish peroxidase

- Neovascularization

CNV	choroidal neovascularization
AMD	age-related macular degeneration
NV	neovascularization
VE	vascular endothelial
CAM	chorioallantoic membrane

- Others

HRA2	Heidelberg Retinal Angiograph 2
CAS	Chemical Abstract Service Registry
FFA	fundus fluorescein angiography

PUBLICATIONS

1. Liming CAO, Huanming LIU, Dennis Shun Chiu LAM, Gary YAM, CP PANG. In vitro screening for angiostatic potential of herbal chemicals. *Invest Ophthalmol Vis Sci*, 2010. [Epub ahead of print]
2. Huanming LIU, Vishal JHANJI, Kasin LAW, Vincent Yau-Wing LEE, Shao-Fen HUANG, Chi-Pui PANG, Gary Hin-Fai YAM. Isoliquiritigenin from licorice root suppressed neovascularization in different experimental ocular angiogenesis models. *Invest Ophthalmol Vis Sci*. Submitted.
3. Li XU, Huanming LIU, Chi-Pui PANG, Gary Hin-Fai YAM, David LIU. Disruption of Bevacizumab (Avastin) activities by vitreous in vitro. *Br J Ophthalmol*. Submitted.

CONFERENCE PRESENTATIONS

1. Huanming LIU, Anita Sin-Yee NG, Nancy Lan LIU, Gary Hin-Fai YAM, Dennis Shun-Chiu LAM, Chi-Pui PANG. Reassessment of corneal neovascularization models in rodent. Association for Research in Vision and Ophthalmology 2009 Annual Meeting, Fort Lauderdale, Florida, USA. May 2-5, 2009. (poster presentation)

2. Huanming LIU, Kasin LAW, Dennis Shun-Chiu LAM, Gary Hin-Fai YAM, Chi-Pui PANG. Isoliquiritigenin Suppressed Ocular Surface Angiogenic Reaction. Chinese Congress for Research in Vision and Ophthalmology 2010. Qingdao, China. March 26-28, 2010. (oral presentation)

CHAPTER 1

INTRODUCTION

1.1 Angiogenesis

1.1.1 Definition and characterization

Angiogenesis is a complex biological process responsible for the formation and development of new blood vessels from a pre-existing vascular network, which carries oxygen and nutrient to cells and tissues. The development and maturation of new blood vessels requiring successive activation of various receptors and ligands and the finely adjusted balance between multiple stimulating and inhibitory signals, however, their imbalance often lead to deregulated angiogenesis and leakages associated with disease manifestation. In development and normal physiological processes, such as embryonic development, reproduction, and repair or regeneration of tissue during wound healing (Folkman et al., 1995), angiogenesis is regulated by endogenous activators and inhibitors. Within adult animals, the levels of endogenous mediators are balanced and endothelial cells (ECs) are largely quiescent (Ferrara et al., 2004; Hoeben et al., 2004; Roskoski et al., 2007). In pathological settings, shifts in the equilibrium between angiogenic stimulators and inhibitors are linked to a broad range of angiogenesis-dependent disease, including tumors and non-neoplastic diseases like atherosclerosis, age-related macular degeneration, diabetic retinopathy and rheumatoid arthritis (Garner et al., 1994). Conversely, insufficient angiogenesis underlies conditions such as cardiovascular disease, stroke and delayed wound healing, where inadequate blood-vessel growth leads to poor circulation and tissue death.

1.1.2 Cellular and molecular mechanisms of angiogenesis

There are two distinct mechanisms responsible for neovascularization: vasculogenesis and angiogenesis. Vasculogenesis is the *in situ* differentiation of endothelial cell precursors (the angioblasts) from mesoderm-derived precursor cells (hemangioblasts) (Poole et al., 1989), gives rise to the heart and the first primitive vascular plexus inside the embryo and in its surrounding membranes, as the yolk sac circulation. In contrast, angiogenesis is the formation of capillaries (new vessels) from the pre-existing vessels in embryo and adult organisms (Patan et al., 1997). These newly formed vasculatures are further restructured to a more mature form with tree-like architecture comprising large and small vessels (Patan et al., 1997). Angiogenesis comprises two different mechanisms: endothelial sprouting and intussusceptive microvascular growth. The sprouting process is based on endothelial cell migration, proliferation and tube formation. Intussusceptive microvascular growth divides existing vessel lumens by the formation and insertion of tissue folds and columns of interstitial tissue into the vessel lumen. They are termed as the interstitial or inter-vascular tissue structures and tissue pillars or posts. Intussusception also includes the establishment of new vessels by *in situ* loop formation in the wall of large veins.

The cellular mechanisms, the molecular regulation of angiogenesis in the pathological state as well as and the differences of physiological and pathological angiogenesis are summarized.

1.1.2.1 The cellular mechanisms of angiogenesis:

Angiogenesis are comprised of two distinct processes after the formation of primary vascular plexus: sprouting of endothelial cells from pre-existing capillary and non-sprouting angiogenesis or splitting of vessel lumens by intussusceptive mi-

crovascular growth.

The sprouting process consists of several consecutive steps that have been described by different studies (Ausprunk *et al.*, 1974; Folkman *et al.*, 1982; 1985; 1986):

- (1) New capillaries originate from small venules or from other capillaries.
- (2) Local degradation of basement membrane on the side of venule closest to the angiogenic stimulus (including collagenase, plasminogen activators).
- (3) Migration of endothelial cells toward the angiogenic stimulus.
- (4) Alignment of endothelial cells in bipolar mode.
- (5) Formation of a lumen (intra-cellular from vacuoles or intercellular) and endothelial cell mitosis distant to the leading tip of the sprout.
- (6) Loop formation by the connection of individual sprouts.
- (7) Flow begins after loop shape formed.
- (8) Pericytes or smooth muscle cells eventually align along the endothelial cell outside the capillary (vessel wall maturation).
- (9) Formation of new basement membrane.

1.1.2.2 The intussusceptive mode of angiogenesis:

The process are summarized in the following steps (Pardanaud *et al.*, 1989; Patan *et al.*, 1993; Patan *et al.*, 1996; Patan *et al.*, 1997; Tardy *et al.*, 1997):

- (1) Growth occurs predominantly on the venous side - intussusception.
- (2) The endothelial layer retreats successively around an organized unit of interstitial tissue (the pillar core) located in the vessel wall.
- (3) Pillar separation from the tissue fold, the division of an interstitial or inter-vascular tissue structures and the thinning of endothelial cells are critical to form

free intraluminal structures or tissue pillars as well as to the in situ formation of vessel loops (Pardanaud et al., 1989).

(4) The synthesis of collagen fibers from peri-endothelial cells (pericytes and smooth muscle cells) is an obligate step to form the interstitial or inter-vascular tissue structures or pillar core and stabilize it. It is yet unknown which types of collagen are involved (Pardanaud et al., 1989; Patan et al., 1993).

(5) Endothelial cell multiplication may occurs.

(6) Flow is permanently present during all these steps.

(7) Finally a basement membrane is formed.

1.1.2.3 Molecular regulation of angiogenesis

In general, the molecular regulation of angiogenesis contains two major groups: angiogenic molecules and angiostatic molecules (angiogenic inhibitors). They are acting at different steps of angiogenesis process and they work in a finely adjusted balance to maintain the angiogenic homeostasis. An imbalance of either group of molecules in any particular step of vessel formation will lead to deregulated vessel formations and sproutings. This is often associated with disease manifestations and tissue damages.

1.1.3 Angiogenesis and its regulatory proteins

Physiologically, angiostatic mediators outweigh the angiogenic molecules and angiogenesis does not occur. Under certain conditions, such as tumor formation or wound healing, the positive regulators of angiogenesis predominate and the endothelium becomes activated. Angiogenesis is initiated by vasodilatation and an increased

permeability. After destabilization of vessel wall, endothelial cells proliferate, migrate and form a tube, which is finally stabilized by pericytes and smooth muscle cells. Numerous soluble growth factors and inhibitors, cytokines and proteases as well as extracellular matrix proteins and adhesion molecules strictly control this multi-step process. The properties and interactions of angiogenic molecules such as fibroblast growth factor (acidic FGF-1 and basic FGF-2), hepatocyte growth factor (HGF), vascular endothelial growth factor (VEGF), transforming growth factor alpha (TGF- α), and interleukin-8 (IL-8) (Ware et al., 1997). Additionally, an important role in angiogenesis has been established for the tie/Angiopoietin and the Eph-B/ephrin-B system of tyrosine kinase receptors and their ligands (Suri et al., 1996; Davis et al., 1996; Wang et al., 1998; Adams et al., 1999) as well as the angiostatic key players including angiostatin, endostatin, thrombospondin, angiopoietin 2, transforming growth factor (TGF) β , tumor necrosis factor (TNF) α , CXC chemokines without ELR motif, thrombospondin (TSP)-1, TSP-2, matrix metalloproteinase family (MMPs), and pigment derived growth factor (PEDF) (Distler et al., 2000).

1.1.4 Vascular endothelial growth factor (VEGF)

Over the past decade, members of vascular endothelial growth factor (VEGF) gene family and their receptors have been extensively studied. It is well supported that they play an important role in the growth and differentiation of vascular as well as lymphatic endothelial cells.

The VEGF gene family are comprised of seven subtypes including VEGF-A, placenta growth factor (PlGF), VEGF-B, VEGF-C, VEGF-D and the *parapoxvirus* genome encoded virus VEGF (viral VEGF, also referred as VEGFE) and recently identified snake venom-derived VEGF (also referred as VEGFF).

In particular, VEGF-A, also referred to as VEGF, is an endothelial cell-specific mitogen and an angiogenic inducer as well as a mediator of vascular permeability (Ferrara et al., 2004). It is a major regulator of physical and pathological angiogenesis, including that associated with tumors, arthritis and several intraocular diseases (Garner et al., 1994; Folkman et al., 1995; Ferrara et al., 2004; Hoeben et al., 2004; Roskoski et al., 2007). Furthermore, VEGF is a critical inducer for the development of embryonic vasculogenesis: inactivation of even a single VEGF allele resulted in defective angiogenesis and early embryonic lethality (Carmeliet et al., 1997).

1.1.4.1 VEGF isoforms

The murine VEGF-A gene is highly conserved, with three splice variants, VEGF120, VEGF164 and VEGF188, equivalent to the human VEGF121, VEGF165 and VEGF189 isoforms, respectively (Ng et al., 2001). Nine major VEGF-A isoforms have been identified in human: VEGF121, VEGF145, VEGF148, VEGF162, VEGF165, VEGF165b (an endogenous inhibitory isoform that binds to VEGFR2 with similar affinity to VEGF165 but does not activate the receptor), VEGF183, VEGF189, and VEGF206 (Neufeld et al., 1999). These isoforms are produced by alternative exon splicing of the human VEGF-A gene on chromosome 6p21.3.1 (Takahashi et al., 2005). An important characteristic of VEGF isoforms is their ability to bind to heparin, and this ability defines whether the secreted protein is in the extracellular matrix and become accessible for the interaction with other cell types. VEGF165 and longer isoforms consist of two major domains: a VEGF receptor-binding domain that is present in all VEGF-A isoforms and a heparin-binding domain that is absent in the shorter diffusible isoforms. Longer isoforms, such as VEGF189 and VEGF206, bind to the extracellular matrix via the heparin-binding

domain (Lee et al., 2005). The VEGF165 isoform is intermediate, and exists as both diffused and partly extracellular matrix-bound forms (Houck et al., 1992; Park et al., 1993). VEGF165 is the most abundantly expressed VEGF-A isoform and has a vital role in angiogenesis (Keyt et al., 1996; Soker et al., 1998). There was another study showing that VEGF121, although less abundant, was more mitogenic than VEGF165 or VEGF189 (Zhang et al., 2000). All VEGF-A isoforms, except VEGF121, contain a plasmin cleavage site and theoretically may be cleaved by plasmin to generate the smaller VEGF110 form (Takahashi et al., 2005; Keyt et al., 1996). VEGF110 stimulates endothelial cell growth and induce vascular permeability in the Miles assay (Houck et al., 1992); however, its mitogenic potency is less than that of VEGF165 (Fairbrother et al., 1998). VEGF121, VEGF165, VEGF183 and VEGF189 are distributed widely in tissue, with VEGF165 having the most abundant expression. In contrast, VEGF145 and VEGF206 are less abundant.

1.1.4.2 VEGF receptors

Member of the VEGF family exert their biological effect via interaction with receptors located on endothelial cell membrane. Five receptors have been identified that bind to different VEGF isoforms: three belong to the receptor tyrosine kinase (RTK) family and are called *fms*-like tyrosine kinase-1 (Flt-1, also known as VEGFR-1) (Neufeld et al., 1999; Dor et al., 2001), kinase insert domain-containing receptor (KDR, VEGFR-2) (Shibuya et al., 1990; Davis et al., 1996) and Flt-4 (VEGFR-3) (Matthews et al., 1991; Terman et al., 1991; Millauer et al., 1993). The others are non-tyrosine kinase-type receptors neuropilin-1 (NP-1) and neuropilin-2 (NP-2), which are believed to function as co-receptors for some VEGF subtypes and their isoforms (Gluzman-Poltorak et al., 2001).

All VEGFR receptors are highly homologous (Shibuya et al., 1990; Alitalo et al., 2002). Like all RTK, VEGF receptors are transmembrane proteins with a single transmembrane domain. The extracellular region of VEGFR is formed by seven immunoglobulin-like domains (Ig I-VII), whereas the intracellular part exhibits tyrosine kinase activity, and the tyrosine kinase domain in these receptors is separated into two fragments (TK-1 and TK-2) by an inter-kinase insert (Shibuya et al., 1990; Terman et al., 1991).

Each VEGF subtype selectively binds to some of these receptors, often with different affinities and selectivities, thereby this demonstrates the diversity of the biological functions exerted by VEGFs. VEGF-A signals through two receptor tyrosine kinases, VEGFR1 and VEGFR2, and is the only member of the VEGF gene family found to be induced by hypoxia (Yonekura et al., 1999). VEGF-B selectively binds to VEGFR1 and has a role in the regulation of extracellular matrix degradation, cell adhesion and migration (Olofsson et al., 1998). Both VEGF-C and VEGF-D bind to VEGFR2 and VEGFR3 and regulate lymphangiogenesis, and VEGF-C may also be involved in wound healing (Olofsson et al., 1998; Stacker et al., 2001; Bauer et al., 2005). PlGF selectively binds to VEGFR1 (Olofsson et al., 1998) and is the most abundantly expressed VEGF family member in endothelial cells (Yonekura et al., 1999). It potentiates VEGF-A to induce endothelial cell proliferation (Ferrara et al., 2002), but on its own PlGF exerts only weak mitogenicity (Yonekura et al., 1999).

1.1.5 VEGF signaling pathway (Figure 1)

Regulation of endothelial cell in angiogenesis is the result of a very complex network of intracellular signalling systems that trigger, control and terminate the process (Mariotti et al., 2006). The transition from a quiescent to an angiogenic phe-

notype in endothelial cells is governed by the activation of several signal transduction pathways as a response to specific stimuli. One of the earliest events in angiogenesis is the up-regulation of endothelial proteolytic enzymes, which degrade the basal lamina underneath the endothelium. The Ras-MAPK pathway is pivotal because it targets the zinc-finger transcription factors Ets-1, which plays a key role in activating the proteolytic system (Mariotti et al., 2006). After the matrix degradation by proteases, the endothelial cell migration occurs. A key role is played by small GTPase and cytosolic tyrosin kinases, which must be activated to stimulate the formation of focal adhesions, a pre-requisite for endothelial migration. Indeed, VEGFR-2 activates the focal adhesion kinase (FAK) that regulates the organization of cytoskeleton and recruits other molecules, including the tyrosine kinase Src (Eliceiri et al., 2002). In short, signaling molecules associate with focal contacts the small GTPases Rho and Rac control cytoskeletal dynamics as well as polarization and migration.

Following migration, endothelial cells begin to proliferate, an event mainly mediated by the extracellular signal-regulated kinase mitogen-activated protein kinases (ERK-MAPK) cascade, which is activated by different signal transduction pathways including phospholipase C gamma and the small GTPase Ras (Schönwasser et al., 1998). VEGFR-2 and FGF receptors, with the contribution of integrins, activate these signal transducers. This leads to translocation of the activated ERK-MAPK to the nucleus and the induction of several transcription factors involved in cell proliferation (Mariotti et al., 2006).

After migration and proliferation, endothelial cells should return to quiescence, survive, undergo a morphogenetic program and recruit to perivascular cells. This is the convergence point for integrin-mediated interactions with the extracellular matrix

and soluble factors such as VEGF and FGF (Mariotti et al., 2006). Although the signaling mechanisms controlling these latter steps are less known, p38 MAPK and JNK pathways seem to be involved. PI3 kinase/Akt pathway is mainly responsible for endothelial cell survival (Mariotti et al., 2006).

1.1.6 Endothelial cells and role in angiogenesis

The initiation of angiogenic cascade from a pre-existing vascular network requires selective departure of individual endothelial cells from differentiated capillaries. The process entails the activation of specific signaling pathways that enable endothelial cells to exit their vessel of origin, invade the underlying stroma and initiate a new vascular sprout. Two major signaling pathways: VEGF and Notch, coordinate this process to select a subset of leading endothelial cells, referred to as tip cells. These cells display long filopodia and are highly migratory, but remain linked to their followers, the stalk cells. The stalk cells constitute the body of sprout and proliferate in response to VEGF to increase the length of incipient capillary. It is the coordination of Notch and VEGF signaling that regulates the extent to which cells become leaders (tip cells) and which become followers (stalk cells). Activation of Notch represses the tip cells in favor of the stalk cell phenotype, in part, by regulating the level of VEGFR2. The resolution of endothelial activation phase requires synthesis and organization of the basement membrane and the recruitment of pericytes and smooth muscle cells (Iruela-Arispe et al., 2008).

During angiogenesis, stimuli that promote proliferation of endothelial cells outweigh the effects of angiostatic factors. Angiogenic molecules include members of VEGF- and FGF families, angiopoietin 1 and 2, angiogenin, epidermal growth factor (EGF), CXC-chemokines and insulin-like growth factor-1 (IGF-1). VEGF and the angiopoietins appear to be specific mitogens for endothelial cells, whereas FGFs,

angiogenin, EGF, CXC-chemokines and IGF-1 induce proliferation in a wide variety of cell types (Iruela-Arispe et al., 2008). The proliferating endothelial cells migrate along a gradient of chemotactic agents through the disintegrated basement membrane into the remodeled and softened perivascular space.

1.2 Deregulated angiogenesis in eye diseases - ocular neovascularization

Ocular neovascularization, the abnormal growth of blood vessels in the eye, is associated with the vast majority of eye diseases that cause transient or permanent loss of vision. The most common type of ocular neovascularization is corneal neovascularization in the anterior segment and it is mainly due to inflammation, limbal stem cell degeneration, or traumatic corneal disorders. Choroidal neovascularization in the posterior part of eye is commonly associated with age-related macular degeneration (AMD), a leading cause of vision loss in the elderly over 65 years old.

1.2.1 Corneal neovascularization in corneal surface wounding

The cornea, the transparent “windscreen” of the eye, is one of the few avascular tissues of the human body (Cursiefen et al., 2006). Corneal clarity and avascularity are important for the proper optical performance of the cornea (Chang et al., 2001) and are actively maintained in all animal species that require high visual acuity (Chang et al., 2001; Cursiefen et al., 2004). This so-called “angiogenic privilege” of the cornea is therefore evolutionary highly conserved and supported by multiple molecular mechanisms (Ambati et al., 2006; Cursiefen et al., 2005; 2006; 2007). Corneal epithelium generates corneal antiangiogenic factors and antiangiogenic MMPs that counterbalance the NV stimuli, which promote corneal NV through breakdown endothelial cell membrane, degradation of corneal antiangiogenic factors and transcriptional upregulation of VEGF, and help maintain corneal angiogenic privilege

(Azar et al., 2006).

1.2.1.1 Epidemiology of corneal neovascularization

Several corneal diseases have the symptomatic pathological corneal neovascularization and reduced corneal transparency. The severity can also affect the survival of corneal transplants, if performed, and eventually results in irreversible blindness.

Corneal NV may occur during corneal surface injuries associated with several inflammatory, infectious, degenerative, and traumatic corneal disorders, including corneal graft rejection, infectious keratitis, contact lens-related hypoxia, alkali burns, stromal ulceration, aniridia, and limbal stem cell deficiency (Chang et al., 2001; Azar et al., 2006).

It is associated with the second most common cause of blindness worldwide (trachoma) and also with the most common form of corneal blindness in industrialized countries (herpetic keratitis) (Lee et al., 1998). Ocular surface disease, especially those leading to corneal NV poses a serious public health that is concerning with considerable morbidity. The incidence of corneal NV in US stands at about 1.4 millions or affecting 4% of the population (Lee et al., 1998). The dreaded complications of corneal NV include corneal edema, lipid deposition, scarring and reduced chances of successful corneal grafts. Thirty per cent of vascularized corneas face with the risk of graft failure following penetrating keratoplasty, making it imperative to identify the molecular mechanisms that may be targeted to prevent or retard its progression (Cursiefen et al., 1998).

The balance between angiogenic and antiangiogenic factors may be tilted in favor of NV due to the upregulation of angiogenic factors and/or the downregulation of antiangiogenic factors (Folkna et al., 1992; Beck et al., 1997; Kato et al., 2001).

1.2.1.2 Molecular mediators of corneal neovascularization

In cancer angiogenesis research, a balance was shown to exist between angiogenic factors (such as fibroblast growth factor and vascular endothelial growth factor) and anti-angiogenic molecules (such as angiostatin, endostatin, or pigment epithelium derived factor) (Chang et al., 2001). Growth factors of VEGF family (VEGF A, C, and D) have been identified as key players in both inflammation-driven hem- and lymphangiogenesis on the normally avascular cornea (Amano et al., 1998; Cursiefen et al., 2004). The pathogenesis of corneal NV may be influenced by matrix metalloproteinases and other proteolytic enzymes (Azar et al., 2006). Lipids also play important roles in the complex inflammatory processes that occur after corneal wounding (Bazan, 2005). Recently Roundabout receptor protein (Robo4), which has an established role in neuronal guidance, was expressed in murine vascular endothelial cells during embryogenesis (ParkK et al., 2003). Robo4 is unique in that it is restricted to endothelial cells, especially at sites of angiogenesis. The soluble extracellular domain of Robo4 receptor inhibits murine VEGF-induced and bFGF-induced endothelial cell migration (Suchting et al., 2005).

1.2.2 Choroidal neovascularization in wet type of age-related macular degeneration

1.2.2.1 Epidemiology and classification of age-related macular degeneration

Age-related maculopathy, also referred to as age-related macular degeneration (AMD), is a leading cause of severe, irreversible visual loss worldwide (Leibowitz et

al., 1980; Tielsch et al., 1995). It is characterized by funduscopy examination, including the presence or not of drusen (yellow deposits below RPE), hyperpigmentary and hypopigmentary changes of RPE, atrophic macular degeneration (well-defined areas of atrophy, called geographic atrophy, or other atrophy of the RPE and chorio-capillaries) and neovascular macular degeneration (choroidal neovascularization CNV, serous or hemorrhagic detachment of RPE, and subsequent scarring of macular area) (Vingerling et al., 1995). The late-stage of AMD is characterized by either the neovascular/exudative (wet-type AMD) or non-neovascular atrophic macular degeneration (dry type AMD) (Bird et al., 1995). The exudative form of AMD, characterized by CNV and its sequelae, is composed of 75% of AMD cases, and the non-neovascular atrophic form is roughly 25%. The development of CNV has devastating effect on the visual capability of the patient and is the major factor contributing to loss of vision in AMD (Bressler et al., 1990).

1.2.2.2 Definition of choroidal neovascularization

The choroid is a thin, highly vascularized layer lying posterior to the neurosensory retina and retinal pigment epithelium (RPE). Its vessels provide oxygen to the outer third of retina including the photoreceptors. Normally, the choroidal vessels are restricted from directly contacting with the adjacent retina by an anatomic barrier, Bruch's membrane. However, in AMD patients, the Bruch's membrane is weakened and the endothelial cells from choroidal vessels are activated to proliferate. The resulting new vessels break through the weakened regions of Bruch's membrane, and fibrovascular tissues are deposited in the sub-RPE space (Husain et al., 2002; Aguilar et al., 2010).

Choroidal neovascularization (CNV) is defined as the formation of new blood

vessels that are located between the RPE and Bruch's membrane and are continuous with the normal choroidal vessels (Green et al., 1986). These newly formed blood vessels are structurally weak, both leaking fluid and lacking of structural integrity, result in hemorrhage, exudates, and accompanying fibrosis often causing blindness.

1.2.2.3 Cellular and molecular mechanism of choroidal neovascularization

The mechanism responsible for the development of CNV is still not well understood. Hypoxia and inflammation play important roles of choroidal new vessel formation. The relative hypoxia caused by the disturbed balance between the limited blood supply in the macula and the high oxygen demand in the photoreceptors may contribute to the formation of CNV by the up-regulation of expression of growth factors, such as VEGF (Penfold, et al., 2001).

The association of inflammation with the neovascular macular lesions has been postulated more than a century. Numerous histological, ultrastructural and immunohistochemical studies have demonstrated that in exudative AMD, the leukocyte is one of the major cellular components of subretinal neovascular membrane derived from the choroid and the distribution of leukocytes is closely related to the development and progression of neovasculation (Penfold, et al., 2001; Kim, et al., 1996; Grossniklaus et al, 2001). Another piece of evidence showing the role of inflammation in the pathogenesis of CNV is that the deposition of complements and Ig has been found in the RPE and choroid in patients with AMD (Ambati, et al., 2003).

The role of macrophage in the pathogenesis of AMD and subsequent CNV is controversial. Although the recruitment of macrophages has been shown to be essential for the elimination of complement and Ig deposition (Ambati, et al., 2003), a

number of histological studies have shown that the infiltration of macrophages is actively involved in the promotion of neovascular proliferation and the exudation from the new vessels in exudative AMD (Penfold, et al., 2001). Furthermore, it is shown that by the release of proteases, growth factors (bFGF, GMCSF, TGF-alpha, IGF-I, PDGF, VEGF/VPF, TGF-beta), and other cytokines (IL-1, IL-6, IL-8, TNF- α , substance P, prostaglandins, interferons, thrombospondin 1), activated macrophages have the capability to influence each phase of the angiogenesis process. These include alteration of local extracellular matrix, induction of endothelial cell proliferation and migration and inhibition of vascular growth with the formation of differentiated capillaries (Sunderkotter, et al., 1994; Grossniklaus, et al., 2002).

1.3 *In vitro* and *in vivo* angiogenesis model for ocular neovascularization

Angiogenic and angiostatic activities can be assessed using both *in vitro* and *in vivo* assays. *In vivo* assays can better mimic the angiogenesis as it occurs in normal and pathologic states, while *in vitro* assays offer several critical advantages over their *in vivo* counterparts. For example, *in vitro* assays allow the identification of direct effects on endothelial cell function, allow the analysis of isolated processes that contribute to angiogenesis, allow the analysis of variables such as matrix components in isolation, and do not require the technical expertise in animal handling required for *in vivo* assays, and typically less expensive than *in vivo* assays, and may be adapted for large-scale screening (Goodwin et al., 2007). However, the critical tests for angiogenesis require a more holistic assessment, and several *in vivo* assays have been developed that permit a more realistic appraisal of the angiogenic response than that can be obtained *in vitro*. The use of animal models to assay angiogenesis is crucial to the search for therapeutic agents that inhibit angiogenesis in the clinical setting, and *in vivo* angiogenesis assays examine the entire spectrum of molecular and cellular processes. The eye provides a useful model system, because it contains several vascular beds sandwiched between avascular tissues. This allows for unequivocal identification and quantification of new vessels (Campochiaro et al., 2003).

1.3.1 *In vitro* scratch-wound HUVEC migration assay

Endothelial cell is the primary constituent of new vessel, and many endothelial

cell functions are required for angiogenesis, including cell migration, proliferation, and tube formation. Numerous techniques have been used to assess these functions in endothelial cells, In my study, I recruited a scratch wound assay to measure the endothelial cell growth and motility in response to angiogenesis stimulators. Cell motility is of particular interest in the design of anti-cancer therapeutics, as cell migration is required for both tumor invasion and tumor angiogenesis (Eccles et al., 2005).

In the scratch wound assay, endothelial cells are grown to confluence and a wound is introduced by clearing an area of the monolayer using a pipet tip, needle, or cell scraper. Cell filling of the cleared space initially occurs by growth and migration (Lampugnani et al., 1999). Since some growth factors stimulate both migration and proliferation, migration can be specifically addressed by adding anti-proliferative agents to the culture medium. Quantification can involve measuring the distance moved by the endothelial cells, the area covered by the endothelial cells, or the amount of cell immigrate into the wound area at specific time, and the amount of cells cover the clear area. This assay can be adapted for large-scale screening (Yarrow et al., 2004), and multiple time points can be assessed using the same wells. Disadvantages include the difficulty of creating scrapped areas of equal size and with even boundaries, variability between wells and experiments due to variations in degree of initial confluence, and difficulty of quantification.

1.3.2 MTT cell viability assay

The MTT (method of transcriptional and translational) assay is a standard colorimetric assay to measure the activity of mitochondria as a mean of assessing number of living cells. Active mitochondria convert the yellow substrate 3-(4,5-dimethylthiazol-2-yl)-2, 5-diphenyltetrazolium bromide (MTT) to formazan, a

purple product (Mosmann et al., 1983). This colorimetric change can be quantified using spectrophotometry and correlated with cell number (Denizot et al., 1986). The main advantages of the colorimetric assay are its rapid assay and precision, and the lack of any radioisotope. The MTT assay is suited to large-scale screening, and can be used to measure cellular cytotoxicity, proliferation or activation. It can also be used to determine cytotoxicity of potential medicinal agents and other toxic materials, since those agents would result in cell toxicity and metabolic dysfunction and therefore decreased performance in the assay.

1.3.3 *In vivo* chick chorioallantoic membrane (CAM) assay

The chick embryonic chorioallantoic membrane is an extraembryonic membrane mediating gas and nutrient exchange until hatching. Due to its dense capillary network, it has been commonly used *in vivo* to study both angiogenesis and anti-angiogenesis in response to normal tissue and cells, to tumor bioptic specimens and cells, or to soluble factors (Leene et al., 1973; Auerbach et al., 1974; Ribatti et al., 2000; Davison et al., 2003).

1.3.3.1 *Embryological origin and development of CAM*

The allantois is an extraembryonic membrane, derived from the mesoderm, in which primitive blood vessels begin to take shape on day 3 after fertilization.

On day 4, the allantois merges with the chorion epithelium, derived from the ectoderm, to form the chorioallantois. All CAM vessels have the appearance of undifferentiated capillaries. Their walls consist of a single layer of endothelial cells lacking a basal lamina (Funk et al., 1996).

Primitive vessels continue to proliferate and to differentiate into an arteriovenous system until day 8 post-fertilization, thus originating a network of capillaries that migrate to occupy an area beneath the chorion and mediate gas exchange with the outer environment. By day 8, the CAM displays small, thin-walled capillaries with a luminal diameter of 10–15 μm beneath the chorionic epithelium, and other vessels with a diameter of 10–15 μm in the mesodermal layer, whose walls have a layer of mesenchymal cells surrounding the endothelium and are completely wrapped by the basal lamina together with the endothelial cells (Funk et al., 1996). At this stage, the chick immunocompetent system is not fully developed and the condition for rejection has not been established (Auerbach et al., 1974). As other vertebrates, chick is protected by a dual immune system composed of B and T cells, controlling the antibody and cell-mediated immunity, respectively. The B cells are differentiated in the bursa of fabricius, the organ equivalent to the bone marrow in mammals, whereas T cells are differentiated in the thymus (Nguyen et al., 1994; Ribatti et al., 1996).

The allantoic vesicle enlarges very rapidly from day 4 to day 10 post-fertilization. In this process, the mesodermal layer of the allantois becomes fused with the adjacent mesodermal layer of the chorion to form CAM. A double layer of mesoderm is thus created: its chorionic component is somatic mesoderm and its allantoic component is splanchnic mesoderm. In this double layer, an extremely rich vascular network develops which is connected to embryonic circulation by the allantoic arteries and veins. Immature blood vessels (lacking the complete basal lamina and smooth muscle cells) scattered in the mesoderm grow very rapidly until day 8 and give rise to a capillary plexus, which comes to be intimately associated with the overlying chorionic epithelial cells and mediates gas exchange with the outer environment. Until day 10, the chick embryo immune system is not completely

developed (Nguyen et al., 1994; Ribatti et al., 1996).

In day 10–12, the capillaries resemble those in the 8-day membrane and are now close to the surface of chorionic epithelium. The mesodermal vessels are distinct arterioles and venules. In addition to the endothelium, the wall of arterioles (10–85 μm in diameter) contains one or two layers of mesenchymal cells and increased amount of connective tissue surrounding them. Venules (10–115 μm in diameter) are surrounded by an incomplete investment of mesenchymal cells, and connective tissue has also accumulated within their walls. The mesenchymal cells are presumed to be developing smooth muscle cells and the wall of CAM arterioles also develops a distinct adventitia containing fibroblast-like cells (Janse et al., 1991).

Rapid capillary proliferation goes on until day 11. Thereafter, the mitotic index declines just rapidly, and the vascular system attains its final arrangement on day 18, just before hatching (Janse et al., 1991). The presence of T cells can be first detected at day 11 and B cells at day 12 (Ausprunk et al., 1977). After day 15, the B cell repertoire begins to diversify and by day 18 the embryo becomes immunocompetent (Nguyen et al., 1994; Ribatti et al., 1996).

1.3.3.2 In ovo and ex ovo model of chick cam assay

The CAM assay is probably the most widely used *in vivo* assay for studying angiogenesis for almost half a century (Folkman et al., 1975; Ribatti et al., 1997). The test substance is prepared either in slow-release polymer pellets, absorbed by filter paper, gel, or gelatin sponges, or air-dried onto plastic discs. These carriers are then implanted onto the CAM through a window cut carefully in the eggshell. The lack of a mature, immune system in 7–8-day old chick embryo allows for the study of tumor-induced angiogenesis (Janse et al., 1991). The angiogenic effect can be measured by counting the number of blood vessels in a given area using a stereomicro-

scope. In this *in ovo* open window CAM model, embryo is left inside the egg shell during development and for the duration of assay, hence this preserves a physiological environment, maintain the normal development of embryo, and keep high embryo survival rate, easy to handle, and embryo can reach hatching. However, it limits the area for use and observation.

In a variation of CAM assay, shell-less embryo is cultured in petri dish prior to applying the test substance (Folkman et al., 1975; Janse et al., 1991). This model also named as *ex ovo* CAM assay. This allows the quantification of blood vessels over a wider area of CAM. Because the entire membrane can be seen, rather than a small portion through the shell window, multiple grafts can be placed on each CAM and photographs can be taken to document vascular changes over time. This method however accompanies with low embryo survival rate, embryos cannot reach hatching, and do not reflect physiological conditions (Ribatti et al., 2000).

1.3.3.3 Advantages and limitations of Chick CAM assay

As pointed out by Auerbach et al., “perhaps the most consistent limitation to progress in angiogenesis research has been the availability of simple, reliable, reproducible, quantitative assays of the angiogenesis response” (Staton et al., 2004). *In vivo* angiogenesis assays have allowed important progress in elucidating the mechanism of action of several angiogenic factors and inhibitors (Taylor et al., 1984). Ideally, assays of angiogenesis should be easy, reproducible, quantitative, cost-effective, and permit rapid analysis.

The main advantages of *in vivo* chick CAM assay are their low cost, simplicity, reproducibility, reliability and suitable for large-scale screening. Among them, the more valuable features of CAM assay are the relative ease of carrying out the assays,

the ready availability of experimental material, and for the explants method, the feasibility of carrying out multiple tests on individual CAMs as well as of monitoring the reaction throughout the course of the assay.

On the contrary, there are only very few restrictions to use CAM, essentially due to (a) nonspecific inflammatory reactions that may develop with an attending secondary stimulation of angiogenesis; (b) preexisting vessels may be present, which make it hard to distinguish the extent of angiogenesis and anti-angiogenesis. In view of these limitations, two different assays should ideally be performed in parallel to confirm the angiogenic or anti-angiogenic activity of test substances and (c) timing of CAM angiogenic response is essential. Many studies determine angiogenesis after 24 hours, when there is no angiogenesis but vasodilation. Measurement of vessel density is to measure visible vessel density, and vasodilation and neovascularization are not readily distinguishable. This drawback can be overcome by using sequential photography to document new vessel formation.

1.3.4 *In vivo* corneal neovascularization assay

Corneal neovascularization assay is still considered as one of the best *in vivo* assays, in as much as the cornea itself is avascular. Thus, any vessels seen in the cornea after stimulation by angiogenesis-inducing tissues or factors are new vessels. The original method was developed for rabbit eyes (Gimbrone et al., 1974), but has been adapted to rats and mice (Fett et al., 1985; Shing et al., 1985), now the most frequently used test animal.

Models of anterior segment neovascularization include the corneal micropocket assay, used to study the influence of specific molecules/proteins in angiogenesis, and corneal chemical and suture-induced injury, which mimic more closely the complex

nature of the human disease.

Briefly, in corneal micropocket assay, a 'pocket' is created in the corneal stroma of an experimental animal (originally rabbits, but is adapted for rats and mice). Angiogenic response can then be initiated by implantation of low-release pellet or polymer containing the angiogenic substance (Silverman et al., 1988; Auerbach et al., 2003).

Also, corneal neovascularization is associated with inflammatory disruption of an exquisitely balanced corneal immune system. Two methods of producing corneal neovascularization in laboratory animals, namely silver nitrate cauterization and suturing, are applied extensively nowadays. Applying silver nitrate solution to central corneal surface with an applicator stick has been proved as an easy and efficient method to stimulate corneal NV sprouting from the limbus vasculature, and can be performed to large amount of animals (Muthukkaruppan et al., 1979; Hartwell et al., 1998). Corneal NV starts on the second day after cauterization, and reach the peak at day 14, while it is occasionally followed by acute inflammation, hypopyon, hyphema, and frequent corneal edema. The other efficient method to induce inflammatory corneal NV is to place three 11-0 sutures intrastromally with 2 stromal incursions, each extending over 120° of corneal circumference. Corneal NV starts to form on 2nd day post-operation, and also reach the peak at day 14. This method demands stringent surgical technique, long training time, labor and time intensive (Mahoney et al., 1985; Presta et al., 1999).

In the last 30 years, the corneal angiogenesis assay has provided insight in various fields of angiogenic research. It is used to study angiogenic agents *in vivo* including angiogenin (Wenk et al., 2003; Bock et al., 2007), chondrosarcoma-derived growth factor, adipose tissue (Phillips et al., 1994; Samolov et al., 2010) and vascular

endothelial growth factor VEGF-A, VEGF-C, and -D (Cao et al., 1998; Marconcini et al., 1999). It is a reliable tool for the investigation of angiogenesis inhibitors, such as protamine, angiostatin, interleukin 12, PEDF, thalidomide and AGM-1470 (Taylor et al., 1982; D'Amato et al., 1994; O'Reilly et al., 1994; Voest et al., 1995; Kenyon et al., 1997; Dawson et al., 1999; Edelman, 2000). The cornea model is also recruited to study mechanisms of angiogenesis and anti-angiogenesis (Ingber et al., 1990; Kusaka et al., 1991; Rohan et al., 2000). Recently, the assay helps to provide an insight into the potential role of platelets for angiogenesis *in vivo* (Kisucka et al., 2006). It is also suggested that cornea is an additional model to identify angiogenic and lymphangiogenic inhibitors (Auerbach et al., 2000; Folkman et al., 2004; Bock et al., 2008).

These assays are reliable, but compared to the *in vitro* assay and chick CAM assay, are more expensive and technically demanding, making them impractical for large-scale screening. Furthermore, although the use of rats and mice make the assay cheaper and increased number of tests can be performed, the surgery becomes more difficult as eye size decreases. Finally, scientists face ethical problem when using an assay that involves a major sensory organ (Carolyn et al., 2004).

1.3.5 *In vivo* laser-induced choroidal neovascularization assay

Until now, there is no suitable animal model for AMD research, however the laser-induced choroidal model can be used to study CNV. In neovascular AMD, which accounts for approximately 80% of severe vision loss, subretinal vessels originating from the choroid develop beneath the retina. The mouse model of laser-induced CNV is well characterized and, in the absence of models which perfectly recapitulate the various aspects of AMD, has been used extensively to study the role of individual angiogenic factors as well as the effect of anti-angiogenic agents or

other therapeutic agents/techniques on CNV (Rakoczy et al., 2006). This model generally utilizes laser photocoagulation to induce break(s) in the Bruch's membrane, a physical barrier that normally mediates separation of the choroidal vasculature from RPE and neural retina. Inflammation, growth factor up-regulation and/or the physical disruption of this barrier results in CNV that can be followed and studied to identify important neovascular factors, or assess various angiostatics (Rakoczy et al., 2004).

1.4 Natural products and potential anti-angiogenic effects

1.4.1 Introduction

Herbs or natural plants have been applied as effective therapeutic agents for more than 5000 years, and is becoming more and more popular nowadays because of its natural origin and inherent safety. It has been estimated that more than 12% of adults in western countries used herbal medicine in 1997 (Sengupta et al., 2004), and herbal medicine plays a major role in the eastern world (Foster et al., 2004). Approximately 25% of the modern medications are developed from plants. They contain many active ingredients with medicinal properties that modern pharmaceuticals cannot reproduce. A wide range of plants contains compounds with angiogenesis-modulating properties, some of them (e.g. Taxol, camptothecin and combretastatin) are antiangiogenic. However, the exact mechanism and preparation involved are still unexplainable. This makes part of the herbal molecules an inexplicable issue in modern medicine world and drug development. The rationale for combining conventional agents and modern biotechnological approaches to the delivery of herbal medicine is an avenue set to revolutionize the future practice of cancer and anti-angiogenic medicine. Further exploitation on the composition, drug efficacy, biological mechanism of single and multiple compounds, safety issue through in vitro or animal studies as well as patient identity warrants a better understanding of this mysterious medicinal approach, and this may well bring on a new dawn of therapeutic strategies where East truly meets West.

1.4.2 Criteria of selecting herbal molecule to study its potent angiostatic character

- (1) it is extracted from a herbal source;
- (2) it has a defined molecular structure;
- (3) it is small-sized and simple in nature;
- (4) it was previously reported to block endothelial cell migration, tube formation or developmental angiogenesis by chick chorioamniotic membrane;
- (5) it was reported to suppress tumorigenesis of various types of cancer in cell or animal models.

1.4.3 Isoliquiritigenin (ISL)

ISL, isoliquiritigenin with molecular formula $C_{15}H_{12}O_4$, isolated from licorice (*Glycyrrhiza uralensis*) (Figure 3), belongs to the family of favoid (Figure 2). It possesses actions against inflammation (Kumar et al., 2007), oxidative stress (Haraguchi et al., 1998), carcinogenesis (Maggiolini et al., 2002; Li et al., 2004) and platelet aggregation (Tawata et al., 1992) as well as inhibition to aldose reductase (Aida et al., 1990). Its anti-carcinogenic activity is mediated by cell cycle arrest, induction of apoptosis (Hsu et al., 2005; Park et al., 2009) and suppression of lipoxygenase (Yamamoto et al., 1991). Its angiostatic effect is the strongest among various licorice-extracted chemicals (Kobayashi et al., 1995). It has been shown to block JNK- or p38/MAPK-responsive pathways to suppress matrix metalloproteinases and increase the level of tissue inhibitor of matrix metalloproteinases (Kwon et al., 2008; Kang et al., 2009).

1.4.4 Epigallocatechin gallate (EGCG)

EGCG (epigallocatechin gallate, molecular formula $C_{22}H_{18}O_{11}$) (**Figure 18**) is one of the polyphenols found in green tea (leaves of *Camellia sinensis*) (**Figure 19**). Green tea consumption has been shown to protect human from the occurrence or progression of cancers in the skin, breast, prostate, lung, colon, liver, stomach and so on (Mukhtar et al., 2000). It possesses anti-oxidative, anti-inflammatory, anti-arteriosclerotic and anti-bacterial activities (Crespy et al., 2004; Cooper et al., 2005). Its angiostatic potential was suggested by its suppression on blood vessel formation and development in chick chorioallantoic membrane model (Oak et al., 2005). When green tea extract was given in drinking water, corneal neovascularization was significantly attenuated in mice (Cao et al., 2007) whereas oxygen-induced retinal neovascularization was suppressed in rats (Saito et al., 2007). Its biological action was hypothesized to mediate through a reduced complex formation between VEGF receptor 2, VE-cadherin and phosphoinositol-3-kinase, which is critical for endothelial cell migration and vessel formation (Lai et al., 2004; Zhang et al., 2009). Activation of certain transcription factors, such as AP-1, NF- κ B and Ets-1 is also blunted (Park et al., 2003; Yamakawa et al., 2004) and the production of metalloproteinases necessary for endothelial cell migration and invasion is attenuated (Oku et al., 2003; Fassina et al., 2004). Finally, EGCG can also inhibit the production of VEGF, bFGF and IL-8 (Sartippour et al., 2002; Trompezinski et al., 2003; Sartippour et al., 2004).

1.4.5 Resveratrol (Rst)

Rst, (trans-3,5,4'-trihydroxystilbene) with molecular formula $C_{14}H_{12}O_3$ (**Figure 33**), is a phytoalexin commonly found in various plantations, including grapes, pea-

nuts, pines and berries (**Figure 34**). It suppressed proliferation of lymphoid and myeloid cancers, cancers of the breast, prostate, stomach, colon, pancreas, and thyroid; melanoma; head and neck squamous cell carcinoma; ovarian carcinoma; and cervical carcinoma (Aggarwal et al., 2004). From botanical studies, it acts as a stress protein responsive to exposure to ozone, heavy metals, change of climate, infection by pathogens and so on (Delmas et al., 2003). In animal study, it is reported with potent chemoprevention to cancers, due to its anti-oxidant and pro-apoptotic activities (Huang et al., 1999; Athar et al., 2007). Its angiostatic potential was revealed in lung cancer and rat gliomas models (Kimura et al., 2001; Tseng et al., 2004). Molecular mechanisms of inhibition of tumor cell proliferation have been partly elucidated and involve suppression of several transcription factors, such as NF- κ B, AP-1 and Egr-1, down-regulation of the expression of anti-apoptotic genes and activation of caspases (Aggarwal et al., 2004). As far as angiogenesis is concerned, Rst has been shown to downregulate the production of several angiogenic cytokines, including VEGF, interleukin-8 (IL-8) and FAK (Cao et al., 2002).

CHAPTER 2

OBJECTIVES AND STUDY DESIGN

The main objective of the work described in this thesis was to investigate the anti-angiogenic properties of three herbal molecules: isoliquiritigenin (ISL) epigallocatechin (EGCG) and resveratrol (Rst) by both *in vitro* and *in vivo* studies.

Study design:

Part I: *In vitro* studies:

1. A first-line examination of cell cytotoxicity by MTT assay on retinal pigment cell line ARPE-19 will be performed to identify the sub-toxic levels of herbal chemicals directly applied to cells.

2. A time-course analysis using a scratch-wound model of human umbilical vein endothelial cell line HUVEC will be used to examine if the herbal chemicals applied at sub-toxic levels suppress the endothelial cell growth and migration.

3. Cells will be collected for the expression analysis of various intracellular signaling pathways, including intracellular level of VEGF, PEDF, Akt activation, focal adhesion kinase activation and metalloproteinases.

Part II: *In vivo* studies:

1. We plan to use the *in vivo* chick chorioallantoic membrane model to test the efficacy of herbal molecules on the regulation of developmental angiogenesis. Gelatin sponge of standard size soaked with a fixed amount of the tested herbal compound will be applied on the chorioallantoic membrane *in vivo* under an open-window manner. At subsequent days, the number of blood vessels converging to sponges will be quantified and analyzed.

2. We shall established animal models of ocular neovascularization to investigate the effect of herbal molecules on the pathological angiogenesis associated with different eye disease: corneal neovascularization and choroidal neovascularization.

(1) The optimal manifestation of corneal neovascularization in BALB/c mice will be explored between 7 to 14 days after central 2-mm corneal epithelial removal in addition to silver nitrate cauterization. Topical treatment by the herbal compounds at different doses will be performed after injury to assess whether the progression of neovascularization would be alleviated. The neovascularization will be examined by immunohistochemistry using anti-CD31 antibody (specific to vascular endothelial cells) and quantified for analysis.

(2) We shall work on establishment of choroidal neovascularization in C57BL/6 mice model. In our model setting, we plan to apply three 532 nm diode laser spots (100 mW power, 100 msec duration, 100 μ m spot size; multi-laser length laser) to the fundus through a slit lamp delivery system of a photocoagulator. Intravitreal injection of the herbal molecules at different doses will be administered immediately after laser photocoagulation. The resultant effects on the progression of choroidal neovascularization will be examined by fundus fluorescence angiography at post-treatment days 4, 7 and 10, or other appropriate periods. The neovascular area will be examined by choroidal flatmount followed by immunohistochemistry for *Griffonia simplifonia* isolectin B4 antibody on day 10.

CHAPTER 3

GENERAL MATERIALS & METHODS

3.1 Materials

3.1.1 Herbal chemicals and angiogenesis controls

Isoliquiritigenin (ISL; 4,2',4'-trihydroxychalcone, or (E)-1-(2,4-dihydroxyphenyl)-3-(4-hydroxyphenyl)-2-propen-1-one; $C_{15}H_{12}O_4$; CAS number: 961-29-5) was purchased from Tauto Biotech. (Shanghai, China). Epigallocatechin gallate (EGCG; (2R,3R)-2-(3,4,5-trihydroxyphenyl)-3,4-dihydro-1(2H)-benzopyran-3,5,7-triol,3-(3,4,5-trihydroxybenzoate; $C_{22}H_{18}O_{11}$; CAS number: 989-51-5), resveratrol (Rst; 3,4',5-trihydroxy-trans-stilbene or 5-[(1E)-2-(4-hydroxyphenyl) ethenyl]-1,3-benzenediol; $C_{14}H_{12}O_3$; CAS number: 501-36-0). Avastin was from Roche (Basel, Switzerland). PP2 (selective inhibitor of src-family tyrosine kinases) was from Sigma-Aldrich Co. Recombinant human vascular endothelial growth factor-165 (VEGF) was from Invitrogen (Carlsbad, CA, US).

3.1.2 Antibodies

Monoclonal anti-mouse glyceraldehyde phosphate dehydrogenase (GAPDH)-horseradish peroxidase (HRP) conjugate was purchased from Sigma-Aldrich Co. (St Louis, MI, US). Monoclonal antibody against human pigment epithelium growth factor (PEDF), PECAM-1 (clone MEC13.3) was from Santa Cruz

Biotech (Santa Cruz, CA, US). Polyclonal antibody against human phospho-FAK (Y576/577) was from Cell Signaling (Danvers, MA, US) and antibody against human FAK from Millipore (Billerica, MA, US). Isolectin-B4 (ALX-650-001F-MC05) was from Enzo Life Sciences International, Inc.

3.1.3 Chemicals for cell culture

Culture media, antibiotics, trypsin (1:250), phosphate buffered saline (PBS), 3-(4,5-dimethylthiazol-2-yl)-2,5-diphenyltetrazolium bromide (MTT), and heat-inactivated fetal bovine serum (FBS) were from Invitrogen (Carlsbad, CA, US). Endothelial cell growth medium was from PromoCell GmbH (Heidelberg, Germany). Dimethylsulfoxide (DMSO), gelatin, isopropanol were from Sigma-Aldrich Co.

3.1.4 Miscellaneous chemicals

PhosSTOP, and protease inhibitor cocktail were obtained from Roche (Basel, Switzerland) and enhanced chemiluminescence from Amersham (Bucks, UK). Silver nitrate was from Sigma-Aldrich, Inc. Potassium nitrate was from Riedel Inc. Pentobarbital sodium (20% Dorminal), 2% xylazine and 10% ketamine were from Alfasan Inc, Netherland. Bouin's Fixative was made with a formula of saturated picric acid 3000 ml, formaldehyde 1000 ml, glacial acetic acid 200 ml.

3.2 Methods

3.2.1 *In vitro* cell viability assay

Human retinal pigment epithelial ARPE19 cell line (CRL-2302, American Type

Culture Collection, Rockville, MD, US) was maintained in DMEM/F12 medium supplemented with 10% FBS and antibiotics (100 U/ml penicillin G and 100 µg/ml streptomycin sulfate). They were seeded at a density of 7×10^3 cells for an overnight and were treated with drug (ISL: 5-50 µM, EGCG: 10-100 µM, Rst: 2.5-50 µM) in medium containing 2% FBS for up to 7 days. The reference concentration range of drug was acquired from literatures (see Discussion). Control cells were kept in medium with 0.1% DMSO. Fresh medium were replenished every 2 days. At time of MTT assay, cells were washed and incubated in MTT solution (5 mg/ml) for 3 hours at 37°C. After washes, isopropanol (300 µl) was added to resolve the purple/blue formazan crystals and was quantified using an ELISA plate reader (PowerWave microplate spectrophotometers, BioTek Instruments Inc., Winooski, VT, US) at emission wavelength of 570 nm. Isopropanol was used as the blank control. Four samples were assayed as each measurement and background-subtracted optical density values were normalized with that of drug-free control and expressed as the viability percentages. The data were analyzed by paired Student's *t-test* and $P < 0.05$ was regarded as statistically significant.

3.2.2 *In vitro* angiogenesis assay

3.2.2.1 *Cell culture*

Human umbilical vein endothelial cell line HUVEC (CRL-2873, American Type Culture Collection) was propagated in complete endothelial cell growth medium with 10% FBS and antibiotics on gelatin-coated surface.

3.2.2.2 Scratch wound HUVEC growth and migration assay

HUVEC grown to confluence on gelatin-coated surface were starved in medium with 0.5% FBS for 6 hours. A scraping tool (1 mm by width) removed a portion of cell monolayer to provide a margin of denuded area. The dislodged cells were removed and drug-added medium in the presence or not with VEGF165 (20 ng/ml) was added. Cells without drug or with Avastin (312 µg/ml) or PP2 (src kinase inhibitor, 10 nM) were controls. The cells in denuded area were monitored at different time points by phase-contrast microscopy using a 5x objective. With Photoshop version CS3, images of the same area at different time points were aligned and cells were quantified and expressed as number of cells per mm² area. Six images were captured for each treatment. The mean density of cells was calculated and compared by time. We used paired Student's t-test to compare two small sets of quantitative data when data in each sample set are organized in pairs. The result was analyzed by paired Student's *t-test* and $P < 0.05$ was statistically significant.

3.2.2.3 Western blot analysis

Cells were lysed in RIPA (radioimmunoprecipitated assay) buffer containing 50 mM Tris-HCl (Sigma), 150 mM sodium chloride, 1% Nonidet P-40 (Sigma), 0.25% sodium deoxycholate (Sigma), and freshly added with PhosSTOP (Roche), protease inhibitor cocktail (CompleteTM, Roche) and 1 mM PMSF on ice for 30 minutes. Lysates were spun at 10,000 g for 30 minutes at 4°C and clear supernatant was collected and denatured in sample buffer with a final concentration of 50 mM Tris HCl (pH 6.8), 2% sodium dodecylsulfate (SDS, BioRad, Hercules, CA), 10% glycerol, 0.002% bromophenol blue, 1% 2-mercaptoethanol, and 50 mM DL-dithiothreitol (DTT, Sigma) and denatured at 95°C for 5 minutes. All protein samples were stored

at -20 °C until Western blot analysis.

The protein samples were analyzed by 10% SDS-polyacrylamide gel electrophoresis (PAGE). Gel and buffer were prepared according to different concentrations of gel. Briefly, for 10% resolving gel, reagents including 6.7 ml 30% acrylamide/Bis solution (29:1, BioRad), 5 ml 4x Tris.HCl/SDS (pH 8.8), 100 µl ammonium persulphate, 20 µl TEMED (AMRESCO) and 8.2 ml distilled water, were mixed and poured to the glass plate sandwich, with distilled water added on top of the gel to prevent evaporation during gel polymerization. Stacking gel solution with 4% acrylamide was prepared by mixing 1.33 ml 30% acrylamide/Bis solution (29:1, BioRad), 2.5 ml 4x Tris.HCl/SDS (pH 6.8), 50 µl 10% ammonium persulphate, 10 µl TEMED and 6.05 ml distilled water, and was added on the top of the resolving gel and a comb with 10 or 15-well was inserted and gel was left to polymerize. After gel polymerization, the wells were rinsed with distilled water and connected to the proper gel setup. Samples equivalent to 7.5×10^4 cells were loaded to each well. Five µl size standard marker (Precision plus proteinTM dual color standards, BioRad) was applied to indicate protein sizes after separation. The electrophoresis was started with a constant 70 voltage (V) for 30 minutes for sample concentration followed by a constant 150 V for 1 hour for protein separation. After gel running, the resolved proteins were immobilized onto the nitrocellulose membrane (BioRad) by blotting at a constant 100 V for 60 to 90 minutes in ice cold transfer buffer (192 mM glycine, 25 mM Tris.base, pH 8.3). After blotting, the membrane was washed in distilled water, then TBST (20 mM Tris-HCl pH 7.4, 150 mM NaCl, and 0.05% Tween 20) for 5 minutes, followed by blocking in 5% skimmed milk in TBST for 1 hour at room temperature.

After blocking, the membrane was incubated with primary antibodies at appropriate dilution (with reference to manufacturer's instruction or after optimization) in

TBS with 0.05% Tween 20 (Sigma) (TBST) for overnight at 4°C. After TBST washes, the membrane was incubated in appropriate HRP-conjugated Ig secondary antibodies (at concentration suggested by manufacturer) in TBST for 1 hr at room temperature. After TBST washes, the staining signal was revealed by enhanced chemiluminescence (ECL, GE Healthcare) using a ChemiDoc™ System (BioRad) (following manufacturer's instruction). Gel imaging and band densitometry was obtained and measured by Quantity One 4.6.2 (BioRad). Except for those specified, all reagents were purchased from Sigma.

3.2.3 *In vivo* angiogenesis assay

One major task of my PhD work was to establish *in vivo* angiogenesis models. This was critical to assess if the selected herbal chemicals contain potential therapeutic effect for anti-angiogenesis. Before my program, no angiogenesis model was established or available in my department. The technical challenges in this work are whether the model setup and outcome reveal the appropriate pathophysiological features of neovascularization development in diseases, whether the setup was effective to develop pathological features in a rather short period of time, rather than a life-long phenotype progression in human, whether the assay was reproducible with consistent and reliable data collection and analysis, as well as whether the assay can be feasibly monitored and handled by other investigators after my graduation. Besides, the assay should be at low cost and financially feasible. The identification, establishment and application of appropriate and practicable models are thus crucial for the exploitation of potential anti-angiogenesis molecules and study their pharmacokinetics.

3.2.3.1 Chick chorioallantoic membrane assay

Source of fertilized eggs Jia Mei fertilized chicken eggs were obtained at day 1 post-laying from Kang Li Farm (Hong Kong) and transferred to the laboratory under clean condition. The egg surface was cleaned immediately with sterilized distilled water and the eggs were put in an sterilized incubator at 37°C for egg development.

Materials and reagents 70% (vol/vol) ethanol in distilled water, sterilized gelatin sponge (Spongostan Standard, Ferrosan A/S, Denmark), Bouin's fixative, recombinant human VEGF165, polyclonal anti-VEGF antibody, Avastin and herbal chemicals were used in the present study.

Choice of polymer for drug application CAM is a growing and developing structure, and it is subject to modification by environmental factors, such as oxygen tension and pH, which could significantly influence the CAM response to stimuli. Also, non-specific inflammatory reactions may occur in the CAM after implantation, which might induce a secondary vasoproliferative response. This non-specific inflammatory response may not be frequent, in particular when the implant is placed at early stages when CAM is developing and the host's immune system is still immature. The reasons why the gelatin sponge was selected for drug application in this study are its immuno-tolerance and low inflammatory induction as well as its high retention of drug and slow releasing characteristics. Alternatives, like filter paper and collagen gel, do not have good biocompatibility to chick CAM tissue. Filter paper is a hard material when compared to the soft nature of polymer sponge and it could induce non-specific inflammatory response, damage vessels and membrane and cause inappropriate leakage, resulting in uncontrollable situations. Collagen gel, due to its high water content and evaporation during 37°C incubation giving rise to inconsis-

tent drug concentration and drug release, may skew the result of drug effect on the CAM vessel development.

Establishment of Chick CAM assay The fertilized hen eggs were incubated at 37°C under 60–70% relative humidity in a clean incubator. In my study, two methods for chick embryo culture were developed. “*In ovo*” or “open-window” method with the embryo development inside the egg shell during treatment and assay period. This model has the advantage of good embryo survival rate, easy to perform, embryo development under a close-to-normal physiological environment (within egg shell), a maintained endogenous calcium level for angiogenic and skeletal development. Such favorable conditions can allow the embryo to reach hatching, even a small window has been opened on the shell. However, the restricted sampling area is the major limitation of this model. The implant can only be placed within the open-window region. And upon embryo growth and enlargement, the implants usually float away from the examination assessable area and observers might have the difficulty to locate the implant after 2-3 days “*in ovo*” development. The other is the “*ex ovo*” method, of which the embryos are cultivated in a shell-less environment. This method can allow a large CAM area available for treatment and examination. Observers can directly visualize the entire chick CAM and able to test different samples in a single embryo so that inter-embryo difference can be minimized or avoided. Easy grafting and monitoring of excised tissues can help the operator to enhance the treatment method. The limitations of this method are the low embryo survival rates as the embryo develops in a totally different condition as that inside the egg. Different gaseous exchange and pH maintenance, evaporation, waste accumulation and so on negatively affect normal embryo development. The embryos will be able to reach hatching. In addition, high risk of inflammation is accompanied with breaking the egg shell and

transferring of embryo to plastic dish. As a whole, *in ovo* model should be easy for beginners to setup their experiments for preliminary study.

In the “*in ovo*” model, there are several important time-points in chick embryo development that are critical for the success of establishing chick CAM angiogenesis assay.

- (1) At day 3 post-fertilization, primitive blood vessels begin to take shape.
- (2) At day 4, the allantois fuses with the chorion and forms the chorioallantois.
- (3) Until day 8, primitive vessels continue to proliferate and to differentiate into an arteriovenous system and originate a network of capillaries.

- (4) The CAM vessels grow rapidly until day 11, afterwards, the endothelial mitotic index decreases.

- (5) At day 18, the vasculature system reaches its final pattern and becomes fully developed .

- (6) At day 21, the chick fetus hatches.

In view of these critical time-points of chick embryo development, the procedure of “open-window” CAM angiogenesis model is adjusted as:

- (1) At day 1 post-fertilization, eggs were transferred to the laboratory. The egg surface was cleaned with 95% ethanol before putting to 37°C incubation with 60–70% relative humidity.

- (2) At day 4, a window of 1.5x2 cm in dimension was made on the egg shell. The opening was sealed with a piece of sterilized parafilm. The egg was then put back to 37°C incubation for another 3 days. This incubation step was to screen out eggs that are prone to immune response upon laboratory manipulation.

- (3) At day 8, a piece of sterilized gelatin sponge (cut to 1 mm³ in size) soaked with drugs to be tested (at appropriate concentration) was implanted on the CAM. In

my experiment, a volume of 3 μ l of drug or vehicle solution was added to each gelatin sponge before implantation.

(4) The placement of gelatin sponge was recorded by photographs taken under stereomicroscopy (Wild MZ8 microscope; Leica, Wetzlar, Germany) equipped with a digital camera and imaging system (Leica EC3, Wetzlar, Germany). The number of blood vessels staying along the edge of gelatin sponge was noted.

(5) At day 9 (24 hours after implantation), the implant images were captured by under stereomicroscopy. The number of blood vessels staying along the edge of gelatin sponge was noted.

(6) Similar imaging procedure can be performed at day 10 (48 hours after implantation)

(7) The difference of number of CAM vessels converging towards the gelatin sponge was calculated. For example, the number of vessel changes upon 24-hour drug treatment was represented as number of vessel converging on the gelatin sponge at day 9 minus that at day 8. CAM vessel index was expressed as the vessel number difference compared to vessel number of 0-hour interval.

Statistical analysis For the experiment of each drug concentration, a minimum of 10 eggs and duplicated experiments were performed. All data were calculated for mean and standard deviation. Statistical significance between control and treatment groups was determined by ANOVA analysis with SPSS version 10. The minimal level of significance was $P < 0.05$.

Drug preparation and treatment Isoliquiritigenin (ISL; $C_{15}H_{12}O_4$; CAS number: 961-29-5) was purchased from Tauto Biotech. (Shanghai, China). Epigallocatechin gallate (EGCG; $C_{22}H_{18}O_{11}$; CAS number: 989-51-5), resveratrol (Rst; $C_{14}H_{12}O_3$; CAS number: 501-36-0) were purchased from Sigma-Aldrich Co. (St

Louis, MI, US). 99% by TLC/high performance liquid chromatography. Stock solution (50 mM) of ISL, EGCG and Rst were prepared in DMSO, stored at -20°C, and then diluted to appropriate working concentrations.

3.2.3.2 Silver nitrate cauterization-induced corneal neovascularization assay

Animals and anesthesia Female BALB/c mice (aged at 6–8 weeks) with 18 to 20 gm body weight were used. Experiments were approved by the Animal Care and Use Committee of The Chinese University of Hong Kong, and were conducted in accordance with the ARVO Statement for the Use of Animals in Ophthalmic and Vision.

Induction of corneal angiogenesis The identification of an appropriate and practicable corneal NV model is crucial for a valid exploitation of potential anti-angiogenesis molecules and study of their pharmacokinetics.

(1) **Literature search and assessment of available corneal neovascularization models (Table 1).**

(2) **Selection of corneal neovascularization model to be used in our laboratory.**

The major criteria of selection are the practicability, economy and demand of skill, setup and technical transfer as well as data analysis and interpretation. The technical challenges include whether the model shows a appropriate pathophysiological features of neovascularization development in corneal diseases, whether the setup is effective to develop pathological features in a rather short period of time, rather than a life-long phenotype progression in human whether the assay, whether the assay is reproducible with consistent and reliable data collection and analysis, as

well as whether the assay can be feasibly monitored and handled by other investigators after my graduation. Besides, the assay should be at low cost and financially feasible. The identification, establishment and application of appropriate and practicable models are thus crucial for the exploitation of potential anti-angiogenesis molecules and study their pharmacokinetics.

(a) Silver nitrate cauterization induced corneal neovascularization

Chemical induction of corneal NV by silver nitrate cauterization was described previously (Mahoney et al., 1985), and with some modifications (Cursiefen et al., 2006). After the removal of central 2 mm (in diameter) corneal epithelium, a solution of 75% silver nitrate /25% potassium nitrate was applied by an applicator (with a diameter of 2 mm) on the central corneas region for 8 seconds, followed by extensive rinsing with sterile BSS. Since the force and duration of application affects the extent of damages and neovascularization, one designated operator for the procedure of cauterization is necessary and an assistant is required to perform an extensive rinsing of eye surfaces immediately after the chemical damage.

(b) Suture-induced inflammatory corneal neovascularization assay

The protocol was adopted from that described previously (Streilein et al, 1996; Cursiefen et al., 2004) with modifications. In brief three 11-0 nylon sutures were placed intrastromally with two stromal incursions extending over 120° of corneal circumference each. The outer point of suture placement was chosen at 1 mm close to the limbus, and the inner suture point was about 1 mm near to the corneal center equidistant from the limbus. This setting could obtain standardized angiogenic responses. Sutures were left in place for the duration of the experiment.

To look for a suitable method of corneal NV induction, I have conducted 4 kinds of injury settings and compared the damage outcome. They were (1) central 2

mm de-epithelization and silver nitrate cauterization, (2) total corneal de-epithelization and silver nitrate cauterization, (3) central 2 mm de-epithelization and suturing, and (4) total corneal de-epithelization and suturing.

We compared the two methods that induce inflammatory corneal neovascularization on BALB/C mice: silver nitrate cauterization (Mahoney et al., 1985) versus suture-induced corneal neovascularization (Streilein et al., 1996; Cursiefen et al., 2004) method on corneas with or without central 2-mm corneal de-epithelization and total corneal de-epithelization (Cursiefen et al., 2006).

In each group of 5 BALB/C mice, after anesthetization with intraperitoneal 75 mg/kg ketamine and 7.5 mg/kg xylazine, the right eyes received the damages at day 0.

At day 4 after injury, suturing and silver nitrate cauterization on corneas with central 2-mm de-epithelization had pronounced corneal angiogenesis. Morphometric analysis of the vascularized area within the boundary of limbal vasculature showed a significant increase of new blood vessel coverage on corneas after the combined treatments than with suturing alone ($P<0.01$) or with silver nitrate cauterization alone ($P<0.01$). Suturing on de-epithelized cornea had greater NV area ratio than that with intact epithelium ($P<0.01$). Suture-induced corneal neovascularization combined with total corneal de-epithelization had severe corneal reaction and with frequent corneal edema and inflammation. At the same time, silver nitrate cauterization with total corneal de-epithelization resulted in higher rate of corneal ulcer and inflammation.

This preliminary work illustrated that the removal of intact corneal epithelium is a crucial determinant for the success of inducing inflammatory corneal neovascularization. For a first start of corneal angiogenesis protocol, silver nitrate cauterization

combined with central 2-mm corneal de-epithelization should be an appropriate model to be selected. Also, this kind of damages is feasible and can be performed on a large number of animals.

Drug preparation and treatment Isoliquiritigenin (ISL; $C_{15}H_{12}O_4$; CAS number: 961-29-5) was purchased from Tauto Biotech. (Shanghai, China). Epigallocatechin gallate (EGCG; $C_{22}H_{18}O_{11}$; CAS number: 989-51-5), resveratrol (Rst; $C_{14}H_{12}O_3$; CAS number: 501-36-0) were purchased from Sigma-Aldrich Co. (St Louis, MI, US). A 50 mM solution of ISL, EGCG and Rst were prepared in DMSO, stored at -20°C , and then diluted to appropriate working concentrations.

Experimental groups and controls Herbal chemicals of appropriate eyedrop concentrations were freshly prepared by diluting the stock solution with sterile BSS. Topical BSS only served as the control. Following damages, the mice were randomly assigned to different groups, with 10 mice in each group. Application of eyedrop was initiated immediately after damage four times daily for a total of 14 days.

In situ photo-taking and mice killing After 7 or 14 days of topical treatment, the mice cornea was photographed under a stereomicroscopy (Wild MZ8 microscope; Leica) equipped with a DCC digital camera and imaging system (Leica). At day 7 and 14, five mice in each group were sacrificed with intraperitoneal overdosed sodium pentobarbital. The eyes were enucleated with special attention of not causing corneal damage.

Corneal wholemount and immunofluorescence Excised corneas were rinsed in PBS and fixed in ice-cold acetone for 30 minutes on ice. After PBS washes for three times, the corneas were blocked with 2% bovine serum albumin (BSA) in PBS for 2 hours, they were incubated in FITC-conjugated rat anti-mouse PECAM antibody (1:50; MEC13.3, Santa Cruz Biotech.) overnight at 4°C . After PBS washes,

all corneas were mounted on glass slides (HistoBond, Paul Marienfeld GmbH & Co., Germany) with epithelial side facing up and covered with GB fluorescence mounting medium, and stored at 4°C in dark.

Vessel examination and quantification analysis Immunostaining results were analyzed with a fluorescence microscope (DMRB microscope; Leica) equipped with a color imaging system (Spot RT, Diagnostic Instruments). Images were captured with a 20x objective. A corneal montage was assembled using Photoshop CS3 version.

Vessel area analysis From the montage image, the corneal NV area revealed by PECAM immunoreactivity was measured using Image J software (National Institutes of Health IMAGE). The NV percentage was calculated by NV area over total corneal area restricted by the innermost limbal arcade vessel.

Statistical analysis The significance of NV area in the whole cornea was calculated using one-way ANOVA analysis of variance. Multiple group comparisons were performed using Tukey's multiple comparisons procedure. P-value < 0.05 was considered significant.

3.2.3.3 Laser-induced choroidal neovascularization assay

Animals and anesthesia All experiments were performed in accordance with the ARVO Statement for the Use of Animals in Ophthalmic and Vision Research and in accordance with protocols reviewed and approved by the Animal Care Committee of the Chinese University of Hong Kong.

Male C57BL-6 mice of age 6 to 8-week-old weighing 18 to 20 g were anesthetized with intraperitoneal injection of 50 mg/kg of ketamine HCl and 10 mg/kg of

xylazine, and the pupils were dilated with 1% tropicamide. To prevent cornea drying and cataract formation when the mice were anesthetized (no blinking movement), a drop of 2% methylcellulose lubricant was applied on the corneal surface.

Protocol of laser induced choroidal NV model

(1) C57BL/6J mice at age of 6 to 8 weeks old were anesthetized with intraperitoneal 50 mg/kg of ketamine HCl and 10 mg/kg of xylazine.

(2) Pupils were dilated with using two drops of cyclopentolate 1% and phenylephrine hydrochloride 10%.

(3) A glass coverslip with a drop of 2% methylcellulose lubricant was placed over the cornea to flatten it and the fundus was visualized under slit lamp biomicroscopy.

(4) A green argon laser set at 100 mW, 0.1 sec duration, and 100 μ m spot size was focused on the RPE and the laser burn was applied at approximately one disc diameter from the optic nerve.

(5) Three separate laser photocoagulation burns were induced to rupture the Bruch's membrane at three separate locations.

(6) Creation of air bubble at the time of laser application indicates the rupture of Bruch's membrane and this ensures the quality and consistency of laser lesions

(7) After laser photocoagulation, a drop of hydroxypropylmethyl-cellulose ointment (Novartis) was applied on the corneal surface.

Comparison with subretinal injection of Matrigel in rabbit model In a recent study (Qiu et al., 2006), CNV was induced in rabbits by sub-retinal injection of VEGF-enriched matrigel matrix. The matrigel serves as a slow-release reservoir of

growth factors and a scaffold for growth of subretinal neovascularization. In this model, the inflammatory response to the matrigel plays a key role in development of CNV. In our laboratory, we also tried to conduct this matrigel-induced CNV, however, the easy solidation of matrigel at ambient temperature and demand of fine surgical technique and sub-retinal injection limit the performance of this assay.

Laser photocoagulation on mouse retina Three 532-nm argon laser spots (100 mW power, 100 msec duration, 100 μ m spot size; multi-laser length laser, Argon laser, Novus Omni, Coherent) were applied to each fundus through the slit lamp delivery system of a photocoagulator (OcuLight GL Photocoagulator; Iridex, Mountain View, CA) and using a hand-held cover slide as a contact lens. The lesions were placed between retinal vessels 2 to 3 disc diameters from the optic nerve. Formation of a bubble at the time of laser application, which indicated the rupture of Bruch membrane, was an important indicator of successful irradiation to induce CNV. Only burns in which a bubble was produced were included in the study. Bubbles formed in accompany with retinal hemorrhage were excluded.

Experimental animal groups and controls Laser-photocoagulated mice were randomly divided to receive drug or control treatment. The drug injection was performed immediately after the laser treatment. The eyes were intravitreally injected with drugs as treated group and the eyes with sterile BSS as control. For various literatures, the vitreal volume of young mice (6-8 weeks old) is ranged from 10~12 μ l (Heiduschka et al., 2007). We estimated the vitreal volume of our experimental mice was ~10 μ l. Hence, the injection concentration should be 10X as that of the working concentration in the chorioidal region and may be 10x as that used in topical application for corneal NV.

Vessel examination and quantification analysis

(a) Fundus Fluorescence angiography (FFA) In order to detect the development of CNV, FFA was performed on day 4, 7 and 10, respectively, as a longitudinal study (Edelman et al., 2000; Campos et al., 2006). Mice exhibiting intact lesions in the control eyes at day 4 were selected for FA analysis. A minimum of 9 lesions were analyzed for each treatment group and experiments were done in duplicates.

FFA was performed in non-anesthetized mice with dilated pupils using a digital fundus camera (Heidelberg Retinal Angiograph 2, HRA2, Heidelberg Engineering company, Germany). Fluorescein injection was administered intraperitoneally (0.02 ml of 5% fluorescein; Akorn, Decatur, IL) at time 0. A PMMA contact lens (base curve, 1.65 mm, power 7.0 D, size 2.5 mm) was placed on the mouse cornea to improve the visualization of retinal structures and prevent corneal drying. Digital images of fundus were taken continuously for a total of 5 minutes. Infrared picture was obtained to illustrate the laser lesion site. After imaging at day 10, the mice were euthanized with overdosed pentobarbital and the eyes were enucleated under PBS in dust-free condition.

(b) Analysis of FFA images Representative digital FA images were selected at 3 time-points of FA examination, namely early (1-2 min), middle (2-4 min) and late (>5 min) stages to illustrate the extent and rate of fluorescein leakage of CNV in the lesion sites. The pictures were analyzed in double blind by at least two masked retinal ophthalmologists or laboratory investigators, including Dr Vincent YW Lee, Dr Gary HF Yam and myself. We followed the grading standards reported earlier (Krzystolik et al., 2002; Zambarakji et al., 2006). Grade 1 lesions have no hyperfluorescence. Grade 2 lesions exhibit hyperfluorescence without leakage. Grade 3 lesions exhibit hyperfluorescence in the early or middle stages and late-stage leak-

age. Grade 4 lesions show bright hyperfluorescence in all stages and late-stage leakage beyond the treated areas. Grade 4 lesions are defined as clinically significant and represent the severe cases of retinopathy in human.

(c) Choroidal flatmount After FFA examination at day 10, mice were sacrificed with intraperitoneal overdosed pentobarbital. Eyes were enucleated and fixed in freshly prepared neutral buffered 4% paraformaldehyde for 1 hour. After PBS washes, the anterior segment, lens and the entire retina was carefully removed from the eye-cup. The remaining choroid and scleral tissue was incubated in a blocking buffer (2% BSA, 0.5% Triton X-100 in PBS) for 1 hour at room temperature. The specimens were then incubated with an isolectin-B4 antibody (Campos et al., 2006) overnight in PBS added with 0.5% BSA with gentle agitation at 4°C. After PBS washes, the choroids-sclera samples were partially cut into 4 quadrants with intact optic nerve region and flattened on glass slides. The samples were mounted with GB fluorescence mounting medium, sealed with a piece of cover glass and stored at -20°C in dark.

(d) Choroidal neovascularization evaluation and analysis Choroidal flatmount were examined with a fluorescence microscope (DMRB microscope; Leica) equipped with a color imaging system (Spot RT). Image of each lesion was taken at 40x magnification. Image J software was used to measure the total CNV area (pixel) in each lesion site. An established and constant threshold in pixels (corresponding to threshold fluorescence) was used to quantify the neovascularization.

Statistical analysis CNV leakage grading was performed from FA images at early, middle and late stages. Total FA grades in different groups and percentage of lesions with different grades were calculated and compared with controls. One-way ANOVA analysis of variance was used to calculate the degree of significance. $P <$

0.05 was considered significant.

CHAPTER 4

RESULTS:

The effect of selected herbal molecules in ocular neovascularization: *in vitro* & *in vivo* studies

4.1 Effect of isoliquiritigenin in ocular angiogenesis

4.1.1 *In vitro* studies

4.1.1.1 *Cytotoxicity analysis*

ISL of working concentrations ranging from 5 to 50 μM was tested for its cytotoxicity. ARPE19 cells were seeded at a density of 7×10^3 cells overnight before drug treatment. At day 0, ISL in medium containing 2% FBS was added to cell culture. Cells were collected at 1, 3 and 5 days for MTT cell proliferation/viability assay (**Figure 4**). At lower doses (5 to 10 μM), ISL promoted ARPE19 cell growth (5 μM : 133%; 10 μM : 145% of untreated cells at day 5). At concentrations higher than 15 μM , ISL prohibited cell proliferation to levels lower than the untreated control at all assay time points.

4.1.1.2 *Scratch wound HUVEC migration assay*

Validation of HUVEC growth and migration assay and controls The assay model and data interpretation was examined by testing with controls, including Avastin (312 $\mu\text{g/ml}$) or PP2 (10 nM) in conditions with or without VEGF (20 ng/ml). Figure 5A showed a time-dependent increase of HUVEC number in the denuded area

after scrapping in our scratch-wound HUVEC migration model. At 24-hour, untreated HUVEC with 14.1 ± 5.7 cells/mm² was observed. In the presence of VEGF, there was increased HUVECs migrated to the wound area (35 ± 9.3 cells/mm²). Treatment with Avastin reduced VEGF-stimulated migration and the cell density was 18.4 ± 4.2 per mm². Application of PP2 in the presence of VEGF further reduced HUVEC migration to 14 ± 5 cells/mm² (**Figure 5B**). Our result validated the scratch-wound model as HUVEC growth and migration assay.

ISL inhibited HUVEC growth and migration To study the potential of ISL in affecting VEGF-induced HUVEC growth and migration, three doses (5, 10 and 15 μ M) were tested. Compared to VEGF control, ISL showed a dose-dependent decrease of HUVEC migration (**Figure 5C**). With reference to 24-hour treatment, the cell density at denuded area was 21.1 ± 6.5 cells/mm² for 5 μ M ISL, 13 ± 1.7 cells/mm² for 10 μ M ISL and 14.3 ± 6.1 cells/mm² for 15 μ M ISL, respectively. These levels were significantly lowered than VEGF control (35 ± 9.3 cells/mm²) ($P < 0.05$, paired Student's *t-test*) and was lowered than that of Avastin-treated cells (18.4 ± 4.2 per mm²) (**Figure 5C**). Since 15 μ M ISL might show toxicity to cells, my result indicated that the non-cytotoxic 10 μ M ISL was potent in suppressing HUVEC growth and migration.

4.1.2 *In vivo* angiogenesis studies

4.1.2.1 *Developmental angiogenesis in chick CAM assay*

Six working concentrations of ISL (2, 5, 10, 25, 50, 100 μ M) were tested by the gelatin-sponge chick CAM model. Recombinant human VEGF was also tested for the induction to angiogenesis. Gelatin sponge with BSS vehicle served as the blank control. Sponge containing 0.6 μ g polyclonal anti-VEGF antibody) or Avastin (75 μ g)

were the negative control, respectively (**Figure 6**). After incubation of fertilized eggs for 8 days, the progression of chick CAM blood vessels was monitored by a micrograph imaging under stereomicroscopy at 0 and 24 hours (day 9 post-fertilization). The number of CAM vessels converging towards the edge of gelatin sponge was quantified. Vessel index was obtained by the difference of vessel converging on the sponge at 24-hour interval compared to that of 0-hour, then divided by vessel number of 0-hour. Application of sponge with 60 ng recombinant human VEGF resulted in the dense appearance of new blood vessels converging towards of the gelatin sponge (**Figures 6C, 6D**). The quantification result showed that at lower ISL concentration (2 μM) (**Figures 7A, 7B**), there was a suppressive effect on chick embryonic blood vessel with reference to that of the BSS control group (**Figures 6A, 6B**). The vessel index was 0.18 ± 0.24 (mean \pm SEM) (n=11) compared to that of control (0.95 ± 0.12 , n=18) ($P=0.009$, one way ANOVA test). ISL at 5 μM showed no clear increase of chick CAM vessel and the angiogenesis ratio was 0 (n=19) (**Figures 7C, 7D**) ($P<0.001$, one way ANOVA). ISL at concentration ≥ 10 μM reduced the number of CAM blood vessels (vessel index of 10 μM was -0.03 ± 0.09 , n=22) (**Figures 7E, 7F**) ($P<0.001$, one way ANOVA test). Treatment with ISL at 25 μM resulted in more inhibition of vessel development than other doses (**Figures 7G, 7H**). Application of sponge with 60 ng recombinant human VEGF resulted in the appearance of new vessels, and the ratio was about 2 folds as that in the BSS blank control measurement (**Figure 8**). Use of polyclonal anti-VEGF antibody (0.6 μg) (**Figures 6E, 6F**) showed significant suppression on CAM vessel growth (0.11 ± 0.06 , n=12, $p=0.01$, one way ANOVA test). Treatment of Avastin did not show similar chick CAM blood vessel number change as that of BSS control (**Figures 6G, 6H**).

4.1.2.2 Pathological angiogenesis of silver nitrate cauterization induced corneal neovascularization assay

This experiment was sought to investigate the efficacy of ISL on corneal angiogenesis. As a common route of administration for treating corneal surface disorders, ISL (ranging from 0.5 to 50 μM) was applied topically on the injured corneal surfaces at a standard 4 times daily. The corneal neovascularization was induced by scraping of the central 2-mm corneal epithelium combined with silver nitrate cauterization (please refer to Materials and Methods) in BALB/c mice. After injury, the mice were randomly divided into 6 groups with 10 mice each and received ISL eye-drops for a total of 14 days. Topical BSS for 4 times daily was employed as control. Half of mice in each group were sacrificed at day 7 (**Figure 9**) and the other half was terminated at day 14 (**Figure 12**). The corneas were harvested for immunofluorescence of CD31 (PECAM)-FITC conjugate (**Figures 10, 13**), which is a vascular endothelial cell marker. The extent of neovascularization was represented as the percentage of NV area in the whole corneal surface area.

In BSS control corneas, the onset of peripheral NV was observed on day 2 after injury. The vessels grew towards the central cornea and reached the center of cornea by day 14. In some control corneas, elevated pannus was found on the corneal surface, indicating a disruption of corneal epithelium. Although phenotypic variations in the NV progression were found in different mice, the onset of NV at day 2 after injury was almost identical.

In ISL treatment groups, the extent of corneal NV justified by the percentage of NV area changes was suppressed by ISL at doses $\geq 1 \mu\text{M}$, applied at 4 times daily for seven days. The ratio of NV area of cornea was 0.24 ± 0.03 (mean \pm SEM) in $1 \mu\text{M}$ ISL treated group ($n=5$), in comparison with BSS control group (0.5 ± 0.04 , $n=5$) ($P=0.000$, one-way ANOVA test). Topical application of ISL $\geq 5 \mu\text{M}$ showed simi-

larly significant suppression on corneal NV formation and growth, accounting for about one third of BSS control group (0.19 ± 0.02 , 0.149 ± 0.025 , 0.17 ± 0.04 for ISL at 5, 10, 50 μM topical administration, respectively, $n=5$ each group, $P = 0.000$, one-way ANOVA test). On the contrary, ISL at 0.5 μM showed no effect in suppressing corneal new blood vessel formation and growth in contrast to BSS control group (0.43 ± 0.08 for 5 μM ISL treatment. And 0.5 ± 0.04 for control groups, $n=5$) ($p=0.282$, one-way ANOVA test) (**Figure 11**). Treatment with ISL at 10 μM resulted in more inhibition of vessel development than other doses.

We found that the outgrowths of blood vessels was inhibited by higher concentration of ISL significantly ($P < 0.05$), this effect last from day 7 to day 14. On day 14, for the BSS control group, the NV area expanded accounting for two third of whole corneal area (0.68 ± 0.04 , $n=5$). Ratio of corneal NV area for 0.5 μM ISL treated mice was decreased to 0.557 ± 0.148 , $n=5$ ($P=0.209$, one-way ANOVA test, compared with control group). In 1 μM ISL treated group, NV area reached about 1/3 of whole corneal area, showing a suppressive effect of corneal NV growth ($P = 0.000$, $n=5$, one-way ANOVA test). In concentration $\geq 5 \mu\text{M}$ ISL treated group, the NV area was about 20% of whole corneal area (0.248 ± 0.012 , 0.221 ± 0.038 , 0.232 ± 0.018 for ISL at 5, 10 or, 50 μM respectively, $n=5$ for each treatment group) ($P = 0.000$, one-way ANOVA test). Treatment with ISL at 10 μM resulted in more inhibition of vessel development than other doses (**Figure 14**). It was concluded that ISL was effective to inhibit corneal NV progress.

4.1.2.3 Pathological angiogenesis of laser-induced choroidal neovascularization assay

This experiment was sought to investigate the efficacy of ISL on choroidal an-

giogenesis. As a common route of administration for treating retinal vessel disorders, ISL was applied intravitreally once immediately laser injury. C57B/L mice with 3 spots of laser injury induced were randomly divided in 4 groups (3 mice each group) and received intravitreal ISL as treated group and intravitreal BSS as control. The laser-injured lesions (n=9) were monitored at day 4, 7 and 10 by fundus fluorescein angiography. At day 10, all mice were sacrificed and choroidal NV was detected by immunofluorescence with isolectin-B4-FITC conjugate (**Figure 15**).

Three concentrations of ISL (10, 50 and 200 μM) were tested in this experiment. The selection of these doses was based on the reported mouse vitreal volume as 10 to 12 μl (Heiduschka *et al.*, 2007). Since our intravitreal injection volume was kept to a minimal of 1 μl to prevent post-injection ocular hypertension and associated ocular injuries, the injection dose was adjusted to 10 times higher in concentration. Hence the injection doses of 10, 50 and 200 μM will be converted to the working doses of 1, 5 and 20 μM , respectively.

Fluorescein leakage in lesions C57BL/c mice were examined in each group by fundus fluorescein angiography (FFA) longitudinally (representative FFA were shown in Figure 14), and the percentages of lesions per eye with leakage illustrated by FFA are shown in Figure 16. At day 4, grade 4 with clinically significant lesion was more prevalent in BSS control mice (accounted in 60% of lesions) whereas it was the least developed in mice with 20 μM ISL (0%). The percentage of grade 4 lesions was 11% in 1 μM ISL group and also in 5 μM group. Lesion scored at or below grade 2 was accounted in two third of lesions in ISL treatment groups, and this was shown by reduced fluorescein leakage. On the contrary, in BSS group, almost 80% lesions showed bright, even sharp bright fluorescein leakage, indicating the success

of choroidal NV establishment. The NV was improved in ISL treatment groups. For day 7 FFA examination, grade 4 lesion was not observed in mice with intravitreal injection of ISL at 1 & 5 μ M, and there is no change in IV ISL 20 μ M group and decreased to 44% in BSS control group. On day 10, choroidal neovascularization usually grows to maximum size, and causes the most severe fluorescein leakage in mouse model. In IV ISL treatment eyes, the proportion of grade 4 lesion leakage was 0, and most of lesions were scored less than grade 2. The percentage of lesion of grade 1 and 2 was 100% in 1 μ M ISL group, 77% for 5 μ M ISL group, and 66% for 20 μ M ISL group. In the control group, there were 44% lesions showing hyperfluorescein leakage (**Figure 16**).

4.1.2.4 Choroidal neovascularization area

At day 10, the mice were sacrificed and choroidal NV area detected by immunofluorescence with isolectin-B4-FITC conjugate was measured by Image J software. Choroidal neovascularization area was 16674 ± 5133 pixels for intravitreal ISL (1 μ M) treated group, 15114 ± 3706 pixels for 5 μ M, and 14060 ± 1822 pixels for ISL 20 μ M treated group. They were compared to 27348 ± 7352 pixels for IV BSS control group ($P < 0.05$, $n = 9$ each group, one-way ANOVA test) (see **Figure 17**). Data were expressed as mean \pm SEM, and our study showed that ISL treatment suppressed laser-induced-choroidal neovascularization in a dose dependent manner.

4.1.3 Protein analysis

4.1.3.1 VEGF expression (Figure 48)

Western blotting and band densitometry analysis followed by the normalization of specific band intensity with housekeeping GAPDH intensity, a lower VEGF ex-

pression was observed in HUVEC under serum-free and growth factor-free starvation (sample 2) when compared to HUVEC in normal culture (sample 1). Supplementation of exogenous VEGF (20 ng/ml) induced a higher cellular VEGF level in sample 3. Simultaneous addition of Avastin (312 μ g/ml, sample 4), on the other hand, effectively suppressed cellular VEGF expression ($P < 0.005$, paired Student's *t*-test). Incubation for 24 hours with ISL (10 μ M, sample 5) significantly down-regulated cellular VEGF level ($P < 0.005$, paired Student's *t*-test).

4.1.3.2 PEDF expression analysis (Figure 48)

By Western blotting and band densitometry analysis followed by normalization of specific band intensity with housekeeping GAPDH, moderate PEDF expression was observed in HUVEC under normal culture condition (full medium, sample 1), starvation (sample 2), VEGF-supplementation (sample 3), treatment with VEGF and Avastin (312 μ g/ml, sample 4). However, treatment of cells with ISL (10 μ M, sample 5) resulted in a significant elevation of PEDF expression ($P < 0.005$, paired Student's *t*-test, compared to VEGF-supplemented sample 3).

4.1.3.3 Akt activation assay (Figure 49)

By Western blotting of phospho-Akt and pan-Akt followed by band densitometry analysis, Akt activation level was represented by the percentage of phospho-Akt in pan-Akt. For HUVEC under normal culture condition (full medium, sample 1), more than 80% of Akt was active. Upon starvation (sample 2), there was a slight reduction of pan-Akt and, in particular, the active Akt level was reduced to about 38%. Supplementation of VEGF (20 ng/ml, sample 3) brought up the Akt expression level and the percentage of active Akt to that of normal cells. This was even less than that

of Avastin treatment (sample 4, down to 51%). However, ISL (10 μ M, sample 5) did not affect the activated Akt levels.

4.1.3.4 Pan-Akt expression (Figure 49)

By Western blotting of pan-Akt and band densitometry followed by normalization with that of housekeeping GAPDH, pan-Akt expression in HUVEC was changed upon various treatments. When compared to cells supplemented with VEGF only, a reduction of Akt expression was observed when cells were treated for 24 hours with VEGF and Avastin (312 μ g/ml, reduced by 40%). On the other hand, higher Akt levels were found in cells with ISL (10 μ M) (up-regulated by 30%).

4.1.3.5 FAK activation assay (Figure 50)

The starved HUVEC was treated with Avastin (312 μ g/ml) or 10 μ M ISL, in the presence of 20 ng/ml VEGF, for 24 hours. Western blotting of soluble cell lysates showed very low expression of FAK and phospho-FAK in starved cells before treatment. In cells incubated with VEGF, FAK was stimulated for more than 10 folds when compared to starved cells. The expression of phospho-FAK (Y576/577) was ~20% of total FAK. This level was unchanged in Avastin treated cells. Treatment with ISL (10 μ M) mildly increased total FAK expression as well as the proportion of phospho-FAK in total FAK (~50%).

4.1.3.6 MMP-2 expression (Figure 51)

In normal culture condition, the proliferating HUVECs (sample 1) had predominant expression of proteolytically active MMP-2 (with molecular size of 55~60

kDa). After starvation, most of the MMP-2 was remained inactive as pro-MMP-2 with molecular size of ~65 kDa and negligible active MMP-2 was observed (sample 2). Starved cells supplemented with VEGF (sample 3) showed about 20% active MMP-2. Similar levels were also observed for cells with Avastin (312 $\mu\text{g/ml}$) (sample 4) and ISL (10 μM) (sample 5). Similar result was observed in duplicated experiments.

4.1.3.7 MMP-9 expression (Figure 51)

Western blotting analysis showed the specific MMP-9 immunoreactive band at ~100 kDa position. Except the starved cells, all cells with or without treatment with Avastin or different herbal chemicals showed moderate expression of MMP-9. There was no distinct difference among treatment groups. Starved cells exhibited negligible MMP-9 expression.

4.1.4 Discussion

Isoliquiritigenin (ISL), which is isolated from licorice, shallot and bean sprouts, is a potent anti-oxidant with anti-inflammatory and anti-carcinogenic effects (Kwon et al., 2009; Kanga et al., 2010; Park et al., 2010). Many studies investigating ISL mechanisms were performed on cancer cells, such as DU145 human prostate cancer cells and HeLa human cervical cancer cells, and ISL was reported to inhibit MAPK and JNK/AP-1 signaling as well as induced G2 and M phase arrest. Recent research has indicated that NF- κ B is tightly involved in the production of VEGF in different cell lines (Jo et al., 2004; Korkolopoulou et al., 2008; Zhang et al., 2009). In the study using ACC cells, ISL down-regulated VEGF production and prevented ACC

cell-induced angiogenesis through the inhibition of NF- κ B activation (Zhang et al., 2006; Zhang et al., 2009).

In this study, ISL when applied at sub-toxic dose of 10 μ M reduced the growth and migration of HUVEC in the *in vitro* scratch-wound model. The effect was even stronger than that of Avastin within 24 hours of examination. Indeed, when comparing different selected herbal chemicals, ISL at 10 μ M demonstrated the best efficacy in reducing HUVEC migration. This effect was not mediated by suppressing VEGF binding to its cognate receptor in endothelial cells or VEGF signaling as similar inhibition was found for condition without VEGF supplementation. Though FAK was activated by ISL, the elevated PEDF could be associated with its inhibitory effect on HUVEC cell growth and migration (Kim et al., 2004).

Also, in this study, proliferating HUVECs at half confluence were recruited to study the suppressive effect of ISL on endothelial cell growth and migration. Treatment of ISL at 10 μ M for 24 hours decreased the intracellular VEGF expression and simultaneously up-regulated PEDF levels. Reported low level of VEGF by ISL application was evidenced in DU145 human prostate cancer cells (Kwon et al., 2009). PEDF is known as a potent anti-angiogenic molecule and its induction by ISL could be one of the mechanisms by which ISL inhibits endothelial cell growth and migration.

Most importantly, the *in vivo* studies verified the *in vitro* findings. ISL treatment effectively reduced developmental blood vessel growth in chick CAM assay and pathological neovascularization on corneal surface and choroid in mice. Two different routes of application, namely topical and intravitreal, were tested and both demonstrated an effective suppression of the corresponding NV. This study, for the first time, demonstrated a dose-dependant NV suppression effect of ISL in developmental

angiogenesis and pathological ocular angiogenesis.

In chick CAM assay, which is the most widely employed *in vivo* model for studying vessel development, ISL markedly and dose-dependently inhibited the development of capillary networks. The inhibitory effect of ISL at 5 μM balanced the endogenous angiogenic effect of chick growth factors in the CAM model. When applied at doses higher than 5 μM (until 100 μM in my assay) effectively regressed the growth of new and preexisting blood vessels. The optimized dose was found to be about 25 μM .

In a mice experiment of silver nitrate cauterization-induced corneal NV, ISL when topically applied at concentration >1 μM also demonstrated a significant reduction in NV area in which new blood vessels sprouted from pre-existing limbal capillary network. In the choroidal NV experiment, vascular leakage was decreased at the dose equivalent to the therapeutic dose of ISL, verified through FFA examination and choroidal flat mount. All the above results are consistent with our *in vitro* findings. The presence of infiltrating cells and other inflammatory cytokines and molecules have been reported at the site of laser burns (Yi et al., 1997; Kwona et al., 2009). It is probable that ISL suppressed the activity of VEGF and simultaneously up-regulated PEDF expression to prohibit angiogenesis and inflammation.

VEGF is a major angiogenic stimulator of hypoxia-induced corneal inflammation and angiogenesis (Singh *et al.* 2007), increased VEGF levels have been shown to be a common pathologic factor in neovascular ocular diseases of humans, as well as in the animal model of alkali-induced corneal disease (Shen et al., 1998). Under certain hypoxic conditions in the cornea, as found in inflammation and injury, angiogenic stimulators are overproduced, whereas angiogenic inhibitors are decreased (Amano et al., 1998). The disruption in the balance between these factors results in

NV. VEGF is a secreted peptide found extensively in the epithelium of vascularized corneas secondary to inflammation (Kvanta, 2006). VEGF binds to tyrosine-kinase receptors, VEGFR1 (Flt-1) and VEGFR2 (Flk-1), and also the neuropilins which lack tyrosine-kinase activity. VEGF signalling is modulated by angiopoietins that bind to Tie-2 receptors (Campochiaro et al., 2004). Soluble Tie-2 receptors curb and regresses corneal NV independent of VEGF in murine models of mechanical-alkali injury-induced corneal NV (Singh et al., 2005b). The avascular cornea owes its transparency to soluble VEGFR-1 (sFlt-1) that acts as a decoy receptor for VEGF-A, a potent stimulator of corneal NV (Ambati et al., 2006). VEGF is also produced at a much higher concentration basally near the VEGF receptors on the choriocapillaris under hypoxic conditions (Blaauwgeers et al., 1999).

Though VEGF is the main regulator in ARMD, increased VEGF alone is not enough to cause subretinal neovascularization. A transgenic model of increased VEGF production by RPE and choroid showed that vasculature is increased but only within the choroid and none had invaded Bruch's membrane. Additional environmental insults and the balance of the angiogenic versus anti-angiogenic factors determine whether choroidal neovascularization will be present (Schwesinger et al., 2001).

PEDF, initially known as a neurotrophic factor, has antiangiogenic properties that maintain the eye free of vascularization by reducing VEGF induced chemotactic endothelial cell migration and proliferation via apoptosis (Mori et al, 2001). It is found abundantly in RPE, iris and cornea (Ortego et al., 1996; Karakousis et al, 2001) and recently has also been detected in the tear fluid of healthy individuals (Abdiu et al., 2008). Its anti-angiogenic activity is selective in that it is effective against newly forming vessels but spares existing ones, and the action is reversible (Bouck et al.,

2002). Since PEDF inhibits bFGF-induced corneal NV (Dawson et al, 1999) it may serve as an additional molecule sustaining the cornea's 'ocular privilege'. It is also highly expressed in the RPE covering choroidal NV at much higher levels when neovascularization first occurs (Ogata et al, 2002). The vitreous concentration of PEDF has been found to be lower in eyes with choroidal neovascularization as compared to age-matched controls (Ogata et al., 2004; Tong et al., 2006). In late stages of ARMD, PEDF is directly related to the oxygen levels in the eye and is reduced in ischemic eyes or those under oxidative stress (Dawson et al. 1999; Matsui et al. 2001).

Our results support the previous findings that ISL inhibits the cascade of angiogenesis and inflammation via suppression of VEGF (Sheela et al., 2006). In addition, we showed a significant up-regulation of PEDF, which showed effectively inhibition of new vessel formation and endothelial cell proliferation.

In my study, treatment with ISL in half-confluent HUVEC showed decreased intracellular VEGF expression and simultaneously up-regulated PEDF levels, which maybe the major contribution to suppress ocular neovascularization. This speculation is supported by a recent clinical study where PEDF concentrations in the vitreous of individuals with choroidal neovascularization because of age-related macular degeneration were found to be significantly lower than that in the vitreous of age-matched controls (Holekamp et al., 2002). ISL also suppressed VEGF-induced endothelial cell migration. We, on the other hand, did not observe that the anti-angiogenic effect of ISL was mediated via Akt or FAK pathways.

MMPs also play an important role in tumor invasion, angiogenesis and inflammatory tissue destruction (Dollery et al., 2006; Nagase et al., 2006). Increased expression of MMPs was observed in benign tissue hyperplasia and in atherosclerotic lesions (Tosetti et al., 2002; Dollery et al., 2006). These enzymes may contribute to a

cell-invasion favoring matrix modification and, thus, to an invasive aggressiveness of tumor cells (John et al., 2001; Tosetti et al., 2002). Invasive cancer cells utilize MMPs to degrade the extracellular matrix (ECM) and basement membrane during metastasis, and MMP-2 has been implicated in the development and dissemination of malignancies (Kargozaran et al., 2007). The interaction between malignant cells and peritumoral benign tissues including the vascular endothelium may serve as an important mechanism in the regulation of tumor invasion and metastasis (Kargozaran et al., 2007). Their proteolytic activities are regulated by inhibitors or activators, such as tissue inhibitors of MMP (TIMPs), membrane-type MMP (MT-MMP) and urokinase-type plasminogen activator (uPA) (Kugler et al., 1999; Bouck et al., 2002; Das et al., 2006). It was also assumed that ISL blockade of MMP production and activation hampered endothelial cell motility (Kanga et al., 2010). However, in my study, the protein analysis did not show any MMP-2 reduction after ISL treatment in HUVECs, nor the MMP-9 expression. This might be due to our experimental setup with the inclusion of VEGF in the medium. This was suggested to surrogate the reduced VEGF caused by ISL and hence, maintaining the MMPs levels. However, in an absolute absence of VEGF, ISL suppressed MMP levels to inhibit endothelial cell motility (Kanga et al., 2010). MMP was involved in the angiogenic and metastatic cascades of knockout or transgenic animals and tumor cell lines overexpressing or down-regulating a specific MMP (Chesler et al., 2007; Blázquez et al., 2008; Pulukuri et al., 2008). It was found ISL decreased EGF-induced secretion of uPA, MMP-9, TIMP-1 and VEGF, but increased TIMP-2 secretion in a concentration-dependent manner (Kwon et al., 2009).

Therefore, ISL down-regulated VEGF and induced PEDF to favor the anti-angiogenesis and, thus, represents a novel mechanism underlying the inhibitory

effect of ISL on ocular NV. Although this implies that blockade of VEGF activity alone is sufficient for the complete inhibition of NV, a synergy might exist between VEGF and PEDF, or other angiogenic factors, which all need to be blocked concurrently for complete inhibition.

4.1.5 Conclusion

The present study demonstrated for the first time that ISL, a natural flavonoid derived from licorice, significantly and specifically suppressed angiogenesis both *in vitro* and *in vivo*, relating to the up-regulated PEDF level. My findings systematically dissected the effects of ISL on the VEGF signaling pathway in endothelial cells, determined the importance of up-regulated PEDF or the anti-angiogenic activity of ISL, and shed new light on the mechanisms of anti-angiogenic activities of ISL, as well as implicated its great therapeutic potential candidate for the tumor and ocular neovascularization diseases.

4.2 Effect of epigallocatechin gallate in ocular angiogenesis

4.2.1 *In vitro* studies

4.2.1.1 *Cytotoxicity by MTT Assay*

By MTT cell proliferation/viability assay, we tested EGCG in the range of 10 to 100 μM . A dose-dependent effect on RPE cell proliferation was observed. At dosages below 50 μM , EGCG promoted cell proliferation at all investigated time points (10 μM : 163% and 50 μM : 121% when compared to untreated cells at day 5) (**Figure 20**). At concentration of 100 μM , EGCG reduced cell proliferation (down to 17% when compared to the untreated control at day 5). This indicated that EGCG at or below 50 μM was not cytotoxic to RPE cells.

4.2.1.2 *Effect on HUVEC migration*

To test if EGCG possesses the potential to affect VEGF-induced HUVEC growth and migration, three doses (10, 20 and 50 μM) were selected for the experiment. Compared to VEGF control (35 ± 9.3 cells/ mm^2), EGCG showed a dose-dependent decrease of HUVEC migration to the denuded area (**Figure 21A**). Among them, 50 μM EGCG exhibited the best suppressive action. With reference to 24-hour of treatment, EGCG at 50 μM had 9.4 ± 2.7 cells/ mm^2 denuded area (**Figure 21C**) which was much lower than that of Avastin control (18.4 ± 4.2 per mm^2) (**Figure 21B**). On the other hand, less inhibitory effect was seen for 10 μM (30.9 ± 8.1 cells/ mm^2) and 20 μM EGCG (20 ± 3.2 cells/ mm^2) (**Figure 21C**), respectively. Since it did not show any cytotoxicity, we suggested that the sub-toxic 50 μM EGCG was more potent in the anti-angiogenic activity.

4.2.2 *In vivo* angiogenesis studies

4.2.2.1 *Suppression of developmental vessel growth in chick CAM assay*

Six working concentrations of EGCG (0.5, 1, 5, 10, 50, 100, 250 μM) were tested by the gelatin-sponge chick CAM model (**Figure 22**). Recombinant human VEGF165 was also tested as the positive control to induce vessel growth towards the sponge. Gelatin sponge with BSS served as the blank control. Sponge containing 0.6 μg polyclonal anti-VEGF antibody (Santa Cruz) or Avastin (75 μg) were the negative control, respectively (**Figure 6**). After incubation of fertilized eggs for 8 days, the progression of chick CAM blood vessels was monitored by a micrograph imaging under stereomicroscopy at 0 and 24 hours (day 9 post-fertilization). The number of CAM vessels converging towards the edge of gelatin sponge was quantified. Vessel index was calculated as the difference of vessel converging on the sponge at 24-hour interval compared to that at 0-hour, then divided by vessel number at 0-hour. Application of sponge with 60 ng recombinant human VEGF165 resulted in the dense appearance of new blood vessels converging towards the gelatin sponge (**Figure 6C, 6D**), and the ratio was about 2 folds (1.85 ± 0.47) as that of the BSS blank control (0.95 ± 0.12 , $n=18$, $P=0.002$, one way ANOVA test) (**Figure 6A, 6B**). Use of polyclonal anti-VEGF antibody (0.6 μg) showed significant suppression on CAM vessel growth (0.11 ± 0.06 , $n=12$, $P=0.012$, one way ANOVA test) (**Figure 6E, 6F**). Treatment of Avastin (vessel index was 0.77 ± 0.48) showed similar chick CAM blood vessel number change as that of BSS control ($P=0.563$, one way ANOVA test) (**Figure 6G, 6H**).

For EGCG treated chick CAM, a dose-dependent reduction of CAM vessel growth towards the sponge was observed (**Figure 22**). The quantification result

showed that at lower EGCG concentration (0.5 μM), the chick embryonic blood vessel growth was suppressed with reference to that of BSS control, and the vessel index was 0.29 ± 0.13 ($n=11$) compared to that of BSS control (0.95 ± 0.12 , $n=18$) ($P=0.025 < 0.05$, one way ANOVA test). EGCG at 1 μM showed a lack of chick CAM vessel growth and the index was 0 ($n=12$) ($P=0.001 < 0.01$, one way ANOVA). EGCG at concentration ≥ 5 μM reduced the number of CAM blood vessels dose-dependently (vessel index was -0.12 ± 0.08 for 5 μM EGCG, -0.19 ± 0.15 for 10 μM EGCG, -0.21 ± 0.08 for 50 μM EGCG, -0.24 ± 0.09 for 100 μM EGCG, $n=10$ in each group) ($P < 0.001$, one way ANOVA test). Treatment with EGCG at 250 μM resulted in the most inhibition of vessel growth (vessel index was -0.28 ± 0.09 for EGCG, $n=10$) (**Figure 23**).

4.2.2.2 Suppression of silver nitrate cauterization-induced corneal neovascularization

This experiment was sought to investigate the efficacy of EGCG on corneal neovascularization. As a common route of administration for treating corneal surface disorders, EGCG (ranging from 0.5 to 250 μM) was applied topically on the injured corneal surfaces at a standard 4 times daily. The corneal neovascularization was induced by scraping the central 2-mm corneal epithelium combined with silver nitrate cauterization in BALB/c mice. After injury, the mice were randomly divided into 6 groups with 10 mice each and received EGCG eyedrops for a total of 14 days. Topical BSS was employed as control. Half of mice in each group were sacrificed at day 7 (**Figure 24**) and the remaining was terminated at day 14 (**Figure 27**). The corneas were harvested for immunofluorescence using monoclonal anti-CD31 (PECAM)-FITC conjugate (Santa Cruz), which labels vascular endothelial cells

(Figures 25, 28). The extent of neovascularization was represented as the percentage of NV area in the whole corneal surface area confined by the limbal vasculature.

In BSS control, the onset of peripheral NV was observed at day 2 after injury. The vessels grew towards the central cornea and reached the center by day 14. In some control corneas, elevated pannus was found on the corneal surface, indicating a disruption of corneal epithelium. Although phenotypic variations of NV progression were found in different mice, the onset of NV at day 2 after injury was almost identical.

In EGCG treatment groups, the extent of corneal NV justified by the percentage of NV area changes was suppressed by EGCG at doses $\geq 1 \mu\text{M}$, applied at 4 times daily for seven days. The ratio of NV area was 0.30 ± 0.06 (mean \pm SEM) in $1 \mu\text{M}$ EGCG-treated group ($n=5$), whereas BSS control was $(0.54 \pm 0.06, n=5)$ ($P=0.001$, one-way ANOVA test). Topical application of EGCG at doses $\geq 5 \mu\text{M}$ showed strong suppression on corneal NV formation and growth (0.25 ± 0.05 for $5 \mu\text{M}$ EGCG, 0.22 ± 0.02 for $10 \mu\text{M}$ EGCG, 0.19 ± 0.01 for $50 \mu\text{M}$ EGCG and 0.22 ± 0.02 for $250 \mu\text{M}$ EGCG, respectively ($n=5$ each group). The reduction of NV area ratio for treatment with doses $\geq 5 \mu\text{M}$ was significant when compared to BSS controls $P < 0.001$, one-way ANOVA test) (Figures 26). On the contrary, EGCG at $0.5 \mu\text{M}$ showed null effect on suppressing corneal NV ($0.52 \pm 0.07, n=5, P=0.763$) (Figure 26). Although, this assay showed that topical treatment with $50 \mu\text{M}$ EGCG, 4 times daily resulted in the most suppression of corneal NV formation.

We found that the outgrowth of corneal blood vessels was significantly inhibited by topical with EGCG ($P < 0.05$, one-way ANOVA test) in the long run. At day 14, the NV area expanded in the BSS control group and accounted for about three quarter of whole corneal surface area (the ratio was $0.74 \pm 0.05, n=5$). In $0.5 \mu\text{M}$ EGCG-treated

mice (n=5), the ratio was decreased to 0.25 ± 0.02 ($P<0.001$, one-way ANOVA test, compared to the control group). In 1 μM EGCG-treated group (n=5), the NV area was about one-fifth of whole corneal surface area and the suppression resulted in a ratio of 0.21 ± 0.01 , $P<0.001$, one-way ANOVA test). For the groups with EGCG doses $\geq 5 \mu\text{M}$, the NV area was reduced to about 20% of whole corneal surface area (0.23 ± 0.01 for 5 μM EGCG, 0.23 ± 0.08 for 10 μM EGCG, 0.16 ± 0.04 for 50 μM EGCG and 0.22 ± 0.01 for 250 μM EGCG, respectively, n=5 for each treatment group) ($P<0.001$, one-way ANOVA test). After all, topical treatment with 50 μM EGCG resulted in the most suppression of corneal NV development (**Figures 29**).

4.2.2.3 Suppression of laser-induced choroidal neovascularization

As a common route of administration for treating retinal vessel disorders, EGCG was applied intravitreally once at time immediately after laser photocoagulation in C57B/L mice. Three doses of EGCG (100, 500 and 2000 μM) were tested. The selection of these doses was based on the reported mouse vitreal volume of 10 to 12 μl (Heiduschka et al., 2007). Since our intravitreal injection volume was kept to a minimal of 1 μl to prevent post-injection ocular hypertension and associated ocular injuries, the injection dose was adjusted to 10 times higher in concentration. Hence the injection doses of 100, 500 and 2000 μM will be converted to the working doses inside the vitreous of 10, 50 and 200 μM , respectively. C57B/L mice with 3 spots of laser injury induced in one eye were randomly divided into 4 groups (5 mice for BSS injection as control and 5 for 10 μM EGCG groups, 3 for 50 μM EGCG group and 4 for 200 μM EGCG group). The laser lesions (15 for BSS and 10 μM EGCG, 9 for 50 μM EGCG and 12 for 200 μM EGCG) were monitored at day 4, 7 and 10 by FFA. The severity of fluorescein leakage in each lesion was scored by 2 independent vit-

reoretinal ophthalmologists using the grading from 1 to 4 (Materials and Methods) and the percentage of each grade was calculated. At day 10, all mice were sacrificed, retinas were harvested for flat-mounting and choroidal NV was detected by immunofluorescence with isolectin-B4-FITC conjugate (**Figure 30**).

Fundus fluorescein angiography The same C57B/L mice were examined by fundus fluorescein angiography at different time intervals (representative FFA images are shown in **Figure 30**), and the percentages of leakage grading for each treatment group are shown in **Figure 31**. At day 4, grade 4 with clinically significant lesion was more prevalent in BSS control mice (accounted in about 60% of lesions) but it was the least developed in mice with 50 and 200 μM EGCG (both were observed as 0%). The percentage of grade 4 lesion was about 13% in 10 μM EGCG group. Lesion scored at or below grade 2 was 100% in 50 μM EGCG treatment group, and this group of lesion was accounted for about 53% and 58% in EGCG 10 & 50 μM treatment groups. On the contrary, the BSS group, showed only 7% lesions in grade 2 and other lesions exhibited bright fluorescein leakage, indicating the severity of choroidal NV development.

For day 7 FFA examination, grade 4 lesion was not observed in mice having intravitreal doses of 10 μM EGCG. Occasional severe lesion with early fluorescein leakage was noted in 50 μM EGCG group (one of 9 lesions) and 200 μM EGCG group (one of 15 lesions). The percentage of grade 4 lesions was increased to 66% in BSS group.

On day 10, choroidal neovascularization usually develops to maximum size and severity as shown by intense fluorescein leakage in mice. In EGCG treated eyes, no severe hyperfluorescein leakage was observed in 10 and 50 μM EGCG treatment

groups, and about 70% lesions were scored below grade 2. The percentage of grade 2 lesions was about 75% in 200 μ M EGCG group and only 8% lesion were scored as grade 4. In contrast, the BSS control group had 87% lesions showing hyperfluorescein followed by end-stage leakage (47% of grade 4, and 40% of grade 3) (Figure 31), whereas the other lesions showed hyperfluorescein without leakage.

Choroidal neovascularization area At day 10, the mice were sacrificed and choroidal NV area detected by immunofluorescence with isolectin-B4-FITC conjugate was measured by Image J. Choroidal neovascularization area in BSS controls was 14847 ± 1074 pixels (mean \pm SEM). This was reduced to 6270 ± 5133 pixels in 10 μ M EGCG group (n=15), 6193 ± 1292 pixels in 50 μ M EGCG (n=9), and 4150 ± 719 pixels in 200 μ M EGCG group (n=12). ($P < 0.001$, one-way ANOVA test) (Figure 32).

4.2.3 Protein analysis

4.2.3.1 VEGF expression (Figure 48)

Western blotting and band densitometry analysis followed by the normalization of specific band intensity with housekeeping GAPDH intensity, lower VEGF expression was observed in HUVEC under serum-free and growth factor-free starvation (sample 2) when compared to HUVEC in normal culture condition (sample 1). Supplementation of VEGF165 (20 ng/ml) to the culture induced a higher cellular VEGF level (sample 3). Simultaneous addition of Avastin (312 μ g/ml, sample 4), on the other hand, effectively suppressed cellular VEGF expression ($P < 0.005$, paired Student's t-test). Incubation for 24 hours with EGCG (50 μ M, sample 7) did not result in a significant change of VEGF level in HUVECs.

4.2.3.2 PEDF expression analysis (Figure 48)

By Western blotting and band densitometry analysis followed by normalization of specific band intensity with housekeeping GAPDH, there was no clear difference in the PEDF expression in HUVECs under normal culture condition (full medium, sample 1), starvation (sample 2), VEGF-supplementation (sample 3), treatment with VEGF and Avastin (312 $\mu\text{g/ml}$, sample 4) and EGCG (50 μM , sample 7).

4.2.3.3 Akt activation assay (Figure 49)

By Western blotting of phospho-Akt and pan-Akt followed by band densitometry analysis, Akt activation level was represented as the percentage of phospho-Akt in pan-Akt level. In HUVEC under normal culture condition (full medium, sample 1), more than 80% of Akt was active. Upon starvation (sample 2), there was a slight reduction of pan-Akt and, in particular, the active Akt level was reduced to about 38%. Supplementation of VEGF (20 ng/ml, sample 3) brought up the Akt expression level and the percentage of active Akt to that of normal cells. In treatment groups, a significant reduced level of active Akt (down to 45% of total Akt) was observed in samples treated with EGCG (50 μM , sample 7) ($P < 0.005$, paired Student's *t*-test, compared to VEGF-supplemented sample 3). This was even less than that of Avastin treatment (sample 4, down to 51%).

4.2.3.4 Pan-Akt expression (Figure 49)

By Western blotting of pan-Akt and band densitometry followed by normalization with that of housekeeping GAPDH, pan-Akt expression in HUVEC was

changed upon various treatments. When compared to cells supplemented with VEGF only, a reduction of Akt expression was observed when cells were co-treated for 24 hours with VEGF and Avastin (312 $\mu\text{g/ml}$, reduced by 40%). On the other hand, higher Akt levels were found in cells with EGCG (50 μM) (up-regulated by 15%).

4.2.3.5 FAK activation assay (Figure 50)

The starved HUVEC was treated with Avastin (312 $\mu\text{g/ml}$) or 50 μM EGCG, in the presence of 20 ng/ml VEGF, for 24 hours. Western blotting of soluble cell lysates showed very low expression of FAK and phospho-FAK in starved cells before treatment. In cells incubated with VEGF, FAK was stimulated for more than 10 folds when compared to starved cells. The expression of phospho-FAK (Y576/577) was ~20% of total FAK. Similar level was observed in Avastin or EGCG-treated cells.

4.2.3.6 MMP-2 expression (Figure 51)

In normal culture condition, the proliferating HUVECs (sample 1) had predominant expression of proteolytically active MMP-2 (with molecular size of 55~60 kDa). After starvation, most of MMP-2 was remained inactive as pro-MMP-2 with molecular size of ~65 kDa and negligible active MMP-2 was observed (sample 2). Starved cells supplemented with VEGF (sample 3) showed about 20% active MMP-2. Similar levels were also observed for cells with Avastin (312 $\mu\text{g/ml}$) (sample 4). However, cells treated with EGCG (50 μM) (sample 7) had almost negligible expression of both pro- and active MMP-2. Similar result was observed in duplicated experiments.

4.2.3.7 MMP-9 expression (Figure 51)

Western blotting analysis showed the specific MMP-9 immunoreactive band at ~100 kDa position. Except the starved cells, all cells with or without treatment with Avastin or different herbal chemicals showed moderate expression of MMP-9. There was no distinct difference among treatment groups. Starved cells exhibited negligible MMP-9 expression.

4.2.4 Discussion

Green tea, the beverage made from the non-fermented leaves of *Camellia sinensis*, is one of the most ancient and widely consumed beverages in the world. Green tea polyphenols - the major constituent is EGCG, have demonstrated significant anti-oxidant, anti-carcinogenic, anti-mutagenic, anti-inflammatory, and anti-microbial properties (Fujiki et al., 1999) and has been proved as an effective chemopreventive agent for many types of cancer in animal models, including those involving tumors of the skin, breast, lung, liver, esophagus, stomach, small intestine, pancreas, and colon (Mukhtar et al., 1999). The anti-carcinogenic properties of green tea polyphenols are likely to be the result of many biological responses (Mukhtar et al., 1999). This includes the inhibition of urokinase activity, which is the enzyme crucial for cancer growth (Jankun et al., 1997). Also, EGCG could have potent inhibitory effect on VEGFR-2 activity (Lamy et al., 2002).

In this study, we consistently detected reduced HUVEC proliferation and migration by EGCG at the sub-toxic dose of 50 μ M. The effect was even stronger than that of Avastin within 24 hours of examination. Indeed, when comparing between different selected herbal chemicals (ISL, EGCG and Rst), EGCG at 50 μ M demonstrated the best efficacy in reducing the HUVEC migration. Fassina and colleagues also re-

ported significant inhibition of endothelial cell migration for 50 μM EGCG ($P < 0.001$) and for 100 μM EGCG ($P < 0.0001$) (Mann-Whitney U test) (Fassina et al., 2004).

In this study, proliferating HUVECs at half confluence were recruited to illustrate the suppressive effect of EGCG on endothelial cell growth and migration. Phospho-Akt level was reduced after 50 μM EGCG treatment to HUVECs with VEGF supplementation. EGCG was also demonstrated to inhibit tube formation probably mediated through the suppression of VE-cadherin tyrosine phosphorylation and inhibition of Akt activation (Tang et al., 2003). This indicates that VE-cadherin and Akt activation, which are the known downstream events in VEGFR-2-mediated cascade, are the potential targets of green tea catechins to effect in inhibiting endothelial cell growth and migration.

Furthermore, MMP-2 expression and its proteolytic activation were also reduced by EGCG. MMPs play an important role in tumor invasion, angiogenesis and inflammatory tissue destruction (Dollery et al., 2006; Nagase et al., 2006). EGCG has shown with anti-invasive property as a potent inhibitor of gelatinases (including MMP-2 and MMP-9), which are enzymes associated with tumor invasion and are frequently over-expressed in cancer (Garbisa et al., 1999; Maeda-Yamamoto et al., 1999; Demeule et al., 2000; Garbisa et al., 2001) and inflammation (Corbel et al., 2002). EGCG inhibited type IV collagenases at low concentrations (MMP-2 and to a slightly lesser extent for MMP-9) with IC_{50} values that were about the levels detected in the serum of moderate green tea drinkers. This suggests another mechanism mediated by EGCG in prevent or treating tumor development. A dose-dependent decrease of MMP-2 production and release in vascular tumor cells was reported after treatment with EGCG and a complete inhibition was achieved at 100 μM level (Makimura et al., 1993).

In this work, *in vivo* animal models of ocular angiogenesis were adopted to verify the *in vitro* findings. It is the first time to investigate the effect of EGCG in ocular angiogenesis of anterior and posterior segments. Silver nitrate cauterization-induced corneal NV with topical drug administration and laser photocoagulation-induced choroidal NV with intravitreal drug administration were conducted to demonstrate the effective suppression of NV by EGCG. On the other hand, EGCG also reduced the developmental blood vessel growth in chick CAM model. Altogether, the present work, for the first time, demonstrated NV suppression effect of EGCG in both developmental and pathological angiogenesis. High concentrations of EGCG in the range of 200~250 μM still demonstrate the safety when applied to cornea and intravitreal. There was no significant adverse effect in topically application of high concentration in mice eyes.

In chick CAM assay, which is the most widely employed *in vivo* model for studying normal vessel development, EGCG markedly and dose-dependently inhibited the development of capillary networks. The inhibitory effect of EGCG at 1 μM balanced the endogenous angiogenic effect of chick growth factors. When applied at doses higher than 5 μM (up to 250 μM in this assay) the growth of new and pre-existing blood vessels were effectively and dose-dependently regressed.

In a mice experiment of silver nitrate cauterization-induced corneal NV, EGCG when topically applied at concentration ≥ 1 μM demonstrated significant reduction in NV area in which new blood vessels were sprouted from pre-existing limbal capillary network. In the choroidal NV experiment, vascular leakage was decreased at the dose equivalent to the therapeutic dose of EGCG, verified through FFA examination and immunofluorescence of CD31 on choroidal flatmount. All these *in vivo* results were consistent with our earlier *in vitro* findings.

The mechanism of inhibition of angiogenesis by green tea or its catechins has not been well-established. A wide variety of mechanisms of action of green tea or green tea polyphenols have been proposed on diverse physiological or pathological situations. The conformation of catechin molecule seems to be crucial in its activity. It was shown that the steric structure of 3-*O*-gallate group is important to inhibit collagenase activity (Makimura et al., 1993). Catechins can scavenge free radicals through their polyphenol group (Mukhtar et al., 1999). Moreover, a pyrogallol-type B-ring structure is required to induce apoptosis, and a 3-*O*-gallate group in *cis*-configuration to the B ring could enhance this activity. Catechins without a pyrogallol-type structure showed no activity on cell apoptosis (Isemura et al., 2000).

EGCG has been reported to induce apoptosis and growth inhibition in a variety of tumor cell lines at doses from 20 to 100 μM . Inhibition of tyrosine kinase activity of growth factor receptors, such as epidermal growth factor receptor, platelet-derived growth factor receptor, and fibroblast growth factor receptor has been observed for EGCG with an IC_{50} of 1–2 μM in A431 human epidermoid carcinoma cells (Liang et al., 1997). Several studies have shown that EGCG at higher concentrations (5–100 μM) perturbed the downstream signaling, repressed the mitogen-activated protein kinase pathway, activator protein-1 and nuclear factor-B (Dong et al., 1997; Barthelman et al., 1998; Chen et al., 1999; Chung et al., 1999; Okabe et al., 1999; Sah et al., 2003; Ahn et al., 2004), although other studies have indicated EGCG could increase mitogen-activated protein kinase and activator protein-1 activity (Balasubramanian et al., 2002; Chen et al., 2003). Decreases in nitric oxide production by 1–10 μM EGCG was also observed, apparently caused by a reduction of inducible nitric oxide synthase gene expression (Chan et al., 1997). All these findings are associated with suppressing downstream signaling in the VEGFR2-mediated

cascade, contributing to inhibition of endothelial cell migration.

4.2.5 Conclusion

The present study demonstrated for the first time that EGCG, a natural polyphenol derived from green tea, suppressed new blood vessel growth and formation in both *in vitro* and *in vivo* neovascularization models. The action could be related with a suppression of VEGF downstream signaling in the VEGFR2-mediated cascade. Even though additional effort is still needed to verify the action of EGCG in suppressing neovascularization, the present findings can shed light on the application of EGCG in ocular neovascularization diseases. This potential therapeutic usage could be efficient and at low cost with minimal side effect to assist the conventional anti-cancer and anti-angiogenesis therapies.

4.3 Effect of resveratrol in ocular angiogenesis

4.3.1 *In vitro* studies

4.3.1.1 *Cytotoxicity by MTT Assay*

Treatment with Rst at concentrations from 2.5 to 50 μM reduced RPE cell proliferation (**Figure 35**). When cells were treated for 5 days with doses below 20 μM , the proliferation was reduced by about one fifth, compared to the untreated control (2.5 μM : reduced by 2%; 10 μM : by 12% and 20 μM : by 17.7%). More reduction of cell viability was found for 25 and 50 μM Rst treatments (reduced by 38% for 25 μM and 68% for 50 μM).

4.3.1.2 *Effect on HUVEC migration*

To test if Rst (5 to 20 μM) affects VEGF-induced HUVEC growth and migration. Compared to VEGF control, Rst at 10 to 15 μM reduced HUVEC growth and migration to the denuded area (**Figure 36**), whereas 5 μM had negligible effect. For the treatment with 10 μM Rst, 18.2 ± 6.5 cells was observed per mm^2 wound area. This was similar to that of Avastin control (18.4 ± 4.2 per mm^2). This dose of 10 μM Rst could have potential anti-angiogenic activity.

4.3.2 *In vivo* angiogenesis studies

4.3.2.1 *Suppression of developmental vessel growth in chick CAM assay*

Six concentrations of Rst (0.1, 0.5, 2, 10, 50, 100 μM) were tested in the gela-

tin-sponge chick CAM model. Recombinant human VEGF165 was also tested as the positive control to induce vessel growth towards the sponge. Gelatin sponge with BSS vehicle served as the blank control. Sponge containing 0.6 μg polyclonal anti-VEGF antibody or Avastin (75 μg) were the negative control, respectively (**Figure 6**). After incubation of fertilized eggs for 8 days, the progression of chick CAM blood vessels was monitored by a micrograph imaging under stereomicroscopy at 0 and 24 hours (day 9 post-fertilization). The number of CAM vessels converging towards the edge of gelatin sponge was quantified. Vessel index was obtained by the difference of vessel converging on the sponge at 24-hour interval compared to that of 0-hour, then divided by vessel number of 0-hour. Application of sponge with 60 ng recombinant human VEGF resulted in a dense appearance of new blood vessels converging towards the gelatin sponge (**Figures 6C, 6D**). The quantification showed that at lower Rst concentration (0.1, 0.5 and 2 μM) (**Figure 37**), there was no distinct suppression of chick embryonic blood vessel growth when compared to the BSS control. The vessel indices were 0.65 ± 0.23 for 0.1 μM Rst, 0.51 ± 0.19 for 0.5 μM Rst and 0.42 ± 0.26 for 2 μM Rst, respectively (n=11 in each group) and the control was 0.95 ± 0.12 (n=18) ($P > 0.05$, one way ANOVA test) (**Figure 38**). Rst at concentration $\geq 10 \mu\text{M}$ reduced the number of CAM blood vessels (the vessel index for 10 μM was 0.31 ± 0.1 , 50 μM was 0.18 ± 0.24 , n=11 in each group) ($P < 0.05$, one way ANOVA test). Rst at 100 μM concentration showed disappearance of chick CAM vessel and the index was -0.04 ± 0.07 (n=11) ($P < 0.01$, one way ANOVA test). Application of sponge with 60 ng recombinant human VEGF165 resulted in an appearance of new vessels, and the index was about 2 folds as that of the BSS blank control (**Figure 38**). Use of polyclonal anti-VEGF antibody (0.6 μg) significantly suppressed CAM vessel growth (0.11 ± 0.06 , n=12, $P < 0.05$, one way ANOVA test). Treatment of

Avastin showed similar chick CAM blood vessel number change as that of BSS control (**Figure 38**).

4.3.2.2 Suppression of silver nitrate cauterization induced corneal neovascularization

As a common route of administration for treating corneal surface disorders, Rst (ranging from 0.5 to 50 μM) was applied topically on the injured corneal surfaces at a standard 4 times daily. The corneal neovascularization was induced by scraping of the central 2-mm corneal epithelium combined with silver nitrate cauterization in BALB/c mice. After injury, the mice were randomly divided into 6 groups with 10 mice each and received Rst eyedrops for a total of 14 days. Topical BSS was employed as control. Half of mice in each group were sacrificed at day 7 (**Figure 39**) and the remaining at day 14 (**Figure 42**). The corneas were harvested for immunofluorescence of with anti-PECAM-FITC conjugate (**Figure 40, 43**), which specifically marks the vascular endothelial cells. The extent of corneal neovascularization was represented as the percentage of NV area in the whole corneal surface area restricted by the limbal vasculature.

In BSS control corneas, the onset of peripheral NV was observed at day 2 after injury. The vessels grew towards the central cornea and reached the center by day 14. Elevated pannus indicating a disruption of corneal epithelium was found on some corneal surface.

In Rst treatment groups, the extent of corneal NV justified by the percentage of NV area changes was suppressed by Rst at doses $\geq 1\mu\text{M}$, applied at 4 times daily for 7 days. Rst at $0.5\mu\text{M}$ showed similar level of new corneal blood vessel formation and growth as BSS control group. The ratio of corneal NV area was 0.5 ± 0.07 (mean

\pm SEM) in 0.5 μ M Rst treated group (n=5), and BSS control group was 0.57 \pm 0.05 (n=5) (P=0.259>0.05, one-way ANOVA test). Topical application of Rst \geq 1 μ M suppressed corneal NV formation and growth, with a level about one half as the BSS control (0.25 \pm 0.06 for 1 μ M Rst, 0.22 \pm 0.01 for 2 μ M Rst, 0.26 \pm 0.02 for 10 μ M Rst and 0.31 \pm 0.03 for 50 μ M Rst, respectively (n=5 in each group). The regression was considered as significant (P<0.001, one-way ANOVA test), when compared with BSS control groups (**Figure 41**).

Similar observation of Rst action on corneal neovascularization was resulted at day 14 of treatment. For the BSS control group, the NV area expanded to about 75% of whole corneal surface area (0.74 \pm 0.05, n=5). The corneal NV area was moderately reduced for 0.5 μ M Rst treatment (0.57 \pm 0.15, n=5) (P=0.063, one-way ANOVA test, compared with the control group). In 1 μ M Rst treatment group, the NV area reached about 1/3 of whole corneal surface area, indicating a suppressive effect of corneal NV (P < 0.001, n=5, one-way ANOVA test). For concentrations \geq 2 μ M, Rst substantially reduced the NV area to about 20% of whole corneal area. It was 0.2 \pm 0.03 for 2 μ M Rst, 0.21 \pm 0.04 for 10 μ M Rst and 0.22 \pm 0.01 for 50 μ M Rst, respectively (n=5 in each treatment group) (P<0.001, one-way ANOVA test) (**Figure 44**).

4.3.2.3 Suppression of laser-induced choroidal neovascularization

As a common route of administration for treating retinal vessel disorders, Rst was applied intravitreally once at time immediately after laser injury. C57B/L mice with 3 spots of laser injury induced in both eyes were randomly divided in 4 groups (3 mice in each group) and received intravitreal Rst as treated eyes and intravitreal BSS as control eyes. The laser-injured lesions (n=9) were monitored at day 4, 7 and 10 by fundus fluorescein angiography. At day 10, all mice were sacrificed and chor-

oidal NV was detected by immunofluorescence with isolectin-B4-FITC conjugate (**Figure 45**)

Three injection doses of Rst (20, 100 and 500 μ M) were selected, based on the reported mouse vitreal volume as 10 to 12 μ l (Heiduschka, et al., 2007) Since our intravitreal injection volume was kept to a minimal of 1 μ l to prevent post-injection ocular hypertension and associated ocular injuries, the injection dose was adjusted to 10 times higher in concentration. Hence the injection doses of 20, 100 and 500 μ M will be converted to the working doses inside the vitreous of 2, 10 and 50 μ M, respectively.

Fluorescein leakage in lesions The mice were examined by FFA at day 4, 7 and 10 (representative FFA images shown in **Figure 45**), and the percentages of leakage grading for each treatment group are shown in **Figure 46**. At day 4, grade 4 lesion was more prevalent in BSS control mice (about 67% of lesions) but not frequently shown in Rst mice. All lesions were scored as grade 2 after 10 μ M Rst treatment and 78% and 89% of lesions were respectively scored below grade 2 after 2 μ M and 50 μ M Rst treatments. On the contrary, the BSS group exhibited bright fluorescein leakages in all lesions (scored as grade 3 and 4).

For day 7 FFA examination, grade 4 lesion was identified in 78% of BSS group and all of them showed complete leakage at the late examination stage (> 5 min) and scored as \geq grade 3., About 11% lesions were scored as grade 4 in mice having intravitreal 2 μ M Rst. When compared to day 4 examination, there was an increased NV severity as noted by higher percentages of lesions with grade 3-4 scoring (2 μ M Rst: 55% at day 7 versus 22% at day 4; 10 μ M Rst: 33% at day 7 versus 0% at day 4 and 50 μ M Rst: 33% day 7 versus 11% at day 4).

At day 10, the choroidal NV in different treatment groups was similar as that in

day 7. There was no specific change in the percentage of NV lesion grades, indicating the healing or recovery process became stable (**Figure 46**).

Choroidal neovascularization area analysis At day 10, the mice were sacrificed and choroidal NV area detected by immunofluorescence with isolectin-B4-FITC conjugate was measured by Image J. In BSS control eyes, the NV area was 14847 ± 1074 pixels (n=9). This was reduced to 7468 ± 1110 pixels for intravitreal $2 \mu\text{M}$ RST ($P < 0.001$, compared to BSS control, one-way ANOVA test), 6002 ± 1009 pixels for $10 \mu\text{M}$ Rst ($P < 0.001$) and 4665 ± 1171 pixels for $50 \mu\text{M}$ Rst treatment ($P < 0.001$), respectively (**Figure 47**).

4.3.3 Protein analysis

4.3.3.1 VEGF expression (Figure 48)

Western blotting and band densitometry analysis followed by the normalization of specific band intensity with housekeeping GAPDH intensity, a lower VEGF expression was observed in HUVEC under serum-free and growth factor-free starvation (sample 2) when compared to HUVEC in normal culture (sample 1). Supplementation of VEGF165 (20 ng/ml) induced a higher cellular VEGF level in sample 3. Simultaneous addition of Avastin ($312 \mu\text{g/ml}$, sample 4), on the other hand, effectively suppressed cellular VEGF expression ($P < 0.005$, paired Student's t-test). However, incubation with Rst ($10 \mu\text{M}$, sample 6) did not result in a significant change of VEGF level in HUVECs.

4.3.3.2 PEDF expression analysis (Figure 48)

By Western blotting and band densitometry analysis followed by normalization

of specific band intensity with housekeeping GAPDH, moderate PEDF expression was observed in HUVEC under normal culture condition (full medium, sample 1), starvation (sample 2), VEGF-supplementation (sample 3), treatment with VEGF and Avastin (312 $\mu\text{g/ml}$, sample 4) and Rst (10 μM , sample 6).

4.3.3.3 Akt activation assay (Figure 49)

By Western blotting of phospho-Akt and pan-Akt followed by band densitometry analysis, Akt activation level was represented as the percentage of phospho-Akt in pan-Akt. For HUVEC under normal culture condition (full medium, sample 1), more than 80% of Akt was active. Upon starvation (sample 2), there was a slight reduction of pan-Akt and, in particular, the active Akt level was reduced to about 38%. Supplementation of VEGF (20 ng/ml, sample 3) brought up the Akt expression level and the percentage of active Akt to that of normal cells. In Rst (10 μM) treatment, a significant reduced level of active Akt (down to 24% of total Akt) was observed (sample 6).

4.3.3.4 Pan-Akt expression (Figure 49)

By Western blotting of pan-Akt and band densitometry followed by normalization with that of housekeeping GAPDH, pan-Akt expression in HUVEC was changed upon various treatments. When compared to cells supplemented with VEGF only, a reduction of Akt expression was observed when cells were treated for 24 hours with VEGF and Avastin (312 $\mu\text{g/ml}$, reduced by 40%) or with Rst (10 μM , reduced by 37%).

4.3.3.5 FAK activation assay (Figure 50)

The starved HUVEC was treated with Avastin (312 µg/ml) or 10 µM Rst, in the presence of 20 ng/ml VEGF, for 24 hours. Western blotting of soluble cell lysates showed very low expression of FAK and phospho-FAK in starved cells before treatment. In cells incubated with VEGF, FAK was stimulated for more than 10 folds when compared to starved cells. The expression of phospho-FAK (Y576/577) was ~20% of total FAK. This level was unchanged in Avastin. However, Rst (10 µM) substantially reduced FAK expression by about 30% as compared to VEGF-only cells and ~20% was phosphorylated.

4.3.3.6 MMP-2 expression (Figure 51)

In normal culture condition, the proliferating HUVECs (sample 1) had predominant expression of proteolytically active MMP-2 (55~60 kDa). After starvation, most MMP-2 remained inactive as pro-MMP-2 with molecular size of ~65 kDa and negligible active MMP-2 was observed (sample 2). Starved cells supplemented with VEGF (sample 3) showed about 20% active MMP-2. Similar levels were also observed for cells with Avastin (312 µg/ml) (sample 4). However, cells treated with Rst (10 µM) (sample 6) had almost negligible expression of both pro- and active MMP-2. Similar result was observed in duplicated experiments.

4.3.3.7 MMP-9 expression (Figure 51)

Western blotting analysis showed the specific MMP-9 immunoreactive band at ~100 kDa position. Except the starved cells, all cells with or without treatment with Avastin or different herbal chemicals showed moderate expression of MMP-9. There was no distinct difference among treatment groups. Starved cells exhibited negligible

MMP-9 expression.

4.3.4 Discussion

Resveratrol (Rst) is a polyphenolic phytoalexin naturally occurring in various plants, including red wine, grapes, berries and peanuts and other 70 other plants. It possesses diverse biochemical and physiological actions, and exhibits pleiotropic health beneficial effects, including anti-oxidant, anti-inflammatory, cardioprotective and anti-tumor activities (Bauer et al., 2005). Rst has been widely investigated for its cardioprotective properties (Das et al., 2006). It also exhibits anti-cancer characteristics, and suppresses the proliferation of various types of tumors, including lymphoid and myeloid cancers, multiple myeloma, melanoma, cancer of breast, ovary, cervix, prostate, stomach, colon, pancreas, and thyroid and head and neck squamous cell carcinoma (Aggarwal et al., 2004). Rst is also reported to affect cell growth, which is mediated through an induction of cell-cycle arrest by the up-regulation of p21^{Cip1/WAF1}, p53 and Bax as well as down-regulation of survivin, cyclin D1, cyclin E, Bcl-2, Bcl-x and cIAPs (Aggarwal et al., 2004). This results in cell death via the activation of caspases. Moreover, Rst suppresses the trans-activation activity of different transcription factors, including NF- κ B, AP-1 and Egr-1 to modify global gene expression (Aggarwal et al., 2004). In particular, it has been shown to inhibit the levels of protein kinases in various pathways, such as JNK, MAPK, Akt, protein kinase C/D and casein kinase II, which are associated with cell survival, metabolism and proliferation (Aggarwal et al., 2004). Moreover, it plays an important role in regulating angiogenesis, vascular and inflammatory activities, through its effect on various gene expressions, including that of COX-2, 5-LOX, VEGF, IL-1, IL-6, IL-8 and PSA (Aggarwal et al., 2004). Recently, it has been reported to inhibit the proliferation and

migration of vascular endothelial cells by its activation of eukaryotic elongation factor-2 kinase, which in turn phosphorylates and inactivates the elongation factor-2, which is a key mediator of ribosomal transfer and protein translation (Khan et al., 2010). Functional inhibition of kinase activity by gene deletion *in vivo* or siRNA as well as pharmacological inhibition *in vitro* completely reversed the effect of Rst on blood vessel growth and endothelial cell proliferation.

It is becoming increasingly clear that Rst has two faces. It can protect cells by potentiating a survival signal whereas it can selectively kill cancer cells. Rst is shown to act as an anti-oxidant, yet it can induce redox signaling. It is an anti-proliferative agent for cancer cells and induces apoptosis and sensitizes cancer cells by inhibiting cell survival signal transduction and anti-apoptotic pathways. In contrast, Rst triggers a cell survival signal in ischemic tissue by inducing anti-apoptotic genes and blocks the apoptosis. At lower doses, Rst can stimulate angiogenesis, while it can lock angiogenic response at higher doses (Das et al., 2006). In my study, Rst at 100 μM balanced with the endogenous angiogenic factor in chick CAM model and the vessel index was 0. When Rst was tested at concentration $>2 \mu\text{M}$, it show substantial suppression on angiogenesis in corneal NV as well as and choroidal NV assay models.

One possible reason for this dichotomy of Rst action could be due to its wide-ranging differences in tissues in pharmacokinetics, bioavailability, and metabolism. At a concentration at or below 0.1 μM , Rst has been -mediated expression of intracellular adhesion molecules and shown to inhibit TNF- such as ICAM-1 (Ferrero et al., 1998). At a concentration of 1 nM, it induces the phosphorylation of ERK1/2, whereas at higher concentration of 50–100 μM , it inhibits MAPK phosphorylation (Miloso et al., 1999).

The angiogenic process is controlled by two major pro-angiogenic factors,

MMPs, which degrade extracellular matrices, and VEGF, which stimulates endothelial cell migration and proliferation and the formation of new blood vessels. The strength of this study was to show the first *in vivo* evidence that Rst dose-dependently suppressed new vessel growth and formation in both developmental and pathological angiogenesis models.

In the CAM assay demonstrating developmental or regulated angiogenesis, the most widely employed *in vivo* model for studying vessel development, Rst dose-dependently suppressed the development of capillary network. The inhibitory effect of 100 μM Rst was able to counteract with the endogenous growth factors in the chick CAM environment, resulting in a null change of vessel number. Rst at doses between 2 to 100 μM could moderately attenuate the vessel growth, causing a slower rate of vessel development. Lower dose of Rst ($<1 \mu\text{M}$) did not show any significant interference on the blood vessel patterning. When compared with ISL and EGCG, Rst was less effective to suppress chick CAM development. In the mouse silver nitrate cauterization-induced corneal NV model, the NV regression was also not as effective as ISL and EGCG. Moderate prevention to vessel growth was demonstrated in RST ($\geq 1\mu\text{M}$) topical treatment, but no complete prevention of NV development was found even higher doses of Rst (50 μM) was applied.

In the laser-induced choroidal NV assay, Rst was found to suppress the NV progression at early examination interval (day 4) but not in later time points (day 7 and 10). At day 4, the optimal preventive effect was observed in 10 μM treatment. This was abrogated at day 7 and 10, with an increased percentage of lesions having more severe NV grades. Similar increase of NV severity was also found for other tested doses. This indicates that, in addition to the less effective action of Rst on anti-angiogenesis, the single injection of Rst might not be able to exhibit a long-lasting

effect to suppress NV development.

VEGF is a major angiogenic molecule in the neovascularization formation. Increased VEGF levels have been shown to be a common pathologic factor in neovascular diseases, including ocular neovascular disorders of humans, as well as induced ocular angiogenesis in the animal model (Amano et al., 1998). It is evident that there is a delicate balance between angiogenesis stimulators and inhibitors, which are crucial in maintaining vasculature homeostasis. As an example, hypoxia occurring in inflammation and traumatic injury in cornea and choroids usually accompanies with altered expression of these molecules. The overproduction of angiogenesis stimulators and reduced level of inhibitors disrupts the homeostatic balance and results in NV development.

In this study, Rst treatment in half-confluent HUVEC did not show any change of intracellular VEGF and PEDF expressions. However, it suppressed endothelial cell growth and migration *in vitro* and neovascularization *in vivo*. By protein analysis, treatment with Rst at 10 μ M reduced Akt activation, as shown by a lower percentage of phosphorylated Akt in total Akt level. Akt activation is an important downstream event of receptor-mediated tyrosine kinase cascade. In spite of neutral influence on VEGF and PEDF expression, it is possible that Rst, with its small molecular mass, can penetrate inside cells and works to inhibit Akt phosphorylation. This could result in a widespread intracellular signaling effect to manifest the effect of Rst on cell migration or metabolism. Also, this could explain the short-term anti-angiogenesis effect of Rst. This could be due to the quick turnover and production of secondary messenger molecule in signaling pathways. Similar finding was reported before (Lin et al., 2003). Furthermore, the suppression of Akt activity by Rst was related to higher apoptosis in cancer treatment, such as ovarian, breast, uterine, and prostate cancer

cells and multiple myeloma cells (Cao et al., 2004; Garvin et al., 2006; Li et al., 2006; Sexton et al., 2006; Aziz et al., 2006).

Inhibition to FAK activation and reduced proteolytic activation of MMP-2 substantiated the effect of Rst on the anti-migratory mechanism in endothelial cells. MMPs, a family of zinc-binding, calcium-dependent endopeptidases that degrade the substrate proteins in the extracellular matrix, play an important role in angiogenesis. Specifically, the gelatinases (MMP-2 and MMP-9) degrade the components of basement membrane such as type IV collagen and fibronectin (Hudson et al., 2007). The inhibitory effect of Rst on MMP-2 expression was observed in lung cancer cell invasion and this was associated with HO-1-mediated NF-kappa B pathway (Bhardwaj et al., 2007). Moreover, it inhibited bovine aortic smooth muscle cell proliferation by blocking G1-S phase entry through a reduced expression of cyclins and cyclin-dependent kinases and this resulted in apoptosis (Gioia et al., 2009; Liu et al., 2010). Exposure of endothelial cells to Rst also led to a concentration-dependent reduction of MMP-2 gelatinolytic activity and marked inhibition of tube formation on matrigel (Poussier et al., 2005).

Rst has been reported to inhibit the expression of HIF-1 α and VEGF in OVCAR-3 cells through the inhibition of Akt and MAP kinases, inhibition of protein translational regulators, and enhancement of proteasomal degradation of HIF-1 α protein (Lee et al., 2005) as well as retarding tumor growth and angiogenesis in ER α /ER β (+) MDA-MB-231 breast tumor xenografts in nude mice and reducing extracellular levels of VEGF in vitro (Cao et al., 2005). Altogether, Rst, in addition to its chemopreventive effects, it also exhibits therapeutic activity against cancer through reduction of VEGF secretion and suppressing its downstream signaling pathway. However, there was no significant reduction of VEGF expression when

HUVECs were treated with 10 μ M Rst in this study. This could be attributed to the use of different cell types, tumor cells versus normal endothelial cells

The molecular mechanism of the *in vivo* anti-angiogenic properties of Rst is not completely clear, the findings in my study indicated that Rst may inhibit several key events of the angiogenic process, such as proliferation and migration of endothelial cells, and suppress downstream signaling in the tyrosine kinase-mediated cascade and this could associate with its inhibitory effect on endothelial cell migration and activation of MMP-2. This suggests an alternative pathway by which red wine polyphenol inhibits angiogenesis.

4.3.5 Conclusion

The present study demonstrated, for the first time, that resveratrol, a natural polyphenol phytoalexin derived from grape and red wine, suppressed angiogenesis both *in vitro* and *in vivo*, relating to the suppression of intracellular signaling in the tyrosine kinase-mediated cascade. Even though additional work is needed to fully understand the mechanisms of action of Rst, the present findings shed light on the application of Rst on ocular neovascular diseases.

CHAPTER 5

GENERAL CONCLUSIONS

This thesis describes an endeavor on the investigation of the anti-angiogenic properties of herbal molecules derived from natural sources. We studied the effects of ISL, EGCG and Rst *in vitro* and *in vivo* angiogenesis assays, especially on the ocular neovascularization in the anterior corneal part as well as the posterior choroidal segment. ISL is a natural flavonoid from licorice root, EGCG is a natural polyphenol from green tea and Rst is a natural polyphenol phytoalexin derived from grapes.

In vitro experiments were conducted and showed anti-angiogenic actions of these three herbal molecules: ISL up-regulated expression of PEDF (endogenic angiogenic inhibitor), and down-regulated VEGF (major angiogenic stimulator) secretion. EGCG and Rst share the similar mode of suppressing angiogenesis by inactivating VEGF downstream signaling cascade: Akt and FAK. AKT is an intracellular signal mediator for endothelial cell migration and survival and FAK can promote endothelial cell proliferation. EGCG and Rst also suppressed MMP expression which is an extracellular metalloproteinases played a major role in degrading endothelial cell membrane and promoting endothelial cell migration. *In vitro* HUVEC migration assay, results showed that these three herbal molecules suppressed VEGF stimulated HUVEC migration in nontoxic dosages dose-dependently, and ISL at 10 μ M, EGCG at 50 μ M and Rst at 10 μ M showed maximal inhibitory effect of endothelial cell migration. This is also set up the proof of principal for *in vivo* angiogenesis studies.

First screening for the suppressive effect of tested herbal molecules was performed by Chick CAM model which new blood vessels were formed under stimula-

tion of endogenic VEGF in chick embryo. We found the consistent suppressive effect on chick CAM new blood vessel formation were achieved by ISL at $\geq 2 \mu\text{M}$, EGCG at $\geq 1 \mu\text{M}$, and Rst at $\geq 10 \mu\text{M}$. ISL at $5 \mu\text{M}$, EGCG at $1 \mu\text{M}$ and Rst at $100 \mu\text{M}$ counteract the stimulatory effect of endogenic VEGF in Chick CAM, vessel index is 0, higher concentration than optimal dosages regressed preexisted blood vessels.

This further prompted us to test these molecules in the established *in vivo* animal models of corneal and choroidal neovascularization in mice eyes in order to shed light on the potential application for ocular NV diseases. These herbal molecules were applied as topical eye drops for chemical burn induced corneal NV model and intravitreal injections for controlling the neovascularization in laser induced choroid lesions respectively. We found that all of these three herbal molecules were effective in suppressing the ocular neovascular response in mice eyes. ISL, EGCG and Rst at as low as $1 \mu\text{M}$ concentration showed the suppressive effect on corneal NV and choroidal NV assays dose-dependently, the most optimal dosage was ISL at $10 \mu\text{M}$, EGCG at $50 \mu\text{M}$ and Rst at $10 \mu\text{M}$, matched with our *in vitro* most optimal doses of suppressing HUVEC migration--- ISL at $10 \mu\text{M}$, EGCG at $50 \mu\text{M}$ and Rst at $10 \mu\text{M}$.

In conclusion, our results showed that ISL, EGCG and Rst contributed to anti-angiogenesis via different biological mechanisms and also verified through our established *in vitro* and *in vivo* angiogenic assays. Natural molecules, therefore, can be used for suppression of abnormal ocular vascularization.

CHAPTER 6

FUTURE PROSPECTS

In the past few years, there have seen major breakthroughs in angiogenesis research, leading to an increased understanding of the pathophysiology. New tractable targets have been identified in key disease pathways, improving the prospects for development of disease-modifying drugs for some devastating disorders causing visual impairment.

The process of neovascularization provides possible targets for cognition enhancement. Some possible interventions that might enhance or repair visual function would be surgical rather than pharmaceutical. These include the use of limited macular translocation, or photodynamic therapy to block abnormal angiogenesis in the macular region. At the other extreme, intravitreal injection or topically application of small molecular anti-VEGF antibody might inhibit new blood vessel formation, are likely to be increasingly popular.

The future study will be mainly related to the development of therapeutic strategies that target the VEGF or prohibit endothelial cell migration and proliferation, or both. Various strategies are under study to use pharmacological therapy instead of surgical or photodynamic therapy.

In the future, biological effects of these three herbal molecules should be further explored in other experimental models, such as oxygen induced retinopathy model in order to detect their effect on retinal neovascularization, also evaluate their other biological effects, such as anti-oxidation and anti-inflammation, and cross interaction with anti-angiogenesis. They can also be combined with Avastin or other an-

ti-angiogenesis inhibitors for the studies of synergistic effects in preventing or reducing the formation of neovascularization, or test the combined effect of these three herbal molecules in inhibiting ocular neovascularization which aimed at different steps of the angiogenesis cascade. The safety and distribution of these three herbal molecules on ocular tissue or cells should also be studies.

Use of these alternative therapies of pharmacological intervention, or a combination of them, would be beneficial in treating devastating diseases of blindness caused by neovascularization. We will probably enter into an era of anti-angiogenic therapy in the near future, and thus alleviate the destructive side effects of current treatment modalities.

TABLES **Table 1: A summary of commonly used corneal neovascularization models**

<p>Silver nitrate cauterization (Mahoney, 1985; Wenk, 2003)</p>	<p>Apply AgNO₃ solution to center of corneal surface with an applicator stick (2-mm diameter) for 10 sec, followed by extensive rinsing with BSS</p>	<p>Easy & efficient, can perform to large no of animals. NV starts on 2nd day post-operation (PO) and peak at day 14</p>	<p>Acute inflammation, hypopyon, hyphema, frequent corneal edema.</p>	<p>1. Central corneal cauterization 2 Central (2-mm dia) de-epithelization 3 75% AgNO₃ /25% KNO₃ is better than 95% AgNO₃. 4. Time of cauterization</p>
<p>Alkali burn (Zhang, 2005; Couriers, 1997)</p>	<p>Apply filter disc soaked in 1 N NaOH to corneal surface for 1-2 minutes, then flush gently with BSS.</p>	<p>Easy & efficient, can perform to large no of animals. NV starts on 4th day PO and peak at day 14</p>	<p>Ulceration, excessive scarring and NV Not as efficient as AgNO₃ to induce NV.</p>	<p>1. Burns to central cornea position 2 Central (2-mm dia) de-epithelization 3 Time of alkali burn</p>
<p>Suturing (Bock, 2007; Samolov, 2008)</p>	<p>Place three 11-0 sutures intrastromally with 2 stromal incisions, each extending over 120° of corneal circumference</p>	<p>Mild & controllable inflammation. Efficient NV induction. NV starts on 2nd day PO and peak at day 14.</p>	<p>Stringent surgical technique, long training time, labor and time intensive.</p>	<p>1 Central (2 mm dia) de-epithelization 2. Firm and even suturing Suture detachment will lead to poor vessel growth 3 Best position of suture - mid-corneal radius</p>
<p>Corneal micropocket assay with implantation of VEGF or bFGF pellet (Fournier, 1981; Schwartz, 2008)</p>	<p>Create a 'pocket' in corneal stroma for the placement of slow release pellet or polymer containing angiogenic molecules.</p>	<p>Reliable and reproducible NV starts on day 3 PO</p>	<p>Stringent surgical technique, long training time, labor and time intensive</p>	<p>1. A 1.5-mm superficial incision is made in central cornea & a micropocket is created by bluntly separating the lamella of stroma 2 The distance between bottom of micropocket and limbus should be <1 mm.</p>
<p>Hemilimbal deficiency (HLD) (Lee, 2002; Javier, 2006)</p>	<p>1. Remove whole epithelium with or without half limbus 2. Remove half limbus with or without corneal epithelium</p>	<p>Easy to handle, but only the combined removal of half limbus and total corneal epithelium induces corneal NV. NV starts on day 4 PO.</p>	<p>Total epithelial debridement & half limbus and half corneal epithelium does not induce NV</p>	<p>Removal of half limbus and total corneal de epithelization</p>

Table 2 Commonly used Chick CAM model (Ribatti, D., 2000; Richardson, 2003; Auerbach, 2003)

Description	Embryos are left inside the eggshell during their development and for the duration of the assay.	After opening the eggshell, the embryo and its extraembryonic membranes are transferred to Petri or plastic dishes and further incubated outside the eggshell.
Advantages	<ul style="list-style-type: none"> ● The source of calcium for building skeletal elements is kept. ● High embryo survival rate. ● Easy methodology. ● Sterility is not required. ● Embryos can reach hatching. 	<ul style="list-style-type: none"> ● The source of calcium for building skeletal elements is kept. ● Evaluation of several samples in one single embryo. ● Easy grafting and monitoring of excised tissues. ● No eggshell falling on CAM. ● Easy access to CAM vasculature. ● Possibility of transillumination. ● In vivo observation of embryo development.
Disadvantages	<ul style="list-style-type: none"> ● Small surface is exposed. ● Difficult monitoring. ● Risk of angiogenesis induced by eggshell pieces. 	<ul style="list-style-type: none"> ● Difficult methodology (e.g. transfer the embryo to plastic dish, sterility requirements). ● Low embryo survival rate. ● Do not reflect physiological conditions. ● Embryos cannot reach hatching.

FIGURES

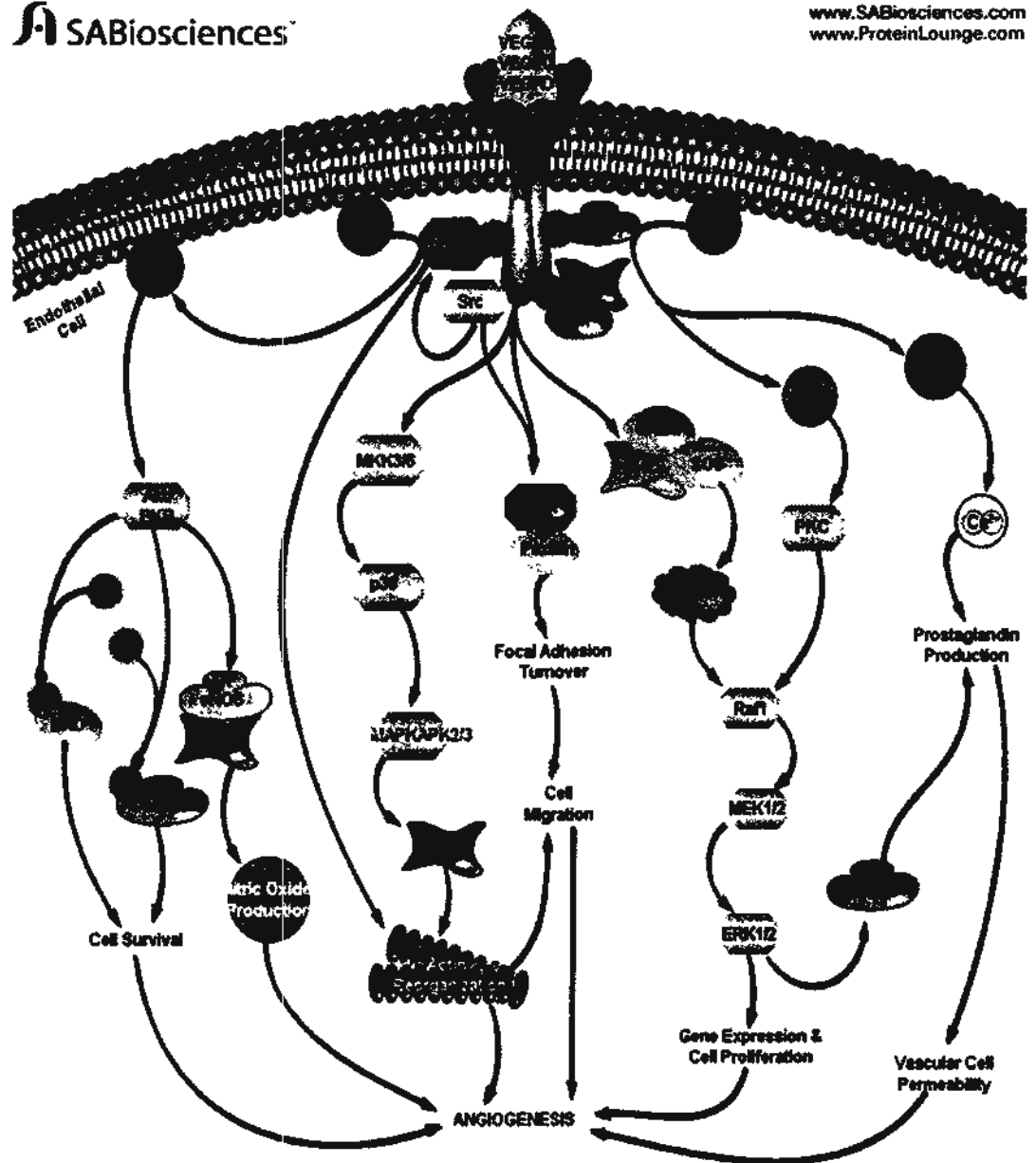


Figure 1: VEGF signaling pathway

Picture is adapted from SABiosciences, <http://www.SABiosciences.com>.

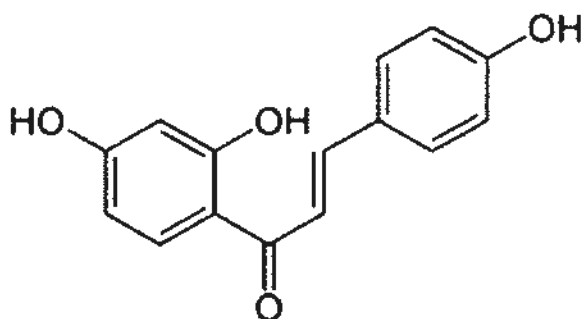


Figure 2: Chemical structure of Isoliquiritigenin.

Chemical name is 4,2',4'-trihydroxychalcone, or (E) -1 -(2,4-dihydroxyphenyl)-3-(4-hydroxyphenyl)-2-propen-1-one; $C_{15}H_{12}O_4$. Molecular mass is 256.25 g/mol. Picture is adapted from ChemBlink, <http://www.chemblink.com>.



Figure 3: Resources of isoliquiritigenin: licorice & licorice root

(Pictures are obtained from <http://www.flowers-cs.com> and www.naturesflavors.com)

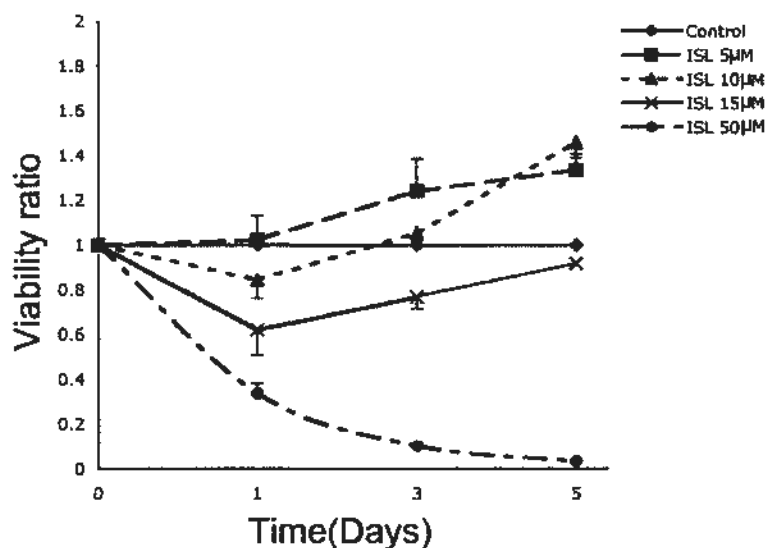


Figure 4: Effect of ISL on cell viability of ARPE-19 cells.

ARPE cells (7×10^3) were seeded and cultured in the presence of ISL (5, 10, 15 & 50 μM , respectively) for 1, 3, 5 days. Untreated cells were used as control. Cytotoxicity of ISL was evaluated by MTT assay. The cell viability was expressed as the ratio of cell under treatment / untreated control cells. Each concentration of ISL was tested in quadruplicate. ISL at 5 & 10 μM showed no inhibitory effect on ARPE cell growth, ISL at 15 μM showed mild cytotoxicity to ARPE cells and, ISL at 50 μM was cytotoxic.

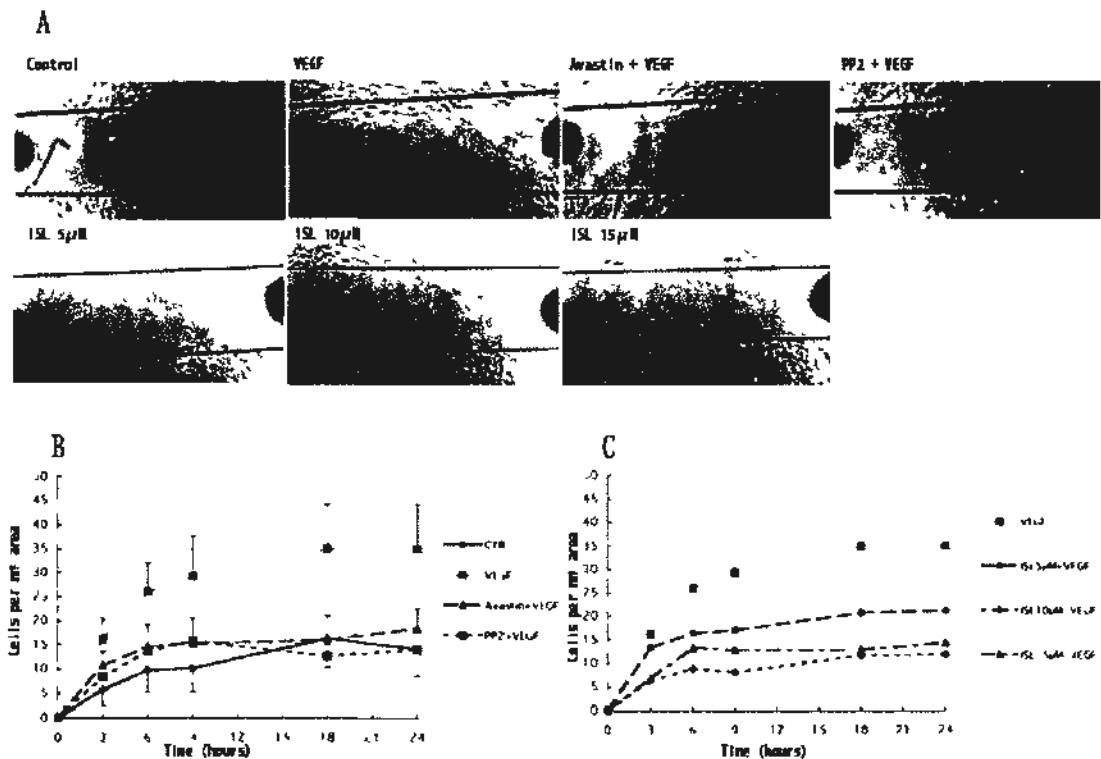


Figure 5: The inhibitory effect of ISL on VEGF-A-induced HUVEC migration in a scratch wound healing assay.

HUVECs grew to 100% confluence were scratched with a scraping tool, and treated with different concentration of ISL (5, 10 & 15 μ M) in the presence of VEGF165 (20 ng/ml). Untreated cells and cells treated with VEGF alone, Avastin (312 μ g/ml) or PP₂ (10 μ M) with VEGF added served as controls. Microphotographs of HUVECs in the denuded area were taken at different time points by phase-contrast microscopy using a 5x objective. Six images were captured for each treatment. HUVEC present in the denuded area were quantified and expressed as number of cells per mm² area. (A) Representative photographs after 24-hour treatment to assess HUVECs migration. (B) A time-dependent increase of HUVEC number in the denuded area in four control groups, compared to untreated cells. Avastin and PP₂ inhibited VEGF stimulated HUVEC migration. (C) A time- and dose-dependent suppression of VEGF-induced HUVECs migration by ISL treatment.

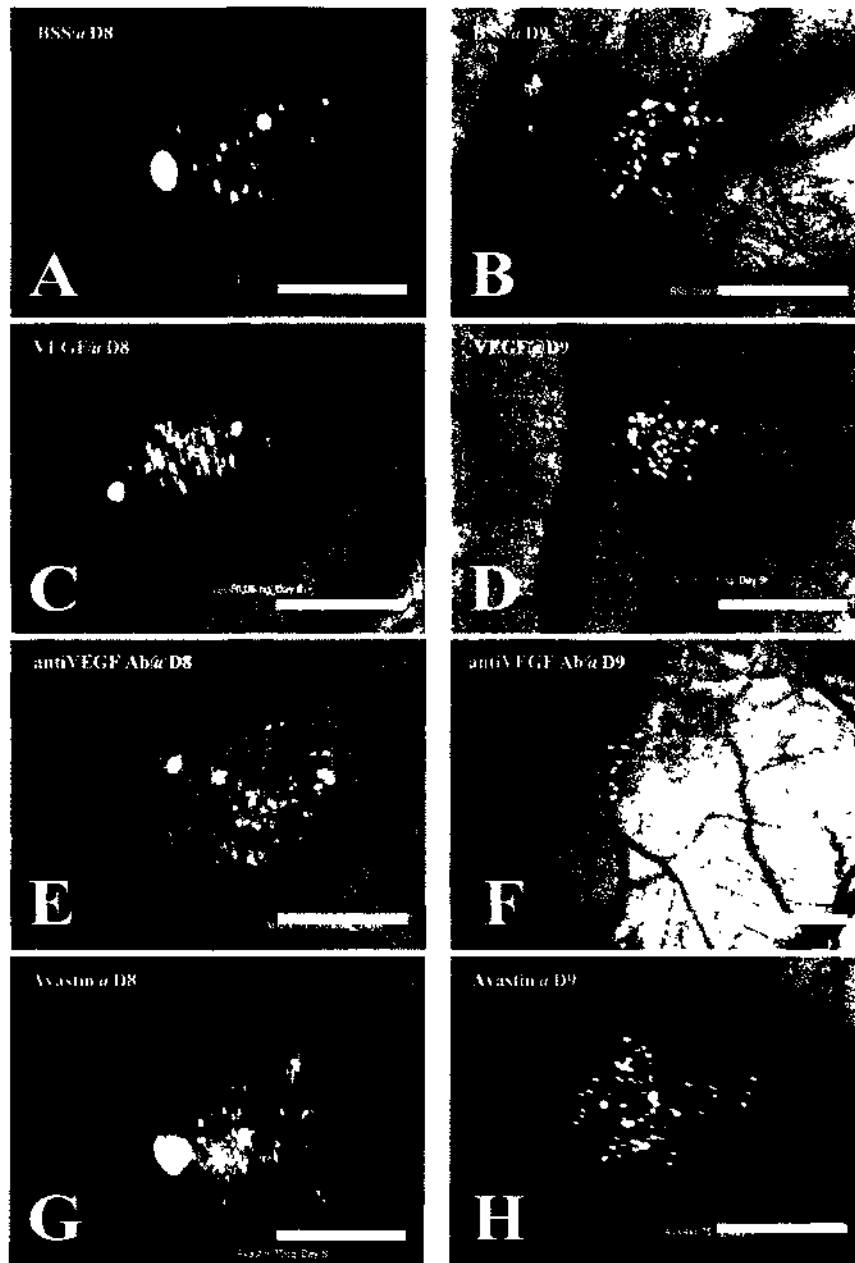


Figure 6: Morphological analysis of blood vessel changes of chick chorioallantoic membrane at 24 hours after treatments.

A and B. gelatin sponge with BSS showing blood vessels converging towards the sponge material; **C and D.** gelatin sponge with VEGF (60 ng); **E and F,** gelatin sponge with polyclonal anti-VEGF antibody (0.6 μ g); **G and H,** gelatin sponge with Avastin (75 μ g). Scale bars = 1 mm.

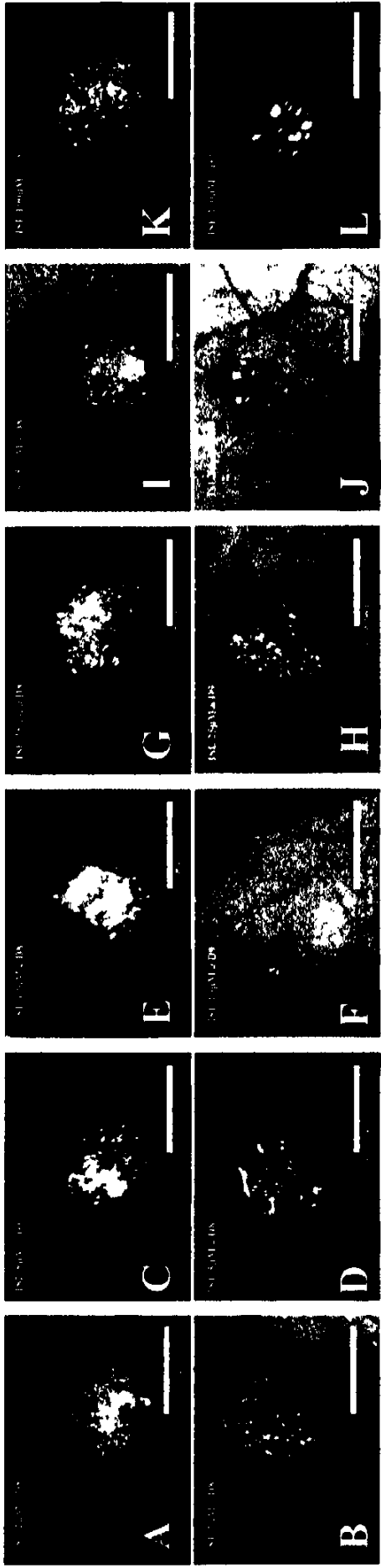


Figure 7: Representative photographs showing the effect of ISL on developmental chick chorioallantoic membrane assay at 24 hours after treatments.

A and B. 2 μ M ISL; C and D. 5 μ M ISL; E and F, 10 μ M ISL; G and H, 25 μ M ISL. I and J, ISL 50 μ M; K and L, 100 μ M ISL.

Scale bars: 1 mm.

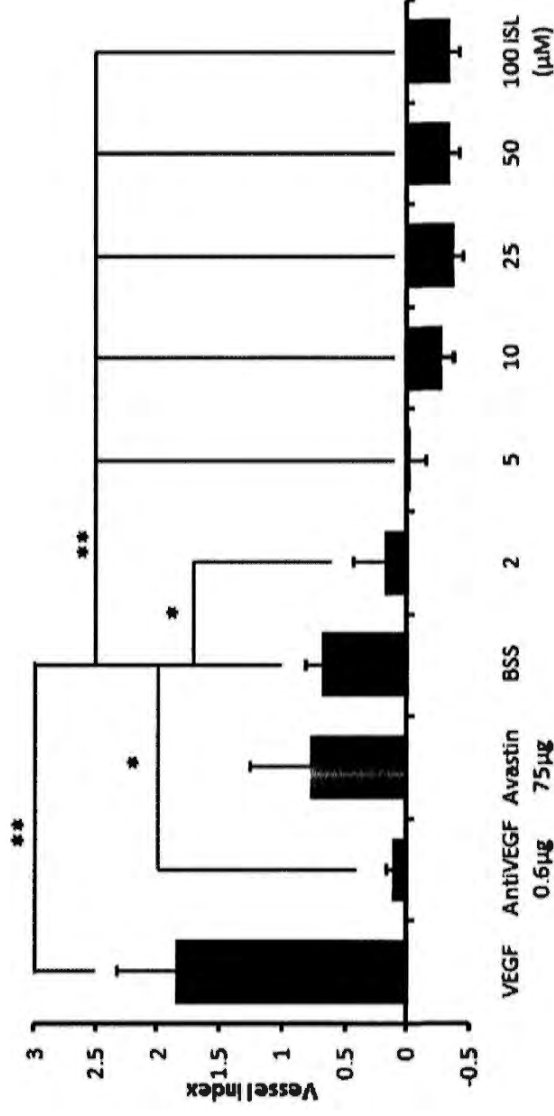


Figure 8: ISL suppressed blood vessel development in the gelatin-sponge chick chorioallantoic membrane assay.

Six concentrations (2, 5, 10, 25, 50, 100 µM) of ISL were tested. BSS only, VEGF (60 ng), polyclonal anti-VEGF antibody (0.6 µg) and Avastin (312 µg/ml) were recruited as control. Each drug was tested on a minimum of 10 sponges. The sequential photographs (0 and 24 hours) were taken using stereomicroscope (Figures 4, 5). Vessel numbers converging toward the gelatin sponge were recorded and CAM vessel number changes between 0 and 24 hours were quantified and represented as vessel index (mean ± S.E.M). The result showed that ISL suppressed CAM vessel development dose-dependently (* $p < 0.05$, ** $p < 0.01$, compared to BSS control group, one-way ANOVA test).

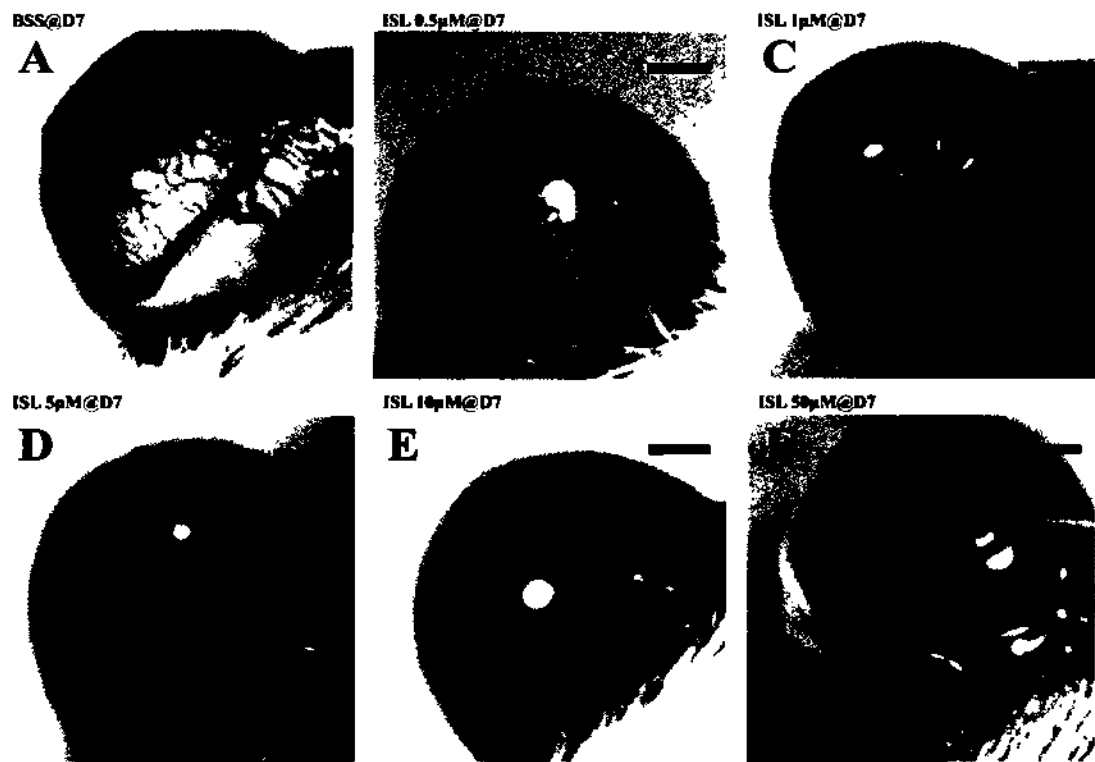


Figure 9: Effect of ISL corneal neovascularization development

Representative photographs of BALB/c mice corneas at 7 days after silver nitrate cauterization, followed by topical treatment with ISL (0.5, 1, 5, 10, 50 μM) four times daily. **A.** BSS control, new vessels grew extensively from limbal vasculature on the corneal surface towards the central region, **B.** 0.5 μM ISL; **C.** 1 μM ISL; **D.** 5 μM ISL; **E.** 10 μM ISL and **F.** 50 μM ISL. ISL at 0.5 μM started to shown suppressive effect on corneal NV formation. When ISL was topically applied at $\geq 1 \mu\text{M}$, effective suppression of corneal NV growth was observed. Scale bars = 1 mm.

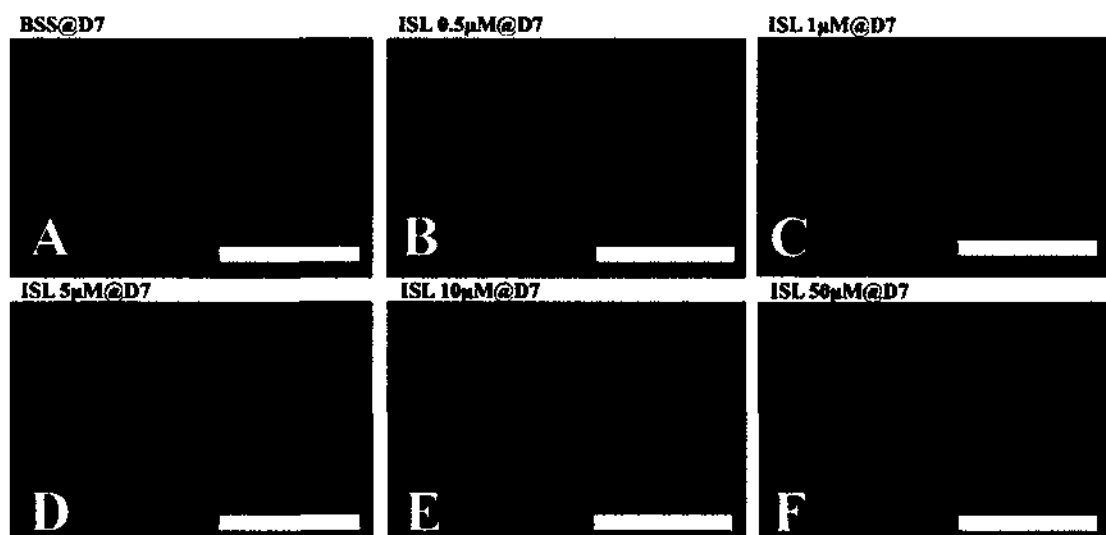


Figure 10: Effect of ISL on blood vessel manifestation in corneal neovascularization assay

Representative segments from corneal flat mounts immunostained with monoclonal anti-PECAM-FITC conjugate after topical treatment with ISL for 7 days. **A.** BSS control. **B.** 0.5 μ M ISL; **C.** 1 μ M ISL; **D.** 5 μ M ISL; **E.** 10 μ M ISL and **F.** 50 μ M ISL. Scale bars = 1 mm.

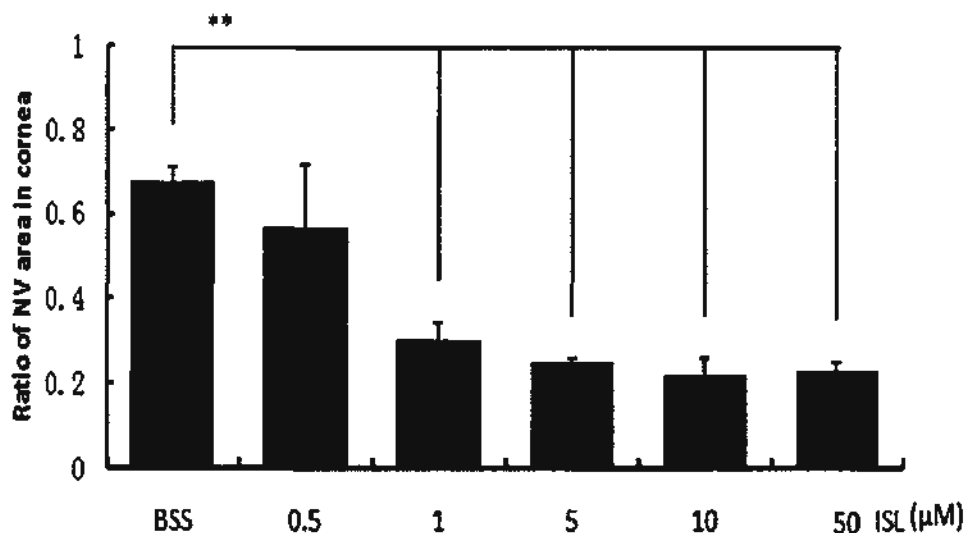


Figure 11: Suppression of neovascularized area after ISL treatment for 7 days.

The vascularized area on mice corneas revealed by immunostaining with monoclonal anti-PECAM-FITC conjugate was quantified and expressed as a ratio to the total corneal surface bordered by limbal vasculature. The result was represented as mean \pm S.E.M. (error bars). A dose-dependent suppression of corneal NV formation and growth was observed for ISL treatment. ISL at ≥ 1 μM effectively suppressed corneal NV. * $P < 0.05$, ** $P < 0.01$ (one-way ANOVA Test), compared to BSS control.

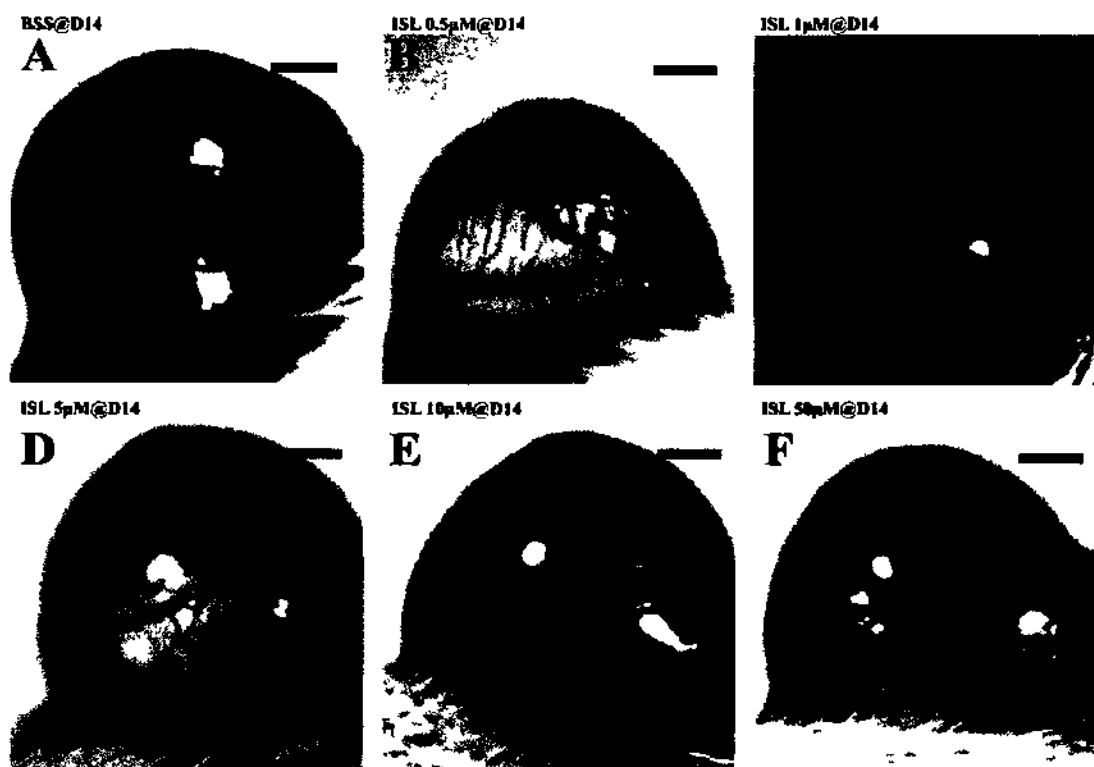


Figure 12: Effect of ISL corneal neovascularization development

Representative photographs of BALB/c mice corneas after silver nitrate cauterization, followed by topical treatment with ISL (0.5, 1, 5, 10, 50 μM) four times daily for 14 days. A. BSS control, new vessels grew extensively from limbal vasculature on the corneal surface towards the central region, B. 0.5 μM ISL; C. 1 μM ISL; D. 5 μM ISL; E. 10 μM ISL and F. 50 μM ISL. ISL at 0.5 μM started to shown suppressive effect on corneal NV formation. When ISL was topically applied at ≥ 1 μM , effective suppression of corneal NV growth was observed. Scale bars = 1 mm.

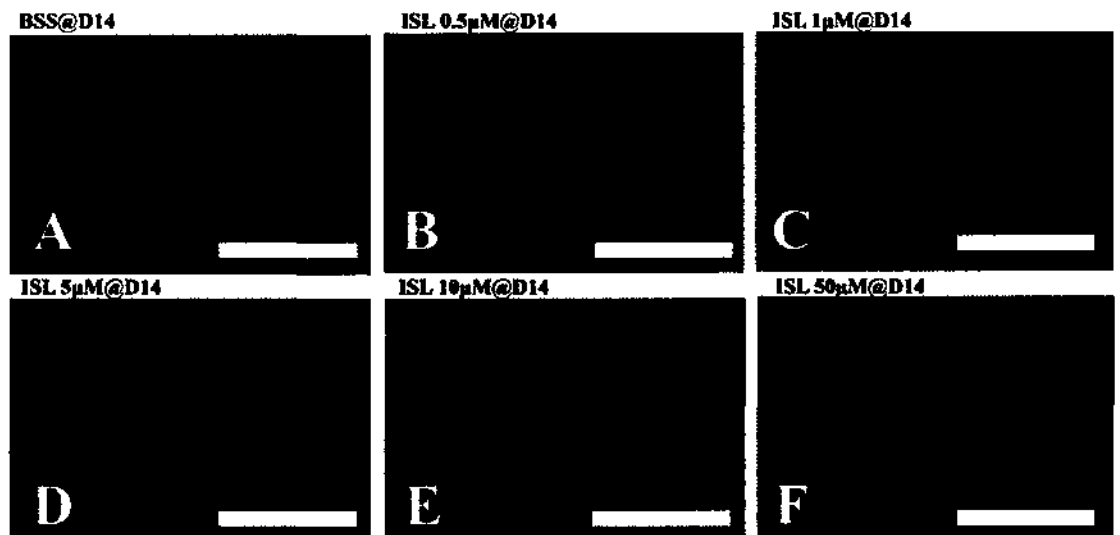


Figure 13: Effect of ISL on blood vessel manifestation in corneal neovascularization assay

Representative segments from corneal flat mounts immunostained with monoclonal anti-PECAM-FITC conjugate after topical treatment with ISL for 14 days. **A.** BSS control. **B.** 0.5 μM ISL; **C.** 1 μM ISL; **D.** 5 μM ISL; **E.** 10 μM ISL and **F.** 50 μM ISL. Scale bars = 1 mm.

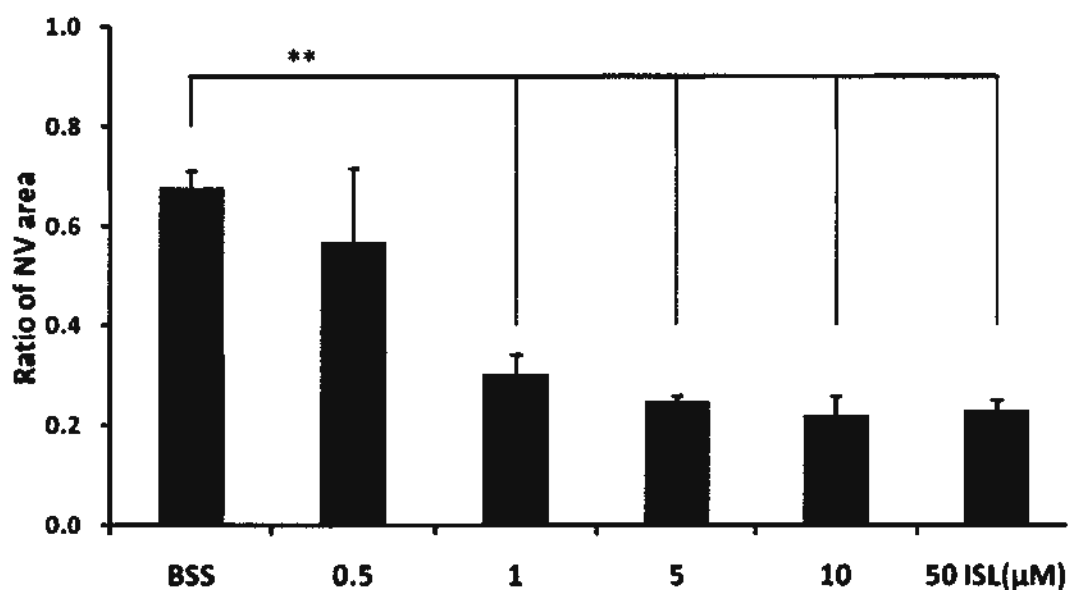


Figure 14: Suppression of neovascularized area after ISL treatment for 14 days.

The vascularized area on mice corneas revealed by immunostaining with anti-PECAM-FITC conjugate was quantified and expressed as a ratio to the total corneal surface bordered by limbal vasculature. The result was represented as mean \pm S.E.M. (error bar). A dose-dependent suppression of corneal NV formation and growth was observed for ISL treatment. ISL at ≥ 1 μM effectively suppressed corneal NV. * $P < 0.05$, ** $P < 0.01$ (one-way ANOVA test), compared to BSS control.

Fundus Fluorescence Angiography

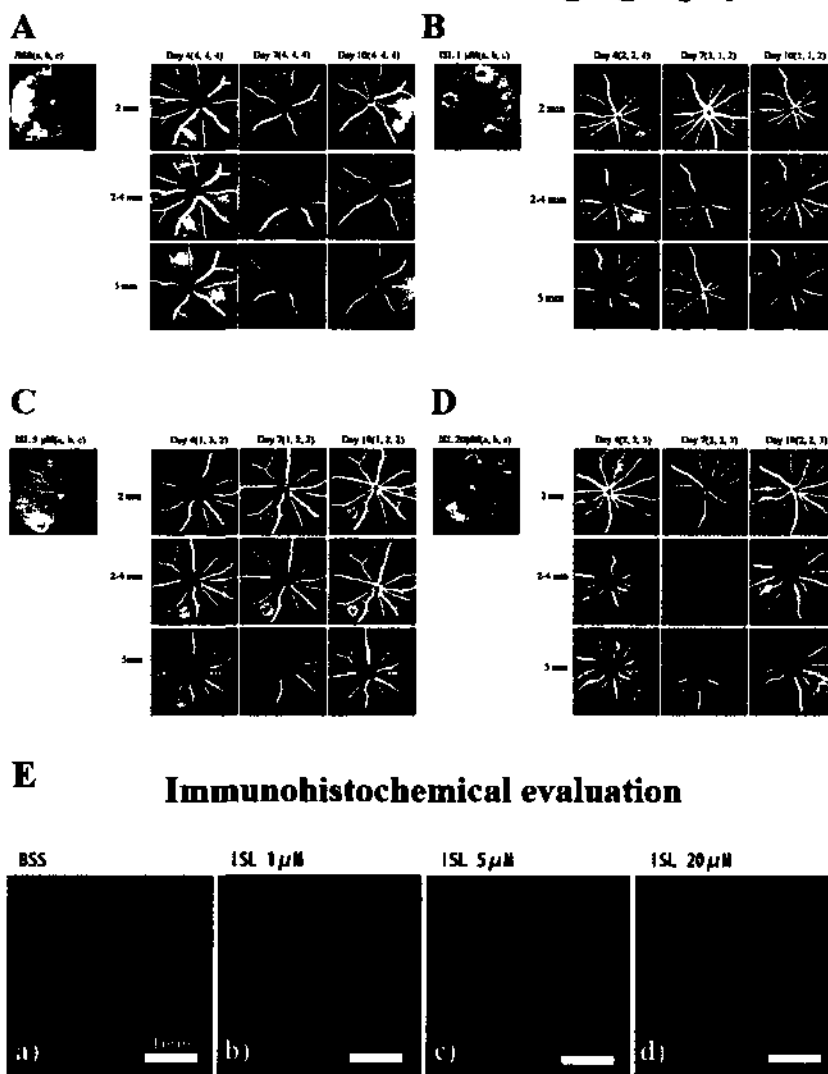


Figure 15: Anti-angiogenic effect of ISL on laser photocoagulation-induced choroidal NV model.

Immediately after diode laser-photocoagulation, ISL (10, 50, 200 μM in BSS) was injected intravitreally at 1 μl volume to achieve a vitreal concentration of 1, 5 and 20 μM . At day 4, 7 and 10, the mice retinas were examined by fluorescein angiography (FA). From images taken at different stage (<2min, 2-4 min and >5 min), the fluorescein leakage of lesions were scored. At day 10, after enucleation, choroidal flat mount was immunostained with isolectin-B4-FITC conjugate for vessel endothelial cells. FA images of A. BSS control; B. 1 μM ISL; C. 5 μM ISL and D. 20 μM ISL. E. Immunofluorescence images of choroidal flat-mounts stained for isolectin-B4. Scale bars = 0.1 mm.

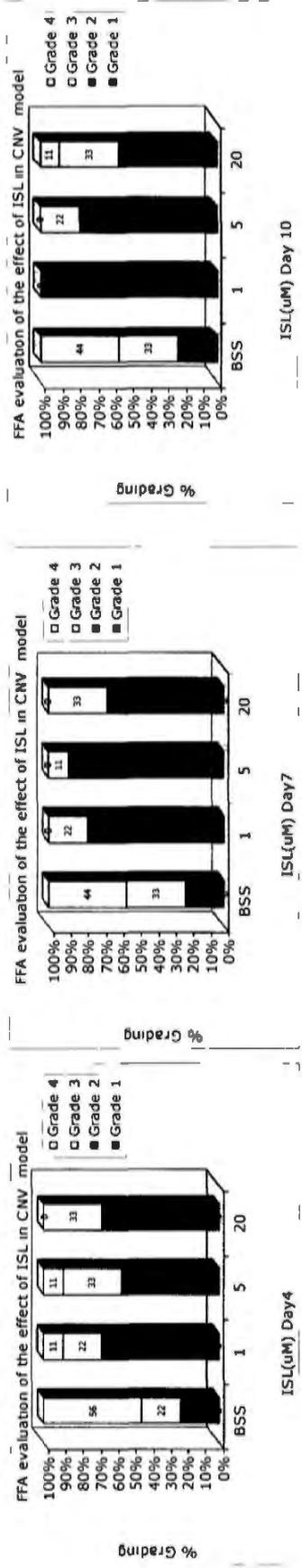


Figure 16: ISL suppressed choroidal NV severity scored after fundus fluorescein angiography.

Fluorescein leakage of choroidal NV lesions was scored from Grade 1 to 4, according to their severity. The percentage of lesions with different severity grades was calculated and compared. A. Day 4; B. Day 7 and C. Day 10 examination.

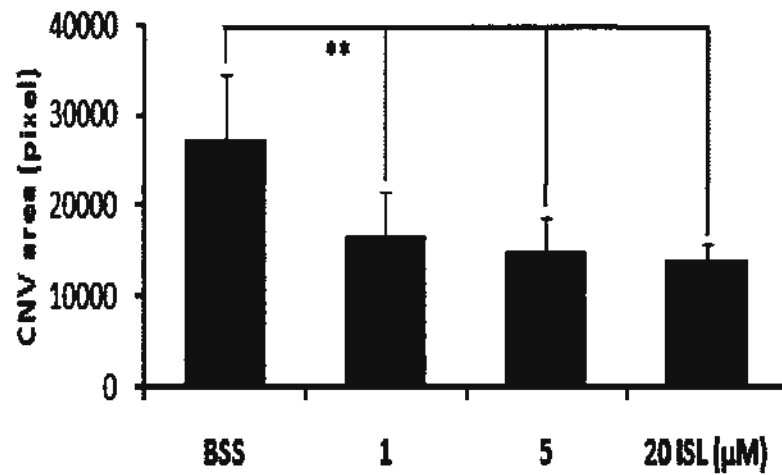


Figure 17: ISL reduced the vascularized area in laser-induced choroidal NV assay.

At day 10 after treatment, choroidal flat mounts were stained for isolectin-B4 to label vessel endothelial cells. The vascularized area in each lesion was measured and expressed as mean \pm S.E.M. (error bars) in each treatment group. Results showed that the vascularized area in ISL treated groups were significantly reduced when compared to BSS control group (* $P < 0.05$, one-way ANOVA test).

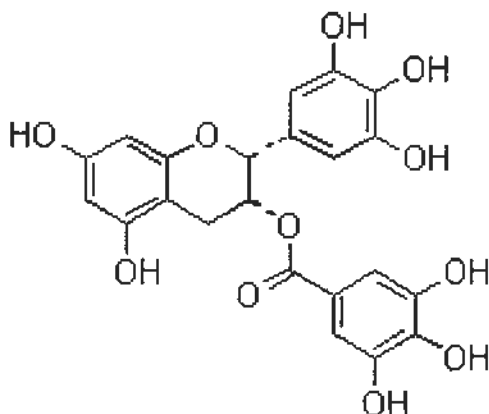


Figure 18: Chemical structure of epigallocatechin-3-gallate

Chemical name is [(2*R*,3*R*)-5,7-dihydroxy-2-(3,4,5-trihydroxyphenyl)chroman-3-yl] 3,4,5-trihydroxybenzoate, (C₂₂H₁₈O₁₁). Molecular mass is 458.37 g/mol. Picture is adapted from ChemBlink, <http://www.chemblink.com>.



Figure 19: Resources of Epigallocatechin-3-gallate: green tea.

(Picture is obtained from <http://antiagingtreatments.blogspot.com>)

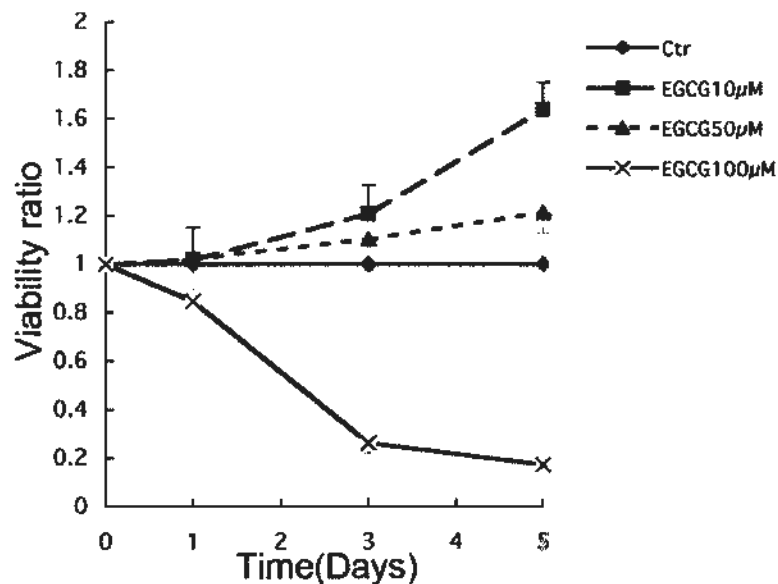


Figure 20: Effect of EGCG on cell viability of ARPE-19 cells.

ARPE-19 cells (7×10^3) were seeded in the presence of EGCG (0, 10, 50 and 100 μM respectively). Cytotoxicity of EGCG was evaluated at 1, 3 and 5 days by MTT assay. The cell viability was expressed as the ratio of cell survival under treatment / cell survival for the untreated control cells. Each concentration of EGCG was tested in quadruplicate. EGCG at 10 & 50 μM showed no cytotoxicity to ARPE-19 cells, EGCG at 100 μM had reduced cell survival.

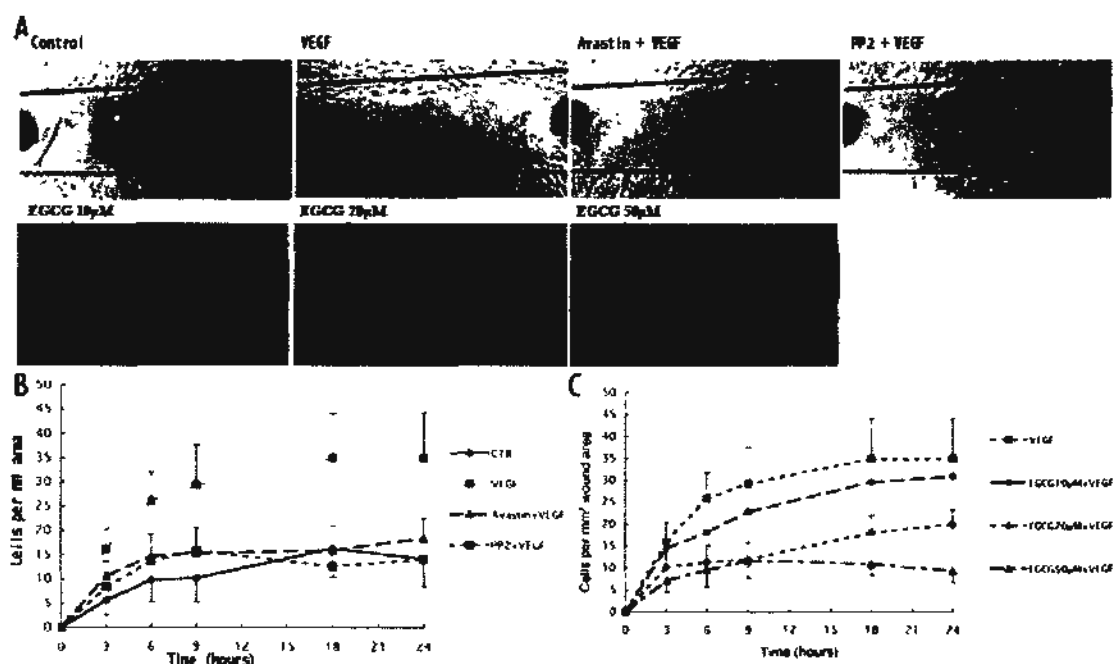


Figure 21: The inhibitory effect of EGCG on VEGF-A-induced HUVEC migration in a scratch wound healing assay.

HUVECs grew to full confluence were scratched with a scraping tool and treated with different concentrations of EGCG (0, 10, 20 and 50 μ M) in the presence of VEGF165 (20 ng/ml). Untreated cells and cells treated with VEGF alone, Avastin (312 μ g/ml) or PP₂ (10 μ M) with VEGF added served as controls. Phase-contrast microphotographs of HUVECs in the denuded area were taken at different time points using a 5x objective. Six images were captured for each treatment. HUVEC present in the denuded area were quantified and expressed as number of cells per mm² area. (A) Representative photographs after 24-hour treatment to assess HUVECs migration. (B) A time-dependent increase of HUVEC number in the denuded area in four control groups, compared to untreated cells. Avastin and PP₂ inhibited VEGF stimulated HUVEC migration. (C) A time- and dose-dependent suppression of VEGF-induced HUVEC migration by EGCG treatments.

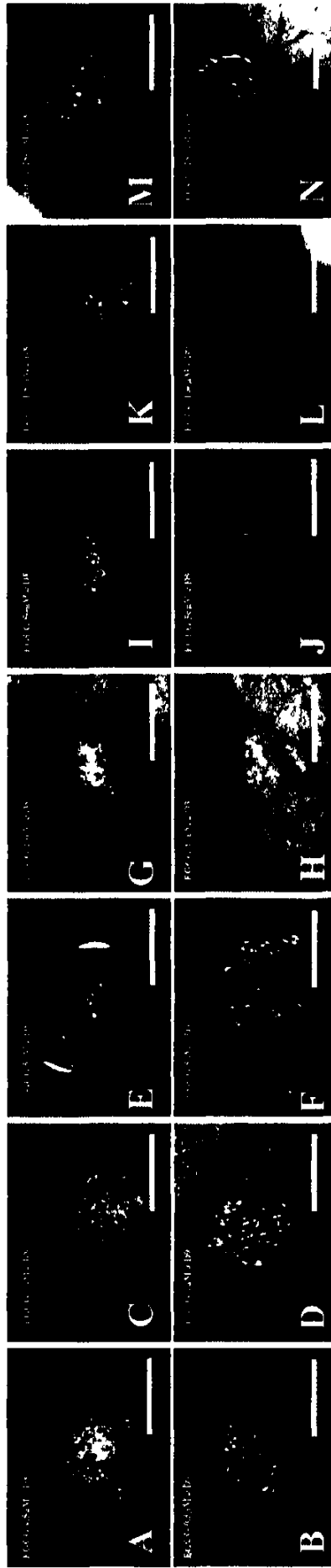


Figure 22: Representative micrographs showing the effect of EGCG on developmental chick chorioallantoic membrane assay at 24 hours.

Gelatin sponge added with **A and B**. 0.5 μM EGCG; **C and D**. 1 μM EGCG; **E and F**, 5 μM EGCG; **G and H**, 10 μM EGCG **I and J**, 50 μM EGCG; **K and L**, 100 μM EGCG **M and N**, 250 μM EGCG Scale bars = 1 mm.

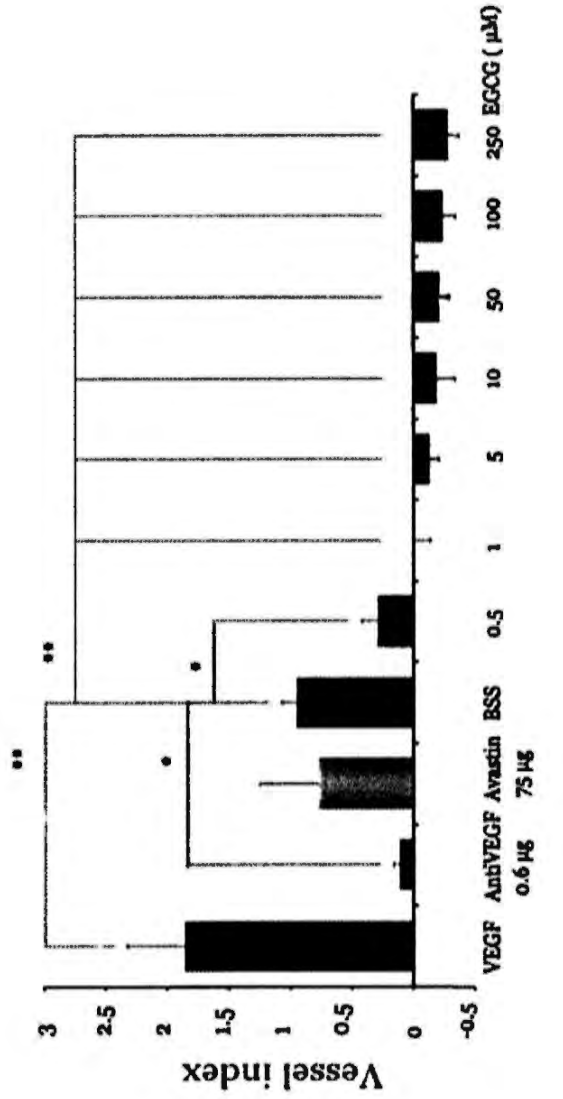


Figure 23: EGCG suppressed blood vessel development in the gelatin-sponge chick chorioallantoic membrane assay.

Seven concentrations (0.5, 1, 5, 10, 50, 100, 250 µM) of EGCG were tested. BSS only, VEGF165 (60 ng), polyclonal anti-VEGF antibody (0.6 µg, Santa Cruz) and Avastin (312 µg/ml) were recruited as control. Each drug was tested on a minimum of 10 sponges. The sequential photographs (0 and 24 hours) were taken using stereomicroscopy (Figures 5 and 21). Vessel numbers converging towards the gelatin sponge were recorded and changes of CAM vessel number between 0 and 24 hours were quantified and represented as vessel index (mean ± S.E.M). The result showed that EGCG at $\geq 0.5\mu\text{M}$ suppressed CAM vessel development dose-dependently (compared to BSS control, one-way ANOVA test, * $P < 0.05$, ** $P < 0.01$).

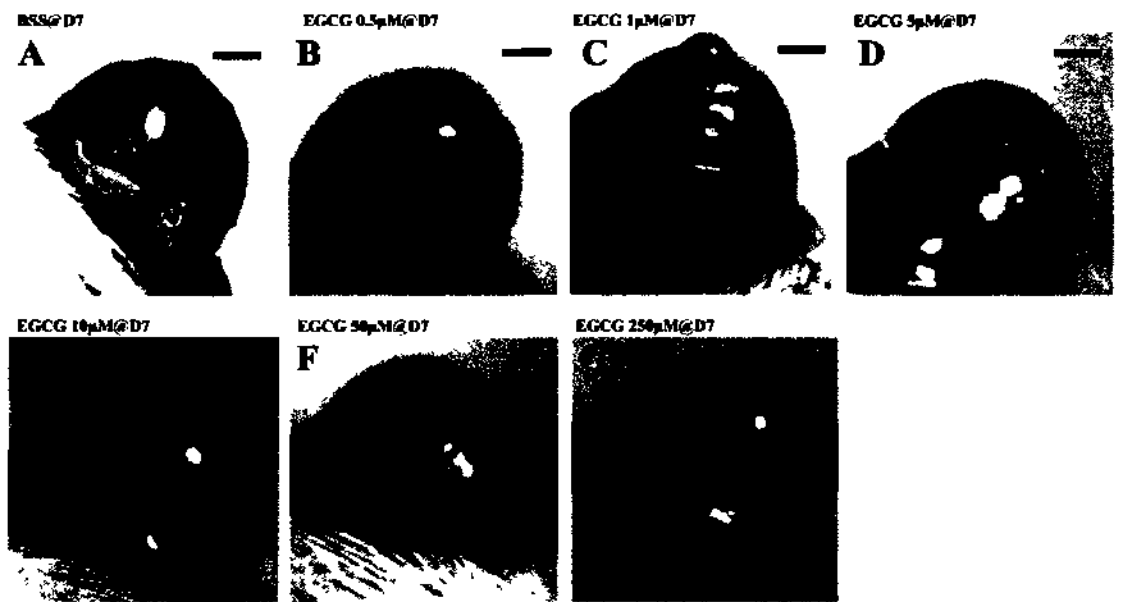


Figure 24. Effect of EGCG corneal neovascularization development.

Representative photographs of BALB/c mice corneas after silver nitrate cauterization, followed by topical treatment with EGCG (0.5, 1, 5, 10, 50, 250 μM) four times daily for 7 days. **A.** BSS control, new vessels grew extensively from limbal vasculature on the corneal surface towards the central region, **B.** 0.5 μM EGCG; **C.** 1 μM EGCG; **D.** 5 μM EGCG; **E.** 10 μM EGCG; **F.** 50 μM EGCG and **G.** 250 μM EGCG. EGCG at 1 μM started to show a suppressive effect on corneal NV formation. When EGCG was topically applied at $\geq 1 \mu\text{M}$, effective suppression of corneal NV growth was observed. Scale bars = 1 mm.

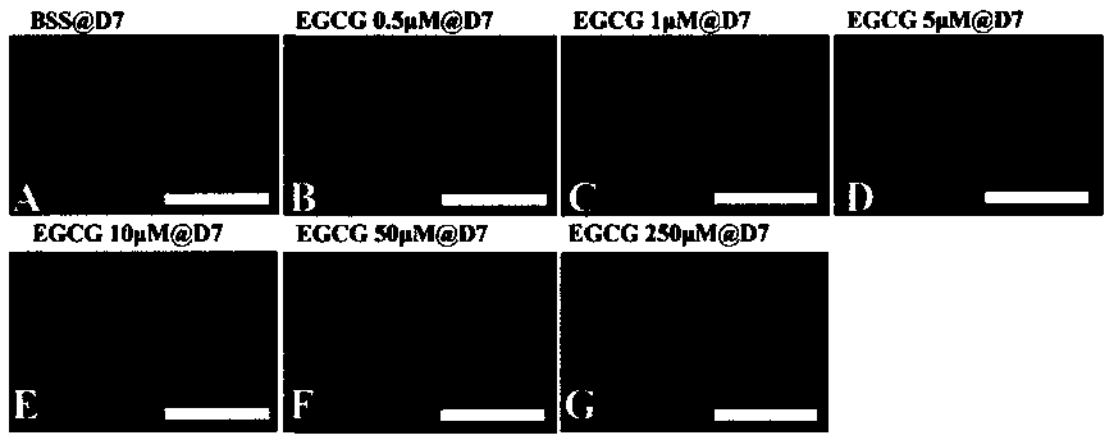


Figure 25: Effect of EGCG on blood vessel manifestation in corneal neovascularization assay

Representative segments from corneal flat mounts immunostained with monoclonal anti-PECAM-FITC conjugate after topical treatment with EGCG for 7 days. **A.** BSS control. **B.** 0.5 μ M EGCG; **C.** 1 μ M EGCG; **D.** 5 μ M EGCG; **E.** 10 μ M EGCG and **F.** 50 μ M EGCG; **G.** 250 μ M EGCG. Scale bars = 1 mm.

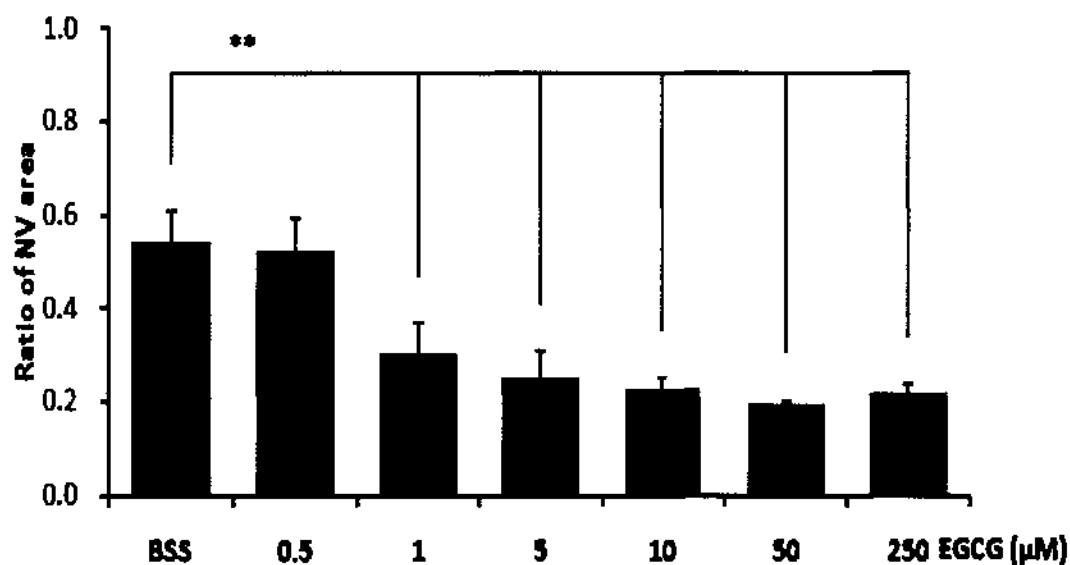


Figure 26: Suppression of neovascularized area after EGCG treatment for 7 days.

The vascularized area on the mice corneas revealed by immunostaining with anti-PECAM-FITC conjugate were quantified and expressed as a ratio to the total corneal surface bordered by limbal vasculature. The result was represented as mean \pm S.E.M. (error bar). A dose-dependent suppression of corneal NV formation and growth was observed for EGCG treatment (n=5). EGCG at $\geq 1 \mu\text{M}$ effectively suppressed corneal NV. $*P < 0.05$, $** P < 0.01$ (one-way ANOVA test), compared to BSS control.

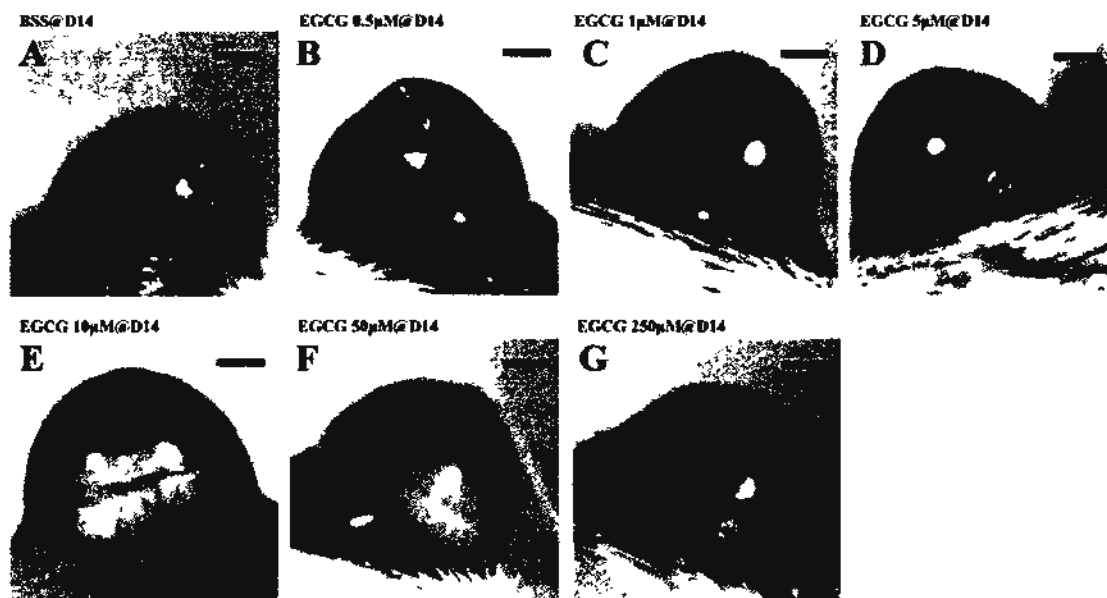


Figure 27: Effect of EGCG corneal neovascularization development.

Representative photographs of BALB/c mice corneas after silver nitrate cauterization, followed by topical treatment with EGCG (0.5, 1, 25, 10, 50 and 250 μM) four times daily for 14 days. **A.** BSS control, new vessels grew extensively from limbal vasculature on the corneal surface towards the central region, **B.** 0.5 μM EGCG; **C.** 1 μM EGCG; **D.** 5 μM EGCG; **E.** 10 μM EGCG; **F.** 50 μM EGCG and **G.** 250 μM EGCG. EGCG at 0.5 μM started to shown suppressive effect on corneal NV formation. When EGCG was topically applied at $\geq 0.5 \mu\text{M}$, effective suppression of corneal NV growth was observed. Scale bars = 1 mm.

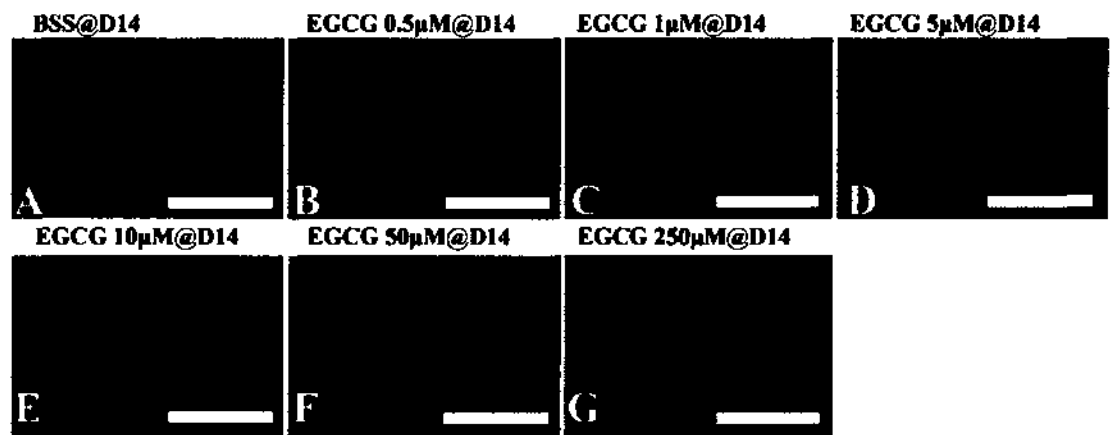


Figure 28: Effect of EGCG on blood vessel manifestation in corneal neovascularization assay

Representative segments from corneal flat mounts immunostained with anti-PECAM-FITC conjugate after topical treatment with EGCG for 14 days. **A.** BSS control. **B.** 0.5 μM EGCG; **C.** 1 μM EGCG; **D.** 5 μM EGCG; **E.** 10 μM EGCG; **F.** 50 μM EGCG and **G.** 250 μM EGCG. Scale bars = 1 mm.

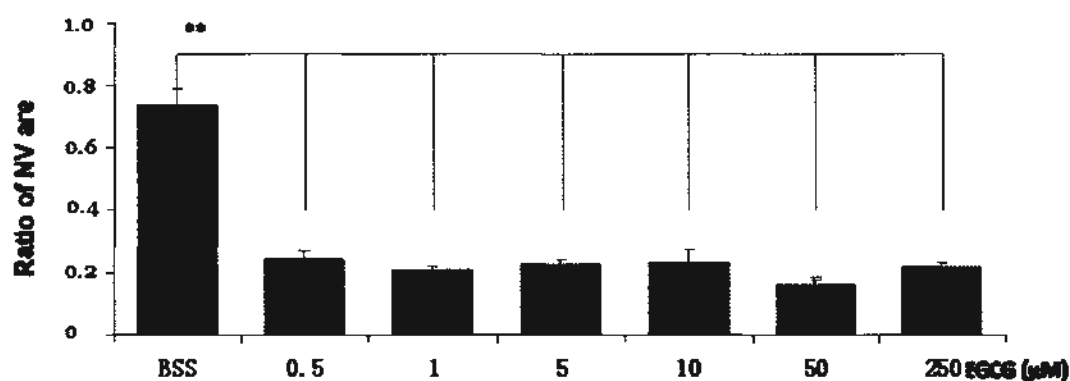


Figure 29: Suppression of neovascularized area after EGCG treatment for 14 days.

The vascularized area on the mice corneas revealed by immunostaining with anti-PECAM-FITC conjugate were quantified and expressed as a ratio to the total corneal surface bordered by the limbal vasculature. The result was represented as mean \pm S.E.M. (error bar). A dose-dependent suppression of corneal NV formation and growth was observed for EGCG treatment (n=5). EGCG at $\geq 0.5 \mu\text{M}$ effectively suppressed corneal NV. * $P < 0.05$, ** $P < 0.01$ (one-way ANOVA test) compared to BSS control.

Fundus Fluorescence Angiography

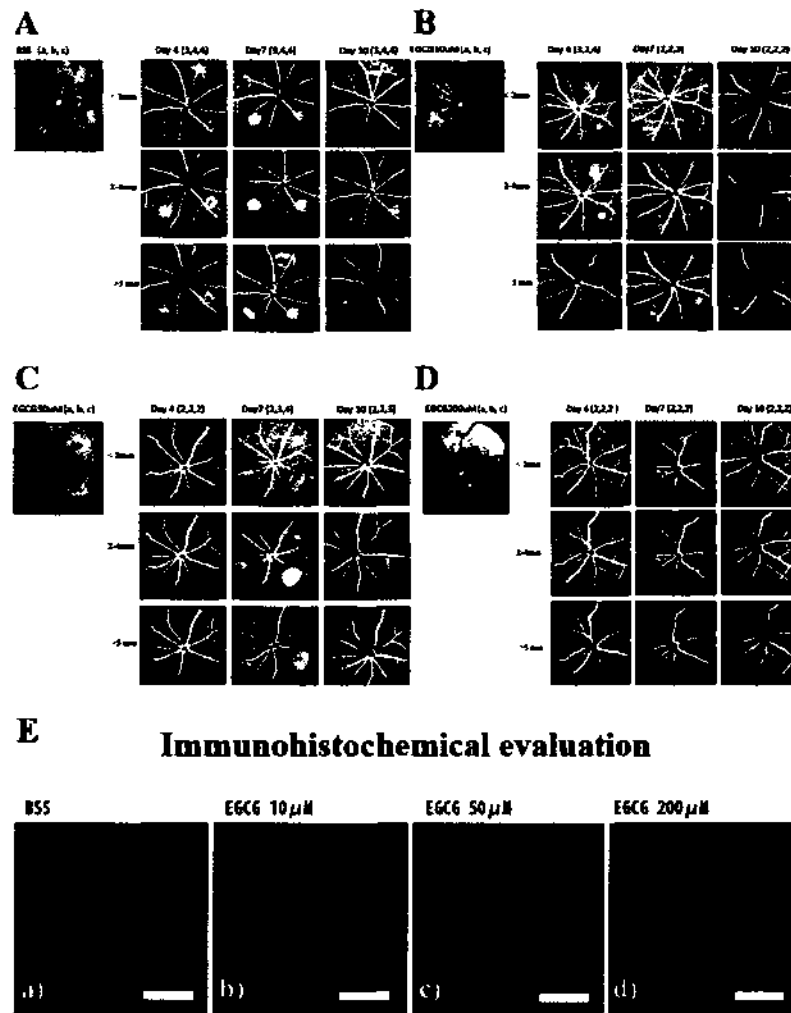


Figure 30: Anti-angiogenic effect of EGCG on laser photocoagulation-induced choroidal NV model.

Immediately after laser-photocoagulation, EGCG (100, 500, 2000 μM in BSS) was injected intravitreally at 1 μl volume to achieve a vitreal concentration of 10, 50 and 200 μM , respectively. At day 4, 7 and 10, the mice retinas were examined by fundus fluorescein angiography (FFA). From images taken at different stage (<2 min, 2-4 min and >5 min), the fluorescein leakage in lesions was scored from Grade 1 to 4. At day 10, choroidal flat mount was immunostained with isolectin-B4-FITC conjugate for vessel endothelial cells. FFA images of **A**. BSS control; **B**. 10 μM EGCG; **C**. 50 μM EGCG and **D**. 200 μM EGCG. **E**. Immunofluorescence images of choroidal flat-mounts stained with isolectin-B4. Scale bars = 0.1 mm.

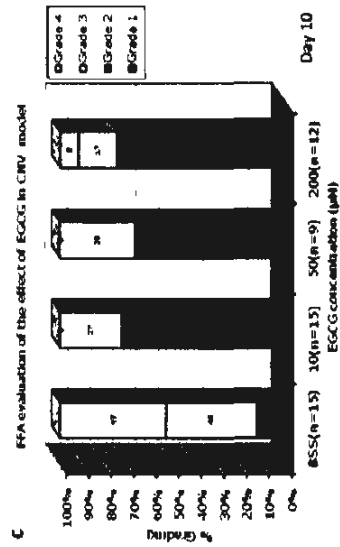
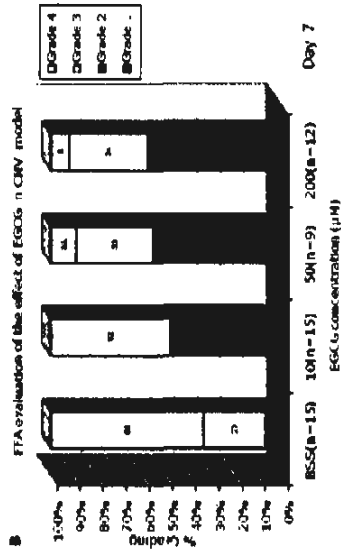
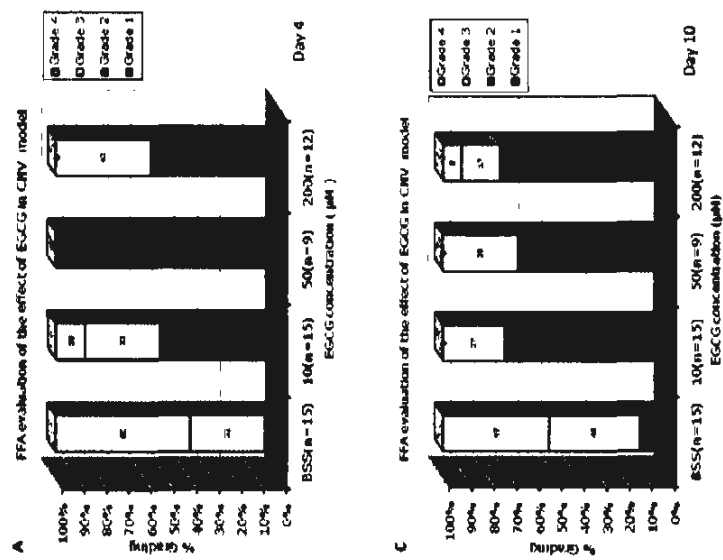


Figure 31: EGCG suppressed choroidal NV examined by fundus fluorescein angiography.

Fluorescein leakage of choroidal NV lesions was scored from grade 1 to 4, according to their severity. The percentage of lesions with different severity grades was calculated. A. Day 4 examination; B. Day 7 and C. Day 10.

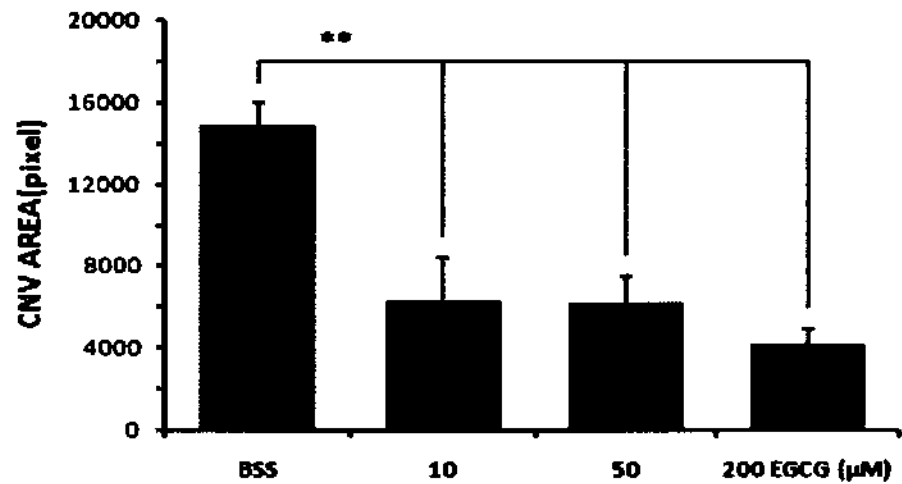


Figure 32: EGCG suppressed the vascularized area in laser-induced choroidal NV assay. At day 10 after treatment, choroidal flat mounts were stained with isolectin-B4 to label vessel endothelial cells. The vascularized area in each lesion was measured and expressed as mean \pm S.E.M. (error bars) for each treatment. Results showed that the vascularized area in EGCG treated groups was significantly reduced when compared to BSS control group (* $P < 0.05$, ** $P < 0.01$, one-way ANOVA test).

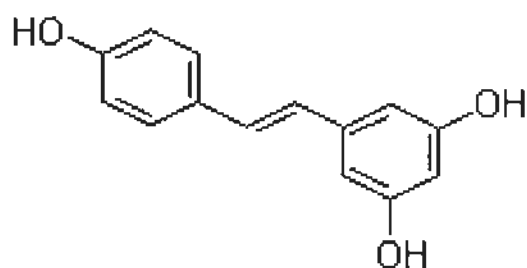


Figure 33: Chemical structure of Resveratrol.

Chemical name is *trans*-3,5,4'-trihydroxystilbene, or 5-

[(1E)-2-(4-hydroxyphenyl) ethenyl] -1,3-benzenediol; (C₁₄H₁₂O₃). Molecular

mass is 228.25 g/mol. Picture is adapted from ChemBlink,

<http://www.chemblink.com>.



Figure 34: Resources of resveratrol: grapes and red wine.

(Picture is obtained from <http://www.learnaboutresveratrol.com>)

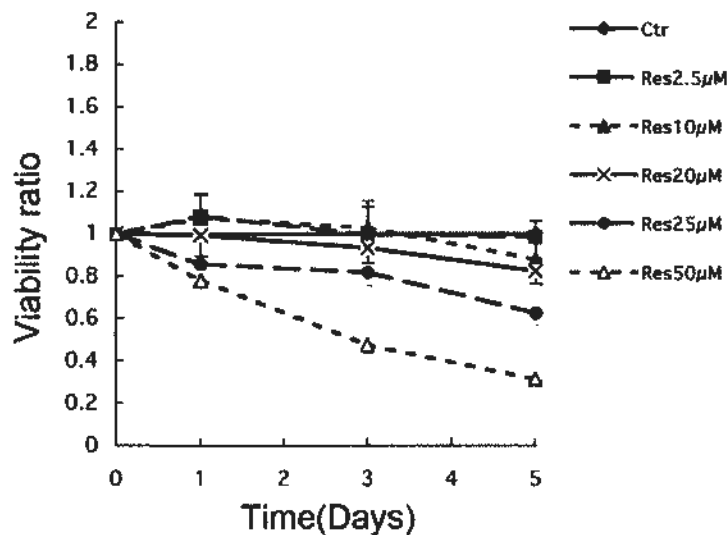


Figure 35: Effect of Rst on cell viability of ARPE-19 cells.

ARPE-19 cells (7×10^3) were seeded and cultured in the presence of Rst (0, 2.5, 10, 20, 25 and 50 μM , respectively). Cytotoxicity of Rst was evaluated by MTT assay at day 1, 3 and 5. The cell viability was expressed as the ratio of cell survival under treatment / cell survival for the untreated control cells. Each concentration of Rst was tested in quadruplicate. Rst at 2.5 and 10 μM showed no effect on ARPE-19 cell growth. Rst at 20 and 25 μM showed mild reduction of ARPE-19 cell number. Rst at 50 μM reduced cell survival.

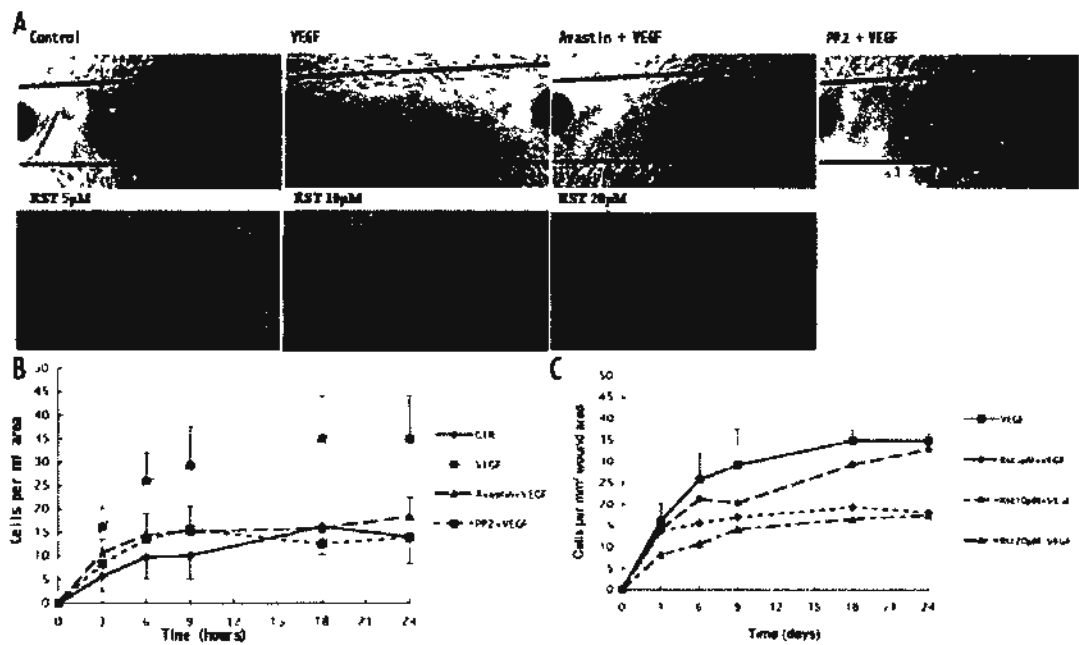


Figure 36: Inhibition of Rst on VEGF-A-induced HUVEC migration.

HUVECs grew to full confluence were scratched with a scraping tool and treated with Rst (5, 10 and 20 μ M) in the presence of VEGF165 (20 ng/ml). Untreated cells and cells treated with VEGF alone, Avastin (312 μ g/ml) or PP₂ (10 μ M) with VEGF were served as controls. Phase-contrast micrographs of denuded area were taken at different time points using a 5x objective. HUVEC migrated to denuded area were counted and expressed as number of cells per mm² area. (A) Representative photographs at 24 hour of treatment to assess HUVECs migration. (B) Number of HUVEC cells in the denuded area in four control groups, compared to untreated cells. Avastin and PP₂ inhibited VEGF-stimulated HUVEC migration. (C) A dose-dependent suppression of VEGF-induced HUVEC migration by Rst treatment.

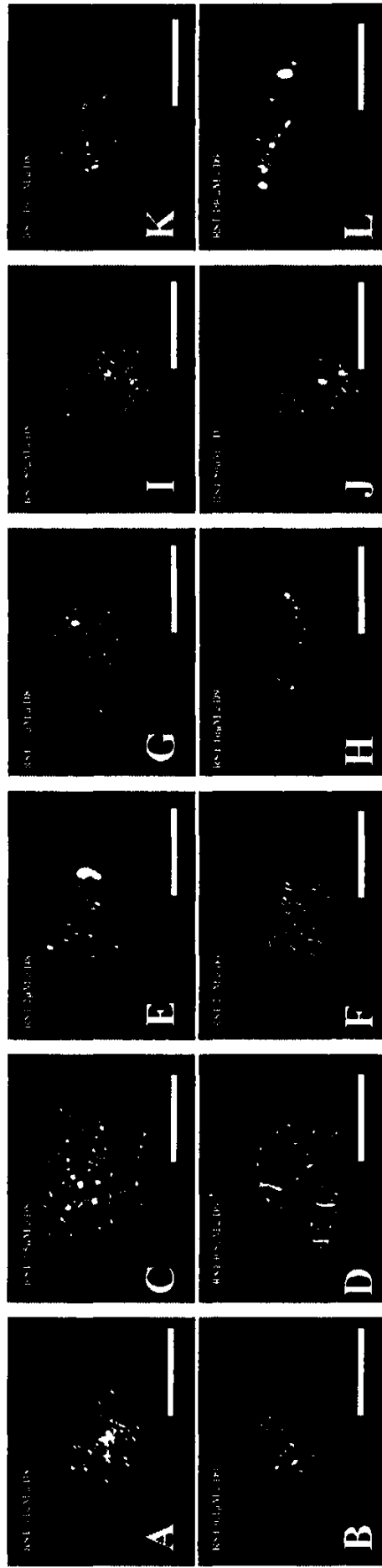


Figure 37: Representative photographs showing chick chorioallantoic membrane changes at 24 hours after Rst treatments.

Gelatin sponge with **A and B**. 0.1 μM Rst; **C and D**. 0.5 μM Rst; **E and F**. 2 μM Rst; **G and H**. 10 μM Rst. **I and J**, 50 μM Rst; **K and L**, 100 μM Rst. Scale bars = 1 mm.

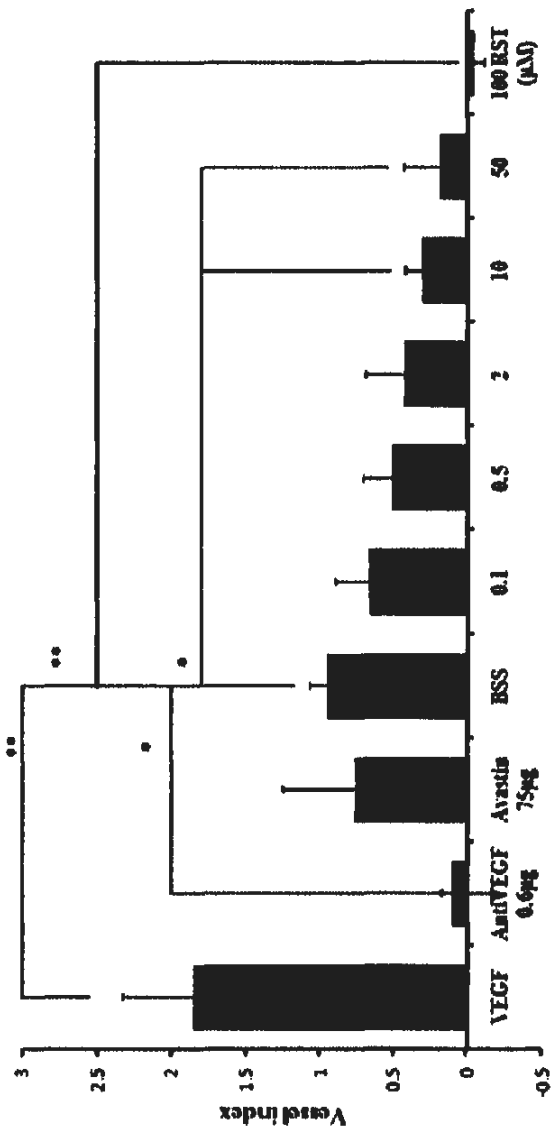


Figure 38: Rst suppressed chick chorioallantoic membrane vessel development.

Six concentrations (0.1, 0.5, 2, 10, 50, 100 µM) of Rst were tested. BSS, VEGF (60 ng), polyclonal anti-VEGF antibody (0.6 µg) and Avastin (312 µg/ml) were recruited as control (See Figure5). Each drug was tested on a minimum of 10 sponges. Micrographs (at 0 and 24 hours) were taken under stereomicroscopy. Blood vessels converging toward the gelatin sponge were quantified and the ratio of CAM vessel changes between 0 and 24 hours were represented as vessel index (mean ± S.E.M). The result showed that Rst at >/= 10 µM suppressed CAM vessel development dose-dependently (compared to BSS control group, one-way ANOVA test, n>/=10, * $P < 0.05$, ** $P < 0.01$).

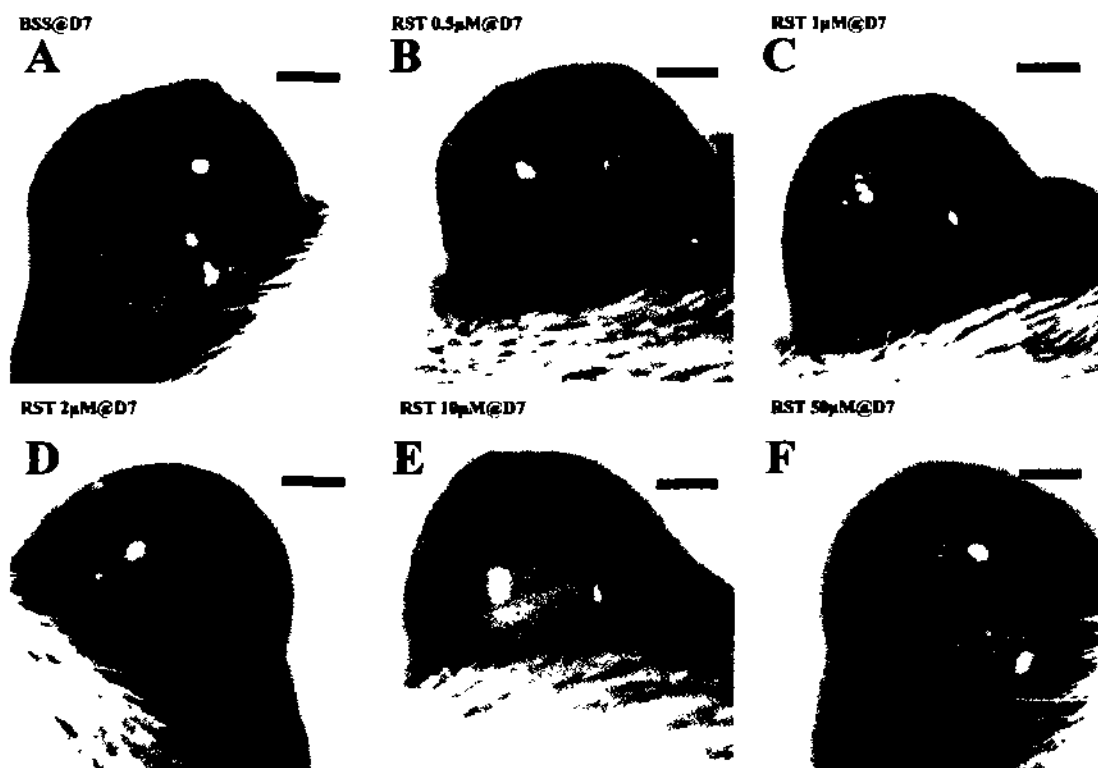


Figure 39: Effect of Rst corneal neovascularization development.

Representative photographs of BALB/c mice corneas after silver nitrate cauterization, followed by topical treatment with Rst (0.5, 1, 2, 10, 50 μM) four times daily for 7 days. **A.** BSS control, new vessels grew extensively from limbal vasculature on the corneal surface towards the central region, **B.** 0.5 μM Rst; **C.** 1 μM Rst; **D.** 2 μM Rst; **E.** 10 μM Rst and **F.** 50 μM Rst. Rst at 1 μM showed suppression on corneal NV. When Rst was topically applied at $\geq 1 \mu\text{M}$, effective suppression of corneal NV was observed. Scale bars = 1 mm.

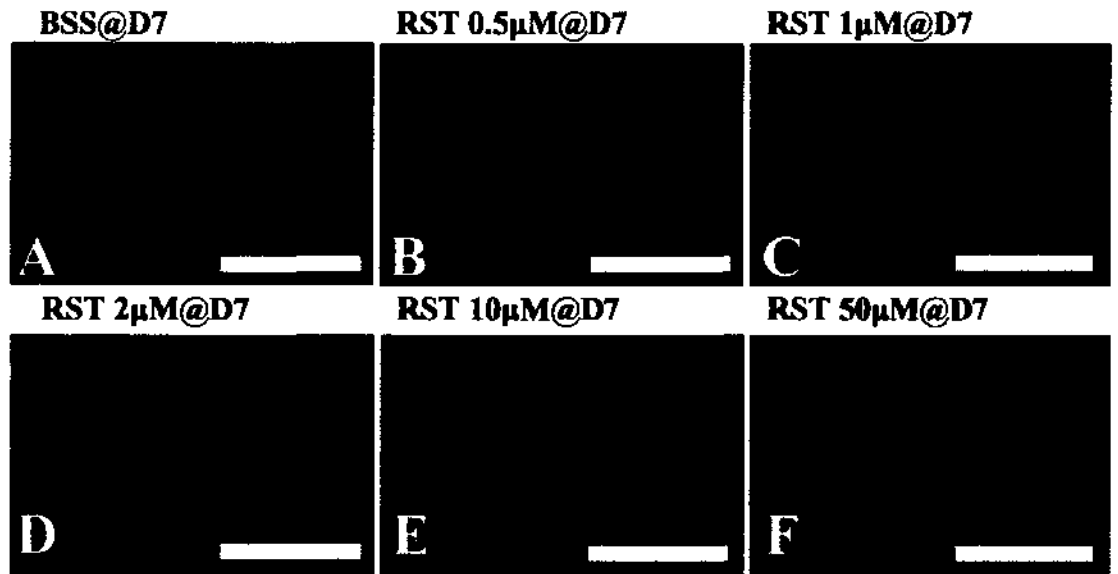


Figure 40: Effect of Rst on blood vessel manifestation in corneal neovascularization assay
Representative segments from corneal flat mounts immunostained with anti-PECAM-FITC conjugate after topical treatment with Rst for 7 days. **A.** BSS control. **B.** 0.5 μM Rst; **C.** 1 μM Rst; **D.** 2 μM Rst; **E.** 10 μM Rst and **F.** 50 μM Rst. Scale bars = 1 mm.

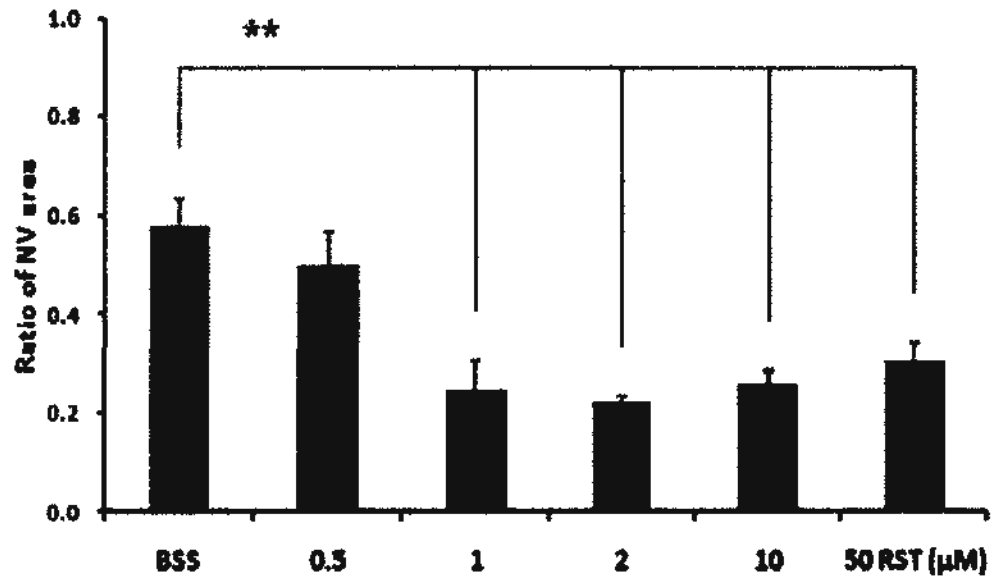


Figure 41: Anti-angiogenic effect of Rst on mice corneal NV after treatment for 7 days.

The vascularized area on mice corneas revealed by immunostaining with anti-PECAM-FITC conjugate was quantified and expressed as a ratio to the total corneal surface bordered by limbal vasculature. The result was represented as mean \pm S.E.M. A suppression of corneal NV formation and growth was observed for Rst treatment (n=5 each group). Rst at $\geq 1 \mu\text{M}$ effectively suppressed corneal NV. * $P < 0.05$, ** $P < 0.01$ (one-way ANOVA test), compared to BSS control.

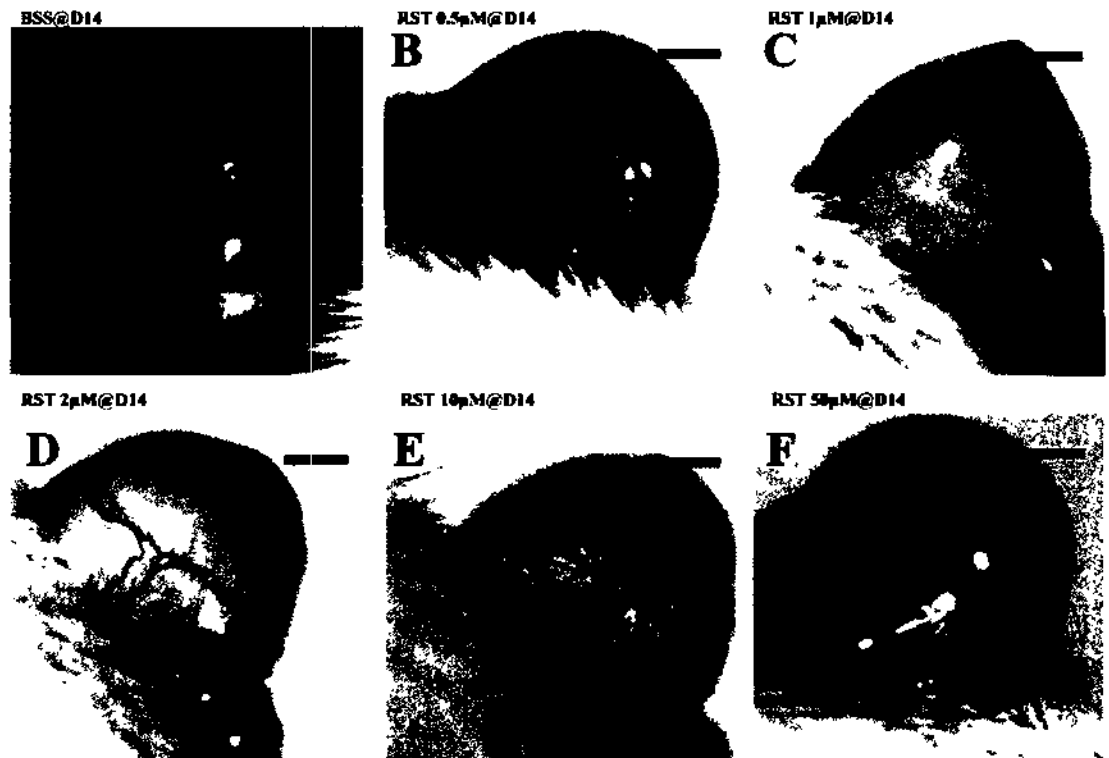


Figure 42: Effect of Rst corneal neovascularization development.

Representative photographs of BALB/c mice corneas after silver nitrate cauterization, followed by topical treatment with Rst (0.5, 1, 2, 10, 50 μM) four times daily for 14 days. A. BSS control, new vessels grew extensively from limbal vasculature on the corneal surface towards the central region, B. 0.5 μM Rst; C. 1 μM Rst; D. 2 μM Rst; E. 10 μM Rst and F. 50 μM Rst. Rst at 1 μM started to suppress corneal NV formation. When Rst was topically applied at $\geq 1 \mu\text{M}$, effective suppression of corneal NV growth was observed. Scale bars = 1 mm.

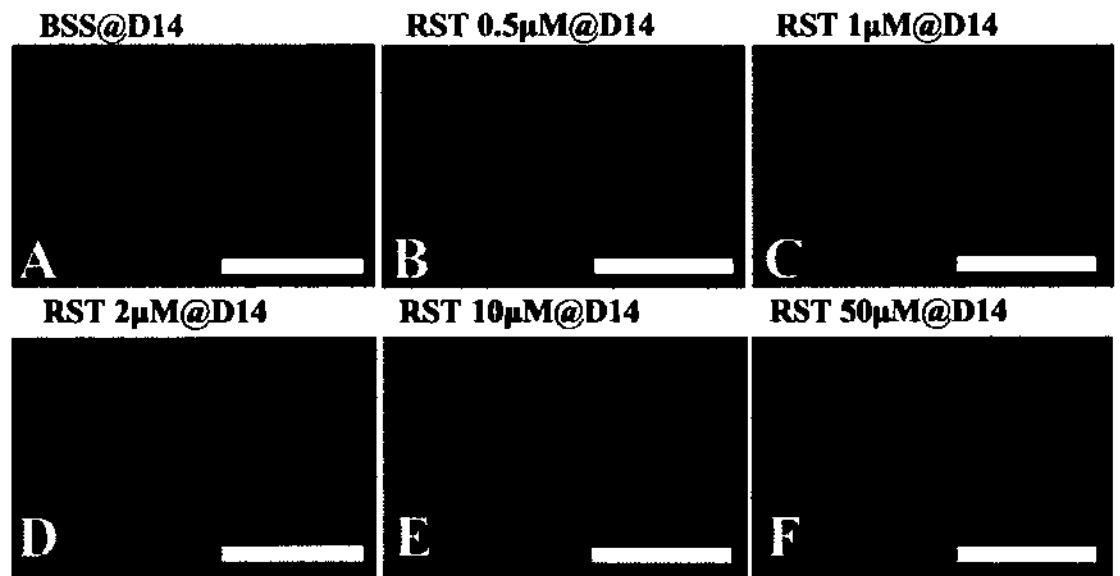


Figure 43: Effect of Rst on blood vessel manifestation in corneal neovascularization assay

Representative segments from corneal flat mounts immunostained with anti-PECAM-FITC conjugate after topical treatment with Rst for 14 days. A. BSS control. B. 0.5 μM Rst; C. 1 μM Rst; D. 2 μM Rst; E. 10 μM Rst and F. 50 μM Rst. Scale bars = 1 mm.

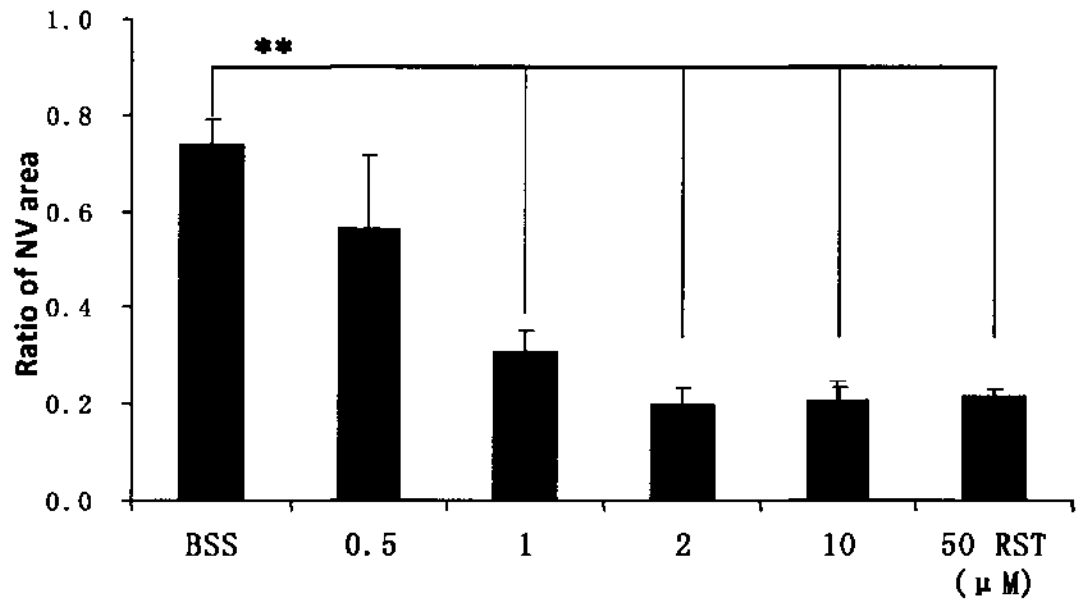


Figure 44: Anti-angiogenic effect of Rst on corneal NV model after treatment for 14 days.

The vascular area on the mice corneas revealed by immunostaining with anti-PECAM-FITC conjugate was quantified and expressed as a ratio to the total corneal surface bordered by limbal vasculature. The result was represented as mean \pm S.E.M. Suppression of corneal NV formation and growth was observed for Rst treatment (n=5 each group). Rst at $\geq 1 \mu\text{M}$ effectively suppressed corneal NV. $*P < 0.05$ $**P < 0.01$ (one-way ANOVA test).

Fundus Fluorescence Angiography

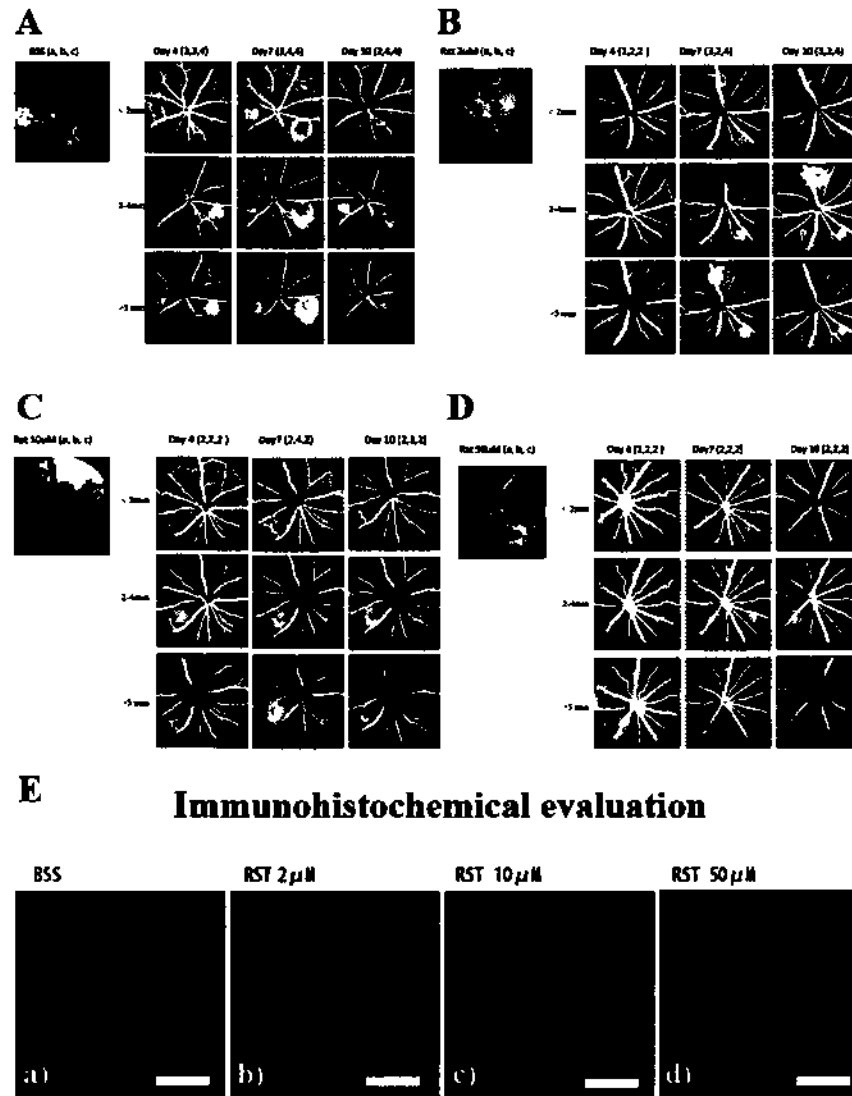


Figure 45: Anti-angiogenic effect of Rst on laser photocoagulation-induced choroidal NV model.

Immediately after laser-photocoagulation, Rst (20, 100, 500 μ M in BSS) was injected intravitreally at 1 μ l volume to achieve a vitreal concentration of 2, 10 and 50 μ M, respectively. At day 4, 7 and 10, the mice retinas were examined by fundus fluorescein angiography (FFA). From images taken at different stage (<2 min, 2-4 min and >5 min), the fluorescein leakage in lesions was scored from Grade 1 to 4. At day 10, choroidal flat mount was immunostained with isolectin-B4-FITC conjugate for vessel endothelial cells. FFA images of **A**. BSS control; **B**. 2 μ M Rst; **C**. 10 μ M Rst and **D**. 50 μ M Rst. **E**. Immunofluorescence images of choroidal flat-mounts stained with isolectin-B4. Scale bars = 0.1 mm.

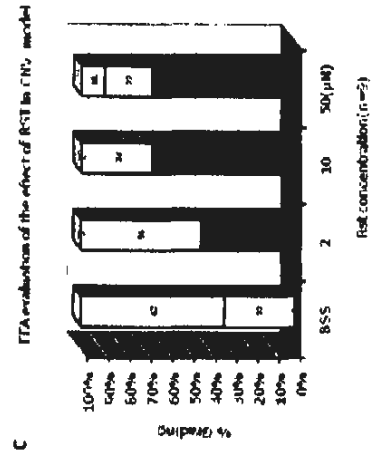
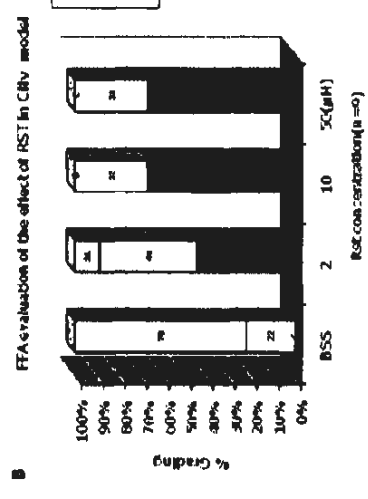
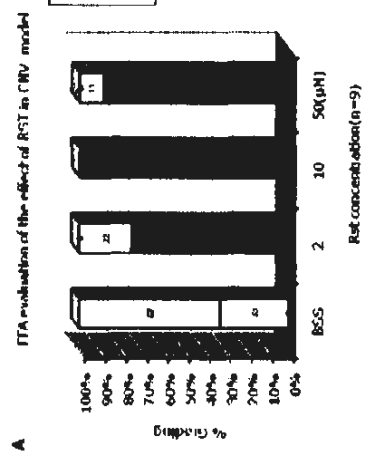


Figure 46: Rst affected choroidal NV development by fundus fluorescein angiography.

Fluorescein leakage of choroidal NV lesions was scored from grade 1 to 4, according to their severity. The percentages of lesions with different severity grades were calculated. **A.** Day 4 examination; **B.** Day 7 and **C.** Day 10.

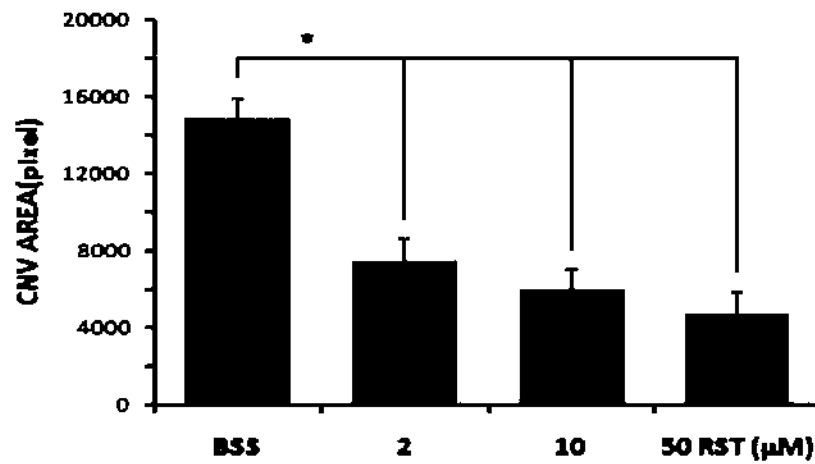


Figure 47: Rst suppressed the vascular area in laser-induced choroidal NV assay.

At day 10 after treatment, choroidal flat mounts were stained for isolectin-B4 to label vessel endothelial cells. The vascular area in each lesion was measured and expressed as mean \pm S.E.M for each treatment groups. Results showed that vascular area of Rst treated groups were significantly smaller than BSS control group (* $P < 0.05$, one-way ANOVA test).

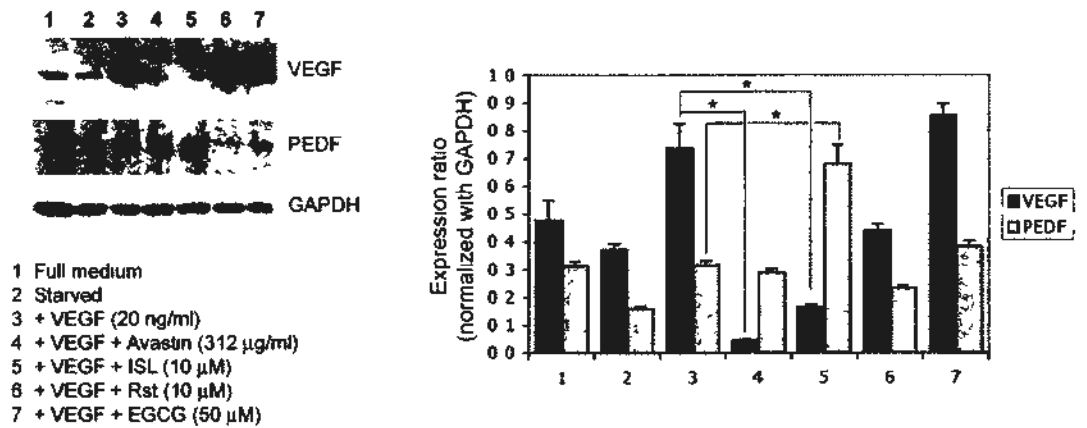


Figure 48: VEGF & PEDF expression by Western blot and quantification analysis by band densitometry.

The histogram showing the mean densitometric measurement in triplicated experiments. * $P < 0.05$, paired Student's *t*-test.

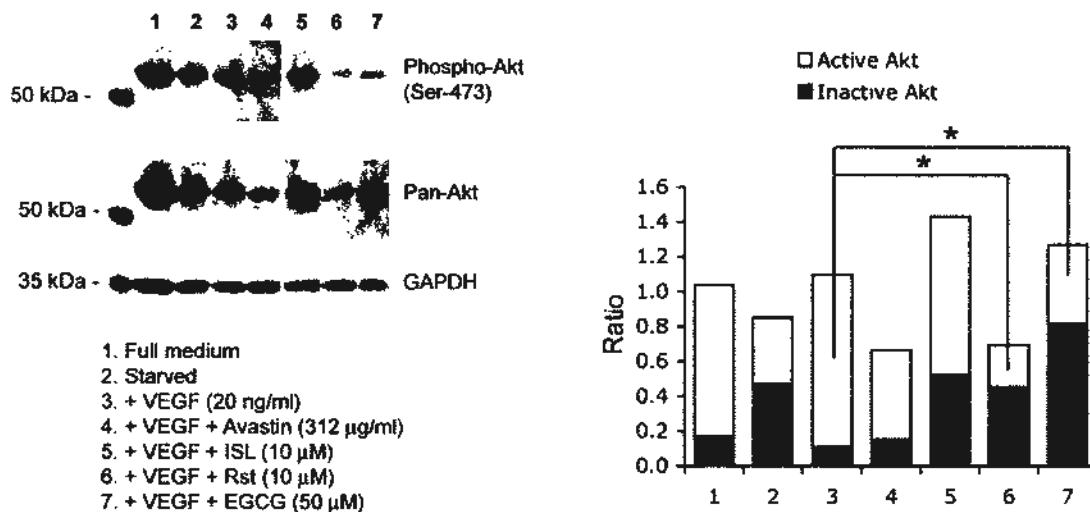


Figure 49: Akt activation assay by Western blot analysis and quantification analysis by band densitometry.

The histogram showing the mean densitometric measurement in triplicated experiments. * $P < 0.05$, paired Student's *t*-test.

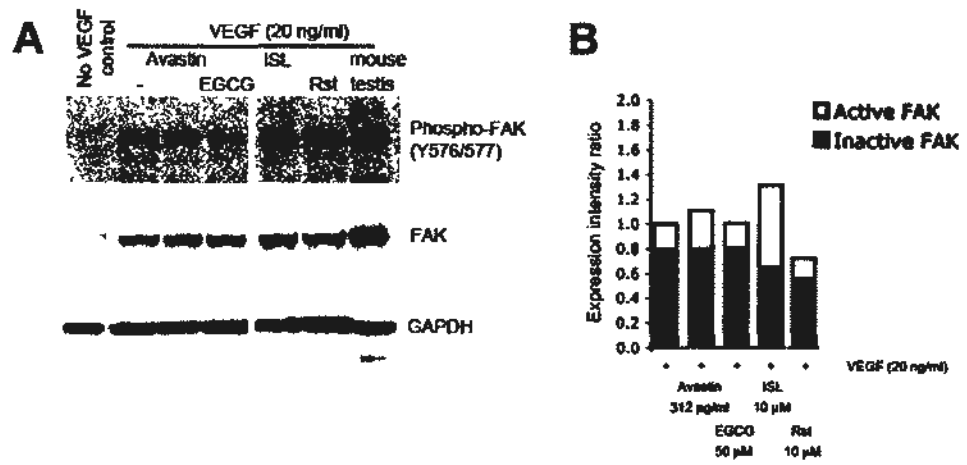


Figure 50: FAK activation assay by Western blot and band densitometry analysis.

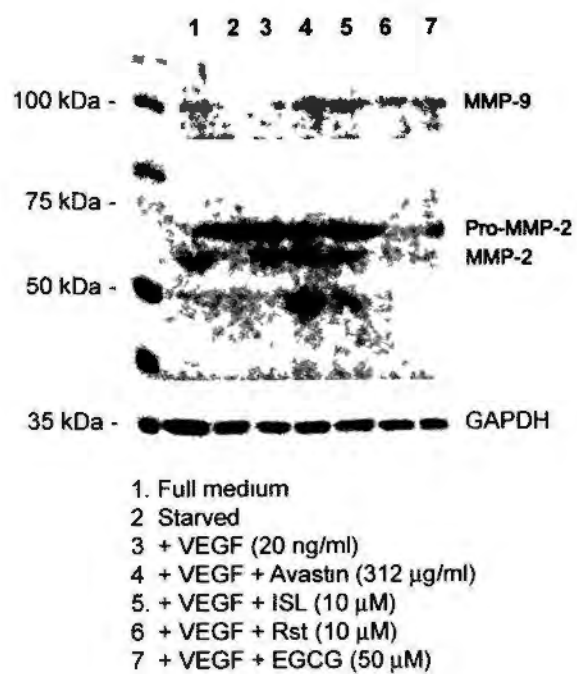


Figure 51: MMP-2 & MMP-9 expression by Western blotting

REFERENCES

- Abdiu, O. and Van Setten, G. (2008) Antiangiogenic activity in tears: presence of pigment-epithelium-derived factor. New insights and preliminary results. *Ophthalmic Research*, 40, 16–18.
- Adams, R. H., Wilkinson, G. A., Weiss, C., Diella, F., Gale, N. W., Deutsch, U., Risau, W., Klein, R. (1999). Roles of ephrin-B ligands and EphB receptors in cardiovascular development: demarcation of arterial/venous domains, vascular morphogenesis, and sprouting angiogenesis. *Genes & Development*, 3: 295–306.
- Aggarwal, B.B., Bhardwaj, A., Aggarwal, R. S. (2004). Role of resveratrol in prevention and therapy of cancer: preclinical and clinical studies. *Anticancer Research*, 24: 2783-840.
- Aguilar, E., Michael, I., Friedlander, D. D. (2010). “Ocular models of angiogenesis”. In: *Methods in Enzymology*. G. Jensen (ed.). Volume 444. Chapter 6, pp.115-158
- Ahmad, N., Gupta, S., Mukhtar, H. (2000). Green tea polyphenol epigallocatechin-3-gallate differentially modulates nuclear factor kappaB in cancer cells versus normal cells. *Archives of Biochemistry and Biophysics*, 376: 338–46.
- Ahn, S. C., Kim, G. Y., Kim, J. H (2004). Epigallocatechin-3-gallate, constituent of green tea, suppresses the LPS-induced phenotypic and functional maturation of murine dendritic cells through inhibition of mitogen-activated protein kinases and NF-kappaB. *Biochemical and Biophysical Research Communications*, 313:148–55.
- Aida, K., Tawata, M., Shindo, H., Onaya, T., Sasaki, H., Yamaguchi, T. (1990). Isoliquiritigenin: a new aldose reductase inhibitor from glycyrrhizae radix. *Planta Medica*, 56: 254-8.
- Alitalo, K., Carmeliet, P. (2002). Molecular mechanisms of lymphangiogenesis in health and disease. *Cancer Cell*, 1: 219-27.
- Amano, S., Rohan, R., Kuroki, M., Tolentino, M., Adamis, A. P. (1998). Requirement for vascular endothelial growth factor in wound- and inflammation-related corneal neovascularization. *Investigative Ophthalmology & Visual Science*,

39:18- 22.

- Ambati, B. K., Nozaki, M., Singh, N., Takeda, A. (2006). Corneal avascularity is due to soluble VEGF receptor-1. *Nature*, 443:993–997.
- Ambati, J., Anand, A., Fernandez, S., Sakurai, E., Lynn, B. C., Kuziel, W. A., Rollins, B. J., Ambati, B. K. (2003). An animal model of age-related macular degeneration in senescent Ccl-2- or Ccr-2-deficient mice. *Nature Medicine*, 9:1390–1397.
- Athar, M., Back, J. H., Tang, X., Kim, K. H., Kopelovich, L., Bickers, D. R., Kim, A. L. (2007). Resveratrol: a review of preclinical studies for human cancer prevention. *Toxicology and Applied Pharmacology*, 224: 274-83.
- Auerbach, R., Kubai, L., Knighton, D., Folkman, J. (1974). A simple procedure for the long-term cultivation of chicken embryos. *Developmental Biology*, 41: 391–394.
- Auerbach, R., Akhtar, N., Lewis, R. L., Shinnars, B. L. (2000). Angiogenesis assays: Problems and pitfalls. *Cancer and Metastasis Reviews*, 19:167–172.
- Auerbach, R., Lewis, R., Shinnars, B., Kubai, L., Aktar, N. (2003). Angiogenesis assays: a critical overview. *Clinical Chemistry*, 49: 32–40.
- Ausprunk, D. H., Knighton, D. R., Folkman, J. (1974). Differentiation of the vascular endothelium in the chick chorioallantois: a structural and autoradiographic study. *Developmental Biology*, 38:237–247.
- Ausprunk, D., Folkman, J. (1977). Migration and proliferation of endothelial cells in preformed and newly formed blood vessels during tumor angiogenesis. *Microvascular Research*, 14:53–65.
- Azar, D. T. (2006). Corneal angiogenic privilege: angiogenic and antiangiogenic factors in corneal avascularity, vasculogenesis, and wound healing. *Transactions of the American Ophthalmological Society*, 104:264-302.
- Aziz, M.H., Nihal, M., Fu, V. X., Jarrard, D. F., Ahmad, N. (2006). Resveratrol-caused apoptosis of human prostate carcinoma LNCaP cells is mediated via modulation of phosphatidylinositol 3'-kinase/Akt pathway and Bcl-2 family proteins. *Molecular Cancer Therapeutics*, 5, 13 .
- Balasubramanian, S., Efimova, T., Eckert, R. L. (2002). Green tea polyphenol stimulates a ras, MEKK1, MEK3, and p38 cascade to increase activator protein 1 factor-dependent involucrin gene expression in normal human keratinocytes.

- Journal of Biological Chemistry*, 277: 1828–36.
- Barthelman, M., Bair, W. B. R., Stickland, K. K. (1998). (-)-Epigallocatechin-3-gallate inhibition of ultraviolet-B-induced AP-1 activity. *Carcinogenesis (London)*, 19: 2201–4.
- Bauer, S. M., Bauer, R. J., Liu, Z. J. (2005). Vascular endothelial growth factor-C promotes vasculogenesis, angiogenesis, and collagen constriction in three dimensional collagen gels. *Journal of vascular surgery*, 41: 699–707.
- Baur, J. A., Sinclair, D. A. (2006). Therapeutic potential of resveratrol: the *in vivo* evidence. *Nature Reviews Drug Discovery*, 5: 493–506.
- Bazan, H. E. P. (2005). Cellular and molecular events in corneal wound healing: significance of lipid signaling. *Experimental Eye Research*, 80: 453–463.
- Beck, L. Jr., D'Amore, P. A. (1997). Vascular development: cellular and molecular regulation. *FASEB Journal*, 11: 365–373.
- Bhardwaj, A., Sethi, G., Vadhan-Raj, S., Bueso-Ramos, C., Takada, Y., Gaur, U., Nair, A. S., Shishodia, S., Aggarwal, B. B. (2007). Resveratrol inhibits proliferation, induces apoptosis, and overcomes chemoresistance through down-regulation of STAT3 and nuclear factor- κ B-regulated antiapoptotic and cell survival gene products in human multiple myeloma cells. *Blood*, 109: 2293–2302.
- Bird, A. C, Bressler, N. M., Bressler, S. B. (1995). An international classification and grading system for age-related maculopathy and age-related macular degeneration. The international ARM epidemiological study group. *Survey of Ophthalmology*, 39: 367–374.
- Blázquez, C., Salazar, M., Carracedo, A., Lorente, M., Egia, A., González-Feria, L. (2008). Cannabinoids inhibit glioma cell invasion by downregulating matrix metalloproteinase-2 expression. *Cancer Research*, 68: 1945–52.
- Blaauwgeers, H. G., Holtkamp, G. M., Rutten, H., Witmer, A. N., Koolwijk, P., Partanen, T. K. et al. (1999) Polarized vascular endothelial growth factor secretion by human retinal pigment epithelium and localization of vascular endothelial growth factor receptors on the inner choriocapillaris. Evidence for a trophic paracrine relation. *American Journal of Pathology*, 155, 421–428.
- Bock, F., Onderka, J., Dietrich, T., Bachmann, B., Pytowski, B., Cursiefen, C. (2008). Blockade of VEGFR3-signalling specifically inhibits lymphangiogenesis in inflammatory corneal neovascularisation. *Graefe's Archive of Clinical and*

- Experimental Ophthalmology*, 246: 115–119.
- Bock, F., Onderka, J., Dietrich, T., Bachmann, B., Kruse, F. E., Paschke, M., Zahn, G., Cursiefen, C. (2007). Bevacizumab as a potent inhibitor of inflammatory corneal angiogenesis and lymphangiogenesis. *Investigative Ophthalmology & Visual Science*, 48: 2545-52.
- Bouck, N. (2002). PEDF: anti-angiogenic guardian of ocular function. *Trends in molecular medicine*, 78: 330-334.
- Bressler, S. B, Maguire, M. G, Bressler, N. M, Fine, S. L. (1990). The Macular Photocoagulation Study Group: relationship of drusen and abnormalities of the retinal pigment epithelium to the prognosis of neovascular macular degeneration. *Archives of Ophthalmology*, 108: 1442–1447.
- Carmeliet, P., Moons, L., Dewerchin, M., Mackman, N., Luther, T., Breier, G., Ploplis, V., Müller, M., Nagy, A., Plow, E., Gerard, R., Edgington, T., Risau, W., Collen, D. (1997). Insights in vessel development and vascular disorders using targeted inactivation and transfer of vascular endothelial growth factor, the tissue factor receptor, and the plasminogen system. *Annual New York Academy Sciociety*, 811:191-206.
- Campa, C., Kasman, I., Ye, W., Lee, W. P., Fuh, G., Ferrara, N. (2008). Effects of an anti-VEGF-A monoclonal antibody on laser-induced choroidal neovascularization in mice:optimizing methods to quantify vascular changes. *Investigative Ophthalmology & Visual Science* , 49(3): 1178-83.
- Campochiaro, P. A., Hachett, S. F. (2003). Ocular neovascularization: a valuable model system. *Oncogene*, 22: 6537–6548.
- Campochiaro, P.A. (2004) Ocular neovascularisation and excessive vascular permeability. *Expert Opinion on Biological Therapy*, 4, 1395–1402.
- Campos, M., Amaral, J., Becerra, S.P., Fariss, R.N. (2006). A novel imaging technique for experimental choroidal neovascularization. *Investigative ophthalmology & visual science*, 47: 5163.
- Cao, W., Tombran-Tink, J., Elias, R., Sezate, S., Mrazek, D., McGinnis, J. F. (2001). In vitro protection of photoreceptors from light damage by pigment epithelium-derived factor. *Investigative Ophthalmology & Visual Science*, 42: 1646–1652.
- Cao, Y., Cao, R. (1999). Angiogenesis inhibited by drinking tea. *Nature*, 398: 381.

- Cao, Y., Cao, R., Brakenhielm, E. (2002). Antiangiogenic mechanisms of diet-derived polyphenols. *Journal of Nutritional Biochemistry*, 13, 380-390.
- Cao, Y., Fu, Z. D., Wang, F., Liu, H. Y., Han, R. (2005). Anti-angiogenic activity of resveratrol, a natural compound from medicinal plants. *Journal of Asian natural products research*, 7: 205–213.
- Cao, Y., Linden, P., Farnebo, J., Cao, R., Eriksson, A., Kumar, V., Qi, J. H., Claesson–Welsh, L., Alitalo, K. (1998). Vascular endothelial growth factor C induces angiogenesis in vivo. *Proceedings of National Academy of Sciences USA*, 95: 14389–14394.
- Cao, Z., Fang, J., Xia, C., Shi, X., Jiang, B. H. (2004). Trans-3,4,5'-trihydroxystibene inhibits hypoxia-inducible factor 1 α and vascular endothelial growth factor expression in human ovarian cancer cells. *Clinical Cancer Research*, 10: 5253–5263.
- Carmeliet, P., Moons, L., Dewerchin, M., Mackman, N., Luther, T., Breier, G., Ploplis, V., Müller, M., Nagy, A., Plow, E., Gerard, R., Edgington, T., Risau, W., Collen, D. (1997). Insights in vessel development and vascular disorders using targeted inactivation and transfer of vascular endothelial growth factor, the tissue factor receptor, and the plasminogen system. *New York Academy of Sciences*, 811,191-206.
- Carmeliet, P., Ferreira, V., Breier, G., Pollefeyt, S., Kieckens, L., Gertsenstein, M., Fahrig, M., Vandenhoek, A., Harpal, K., Eberhardt, C., Declercq, C., Pawling, J., Moons, L., Collen, D., Risau, W., Nagy, A. (1996). Abnormal blood vessel development and lethality in embryos lacking a single VEGF allele. *Nature*, 380: 435–9.
- Campa, C., Kasman, I., Ye, W., Lee, W. P., Fuh, G., Ferrara, N. (2008) Effects of an anti-VEGF-A monoclonal antibody on laser-induced choroidal neovascularization in mice:optimizing methods to quantify vascular changes. *Investigative Ophthalmology and Visual Science*, 49: 1178-83
- Campos, M., Amaral, J., Becerra, S. P., Fariss, R. N. (2006) A novel imaging technique for experimental choroidal neovascularization. *Investigative ophthalmology & visual science*, 47: 12
- Cayouette, M., Smith, S. B., Becerrac, S. P., Gravel, C. (1999). Pigment epithelium derived factor delays the death of photoreceptors in mouse models of inherited

- retinal degenerations. *Neurobiology of Disease*, 6:523–532.
- Chan, M. M., Fong, D., Ho, C. T., Huang, H. I. (1997). Inhibition of inducible nitric oxide synthase gene expression and enzyme activity by epigallocatechin gallate, a natural product from green tea. *Biochemical Pharmacology*, 54: 1281–6.
- Chang, J. H., Gabison, E. E., Kato, T., Azar, D. T. (2001). Corneal neovascularization. *Current opinion ophthalmology*, 12: 242-249.
- Chen, C., Shen, G., Hebbar, V., Hu, R., Owuor, E. D., Kong, A. N. (2003). Epigallocatechin-3-gallate-induced stress signals in HT-29 human colon adenocarcinoma cells. *Carcinogenesis (Lond.)*, 24: 1369–78.
- Chen, W., Dong, Z., Valcic, S., Timmermann, B.N., Bowden, G. T. (1999). Inhibition of ultraviolet B-induced c-fos gene expression and p38 mitogenactivated protein kinase activation by (-)-epigallocatechin gallate in a human keratinocyte cell line. *Molecular Carcinogenesis*, 24: 79–84.
- Chesler, L., Goldenberg, D. D., Seales, I. T., Satchi-Fainaro, R., Grimmer, M., Collins, R. (2007). Malignant progression and blockade of angiogenesis in a murine transgenic model of neuroblastoma. *Cancer Research*, 67: 9435–42.
- Chung, J. Y., Huang, C., Meng, X., Dong, Z., Yang, C. S. (1999). Inhibition of activator protein 1 activity and cell growth by purified green tea and black tea polyphenols in H-ras-transformed cells: structure-activity relationship and mechanisms involved. *Cancer Research*, 59,: 4610–7.
- Cooper, R., Morre, D. J., Morre, D. M. (2005). Medicinal benefits of green tea: Part II. Review of anticancer properties. *Journal of Alternative and Complementary Medicine*, 11: 639-52.
- Corbel, M., Belleguic, E., Boichot, E., Lagente, V. (2002). Involvement of gelatinases (MMP-2 and MMP-9) in the development of airway inflammation and pulmonary fibrosis. *Cell Biology and Toxicology*, 18: 51–61.
- Crespy, V., Williamson, G. A. (2004). A review of the health effects of green tea catechins in in vivo animal models. *Journal of Nutrition*, 134: 3431S-40.
- Cursiefen, C., Kuchle, M., Naumann, G. O. (1998). Angiogenesis in corneal diseases: histopathologic evaluation of 254 human corneal buttons with neovascularization. *Cornea*, 17: 611–613.
- Cursiefen, C., Masli, S., Ng, T. F., Dana, M. R., Bornstein, P., Lawler, J. Streilein, J. W. (2004). Roles of thrombospondin-1 and -2 in regulating corneal and iris

- angiogenesis. *Investigative Ophthalmology & Visual Science*, 45: 1117–1124.
- Cursiefen, C., Chen, L., Borges, L., Jackson, D., D'Amore, P. A., Dana, M. R., Wiegand, S. J., Streilein, J. W. C. (2004). VEGF-A stimulates lymphangiogenesis and hemangiogenesis in inflammatory neovascularization via macrophage recruitment. *Journal of Clinical Investigation*, 113: 1040–1050.
- Cursiefen, C., Kruse, F. E. (2005). New aspects of corneal angiogenesis. In “*Essentials in Ophthalmology*” W. R. Krieglstein (ed.) New York. Springer.
- Cursiefen, C., Chen, L., Saint-Geniez, M., Hamrah, P., Jin, Y., Rashid, S., Pytowski, B., Persaud, K., Wu, Y., Streilein, J. W., Dana, R. (2006). Nonvascular VEGF receptor 3 expression by corneal epithelium maintains avascularity and vision. *Proceedings of the National Academy of Sciences*, 103:1405–11410.
- Cursiefen, C., Maruyama, K., Jackson, D. G. (2006). Time course of angiogenesis and lymphangiogenesis after brief corneal inflammation. *Cornea*, 25:443–447.
- Cursiefen, C. (2007). Immune privilege and angiogenic privilege of the cornea. *Chemical Immunology and Allergy*, 92: 50–57.
- D'Amato, R. J., Loughnan, M. S., Flynn, E., Folkman, J. (1994). Thalidomide is an inhibitor of angiogenesis. *Proceedings of the National Academy of Sciences*, 91: 4082–4085.
- Das, A., McGuire, P. (2006). Role of urokinase inhibitors in choroidal neovascularization. *Seminars of Ophthalmology*, 21: 23–7.
- Das, D.K., Maulik, N. (2006). Resveratrol in cardioprotection: a therapeutic promise of alternative medicine. *Molecular Informatic*, 6: 36-47.
- Davis, S. A. (1996). Isolation of angiopoietin-1, a ligand for the angiogenic TIE2 receptor, by secretion-trap expression cloning. *Cell*, 87:1161.
- Davison, T. F. (2003). The immunologists' debt to the chicken. *British Poultry Science*, 44: 6–21.
- Dawson, D. W., Volpert, O.V., Gillis, P., Crawford, S. E., Xu, H., Benedict, W., Bouck, N. P. (1999). Pigment epithelium-derived factor: a potent inhibitor of angiogenesis. *Science*, 285: 245–248.
- de Vries, C., Escobedo, J. A., Ueno, H., Houck, K., Ferrara, N., Williams, L. T. (1992). The fms-like tyrosine kinase, a receptor for vascular endothelial growth factor. *Science*, 255: 989-91.
- Delmas, D., Rebe, C., Lacour, S., Filomenko, R., Athias, A., Gambert, P. (2003).

- Resveratrol-induced apoptosis is associated with Fas redistribution in the rafts and the formation of a death-inducing signaling complex in colon cancer cells. *Journal of Biological Chemistry*, 278: 41482.
- Demeule, M., Brossard, M., Page, M., Gingras, D., Beliveau, R. (2000). Matrix metalloproteinase inhibition by green tea catechins. *Biochimica et Biophysica Acta*, 1478: 51–60.
- Denizot, F., Lang, R. (1986). Rapid colorimetric assay for cell growth and survival. Modifications to the tetrazolium dye procedure giving improved sensitivity and reliability. *Journal of Immunological Methods*, 89: 271–277.
- Distler, J. H., Hirth, A., Kurowska-Stolarska, M., Gay, R.E., Gay, S., Distler, O. (2000). Angiogenic and angiostatic factors in the molecular control of angiogenesis. *The quarterly journal of nuclear medicine and molecular imaging*, 47(3):149-61.
- Dollery, C. M., Libby, P. (2006). Atherosclerosis and proteinase activation. *Cardiovascular Research*, 69: 625–35.
- Dong, Z., Ma, W., Huang, C., Yang, C. S. (1997). Inhibition of tumor promoter-induced activator protein 1 activation and cell transformation by tea polyphenols, (-)-epigallocatechin gallate, and theaflavins. *Cancer Research*, 57: 4414–9.
- Dor, Y., Porat, R., Keshet, E. (2001). Vascular endothelial growth factor and vascular adjustments to perturbations in oxygen homeostasis. *American Journal of Physiology*, 280: C1367-74.
- Eccles, S.A., Box, C., Court, W. (2005). Cell migration/invasion assays and their application in cancer drug discovery. *Biotechnology Annual Reviews*, 11: 391–421.
- Edelman, J. L., Castro, M. R. (2000). Quantitative image analysis of laser-induced choroidal neovascularization in rat. *Experimental Eye Research*, 71(5):523-33.
- Fairbrother, W. J., Champe, M. A., Christinger, H. W. (1998). Solution structure of the heparin-binding domain of vascular endothelial growth factor. *Structure*, 6:637–48.
- Fassina, G., Vene, R., Morini, M., Minghelli, S. (2004). Mechanisms of inhibition of tumor angiogenesis and vascular tumor growth by epigallocatechin-3-gallate. *Clinical Cancer Research*, 10: 4865–4873.

- Ferrero, M. E., Bertelli, A. A. E., Fulgenzi, A., Pellegatta, F., Corsi, M. M., Bonfrate, M., Ferrara, F., De Caterina, R., Giovannini, L., Bertelli, A. (1998). Activity in vitro of resveratrol on granulocyte and monocyte adhesion to endothelium. *American Journal of Clinical Nutrition*, 68: 1208–1214
- Ferrara, N. (2002). Role of vascular endothelial growth factor in physiologic and pathologic angiogenesis: therapeutic implications. *Seminars in oncology*, 29:10–14.
- Ferrara, N. (2004). Vascular endothelial growth factor: basic science and clinical progress. *Endocrine Reviews*, 25: 581-611.
- Fett, J. W., Strydom, D. J., Lobb, R. R., Alderman, E. M., Bethune, J. L., Riordan, J. F., Vallee, B. L. (1985). Isolation and characterization of angiogenin, an angiogenic protein from human carcinoma cells. *Biochemistry*, 24: 5480–5486.
- Folkman, J. (1975). Tumor angiogenesis. *Advanced Cancer Research*, 43: 175–203.
- Folkman, J. (1982). Angiogenesis: initiation and control. *Annals of New York Academy of Sciences*, 401: 212–227
- Folkman, J. (1986). How is blood vessel growth regulated in normal and neoplastic tissue. *Cancer Research*, 46:467–473.
- Folkman J, Shing Y. (1992). Angiogenesis. *Journal of Biology Chemistry*, 267: 10931-10934.
- Folkman, J. (1995). Angiogenesis in cancer, vascular, rheumatoid and other disease. *Nature Medicine*, 1, 27–31.
- Folkman, J. (2004). Endogenous angiogenesis inhibitors. *Acta Pathologica Microbiologica et Immunologica Scandinavica*, 112: 496–507.
- Foster, B. C., Arnason, J. T., Briggs, C. J. (2004). Natural Health Products and Drug Disposition. *Annual Review of Pharmacology and Toxicology*, 45: 203-226.
- Fujiki, H. (1999). Two stages of cancer prevention with green tea. *Journal of Cancer Research and Clinical Oncology*, 125: 589–597.
- Funk, P. Thompson, C. B. (1996). Current concepts in chicken B cell development. *Current Topics in Microbiology and Immunology*, 212: 17.
- Garbisa, S., Biggin, S., Cavallarin, N., Sartor, L., Benelli, R., Albini, A. (1999). Tumor invasion: molecular shears blunted by green tea. *Nature Medicine*, 5: 1216.
- Garbisa, S., Sartor, L., Biggin, S., Salvato, B., Benelli, R., Albini, A. (2001). Tumor

- gelatinases and invasion inhibited by the green tea flavanol epigallocatechin-3-gallate. *Cancer*, 91: 822–32.
- Garner, A. (1994). Vascular diseases. In: “*Pathobiology of ocular disease*” K. G. Garner (ed.) pp 1625–1710. New York. Marcel Dekker.
- Garvin, S., Ollinger, K., Dabrosin, C. (2006). Resveratrol induces apoptosis and inhibits angiogenesis in human breast cancer xenografts in vivo. *Cancer Letter*, 231: 113–122.
- Gazmararian, J. A. (1995). Vision problems in the United States: a report on blindness and vision impairment in adults age 40 and older: prevent blindness America. 1–20.
- Gimbrone, M. A. J., Cotran, R. S., Leapman, S. B., Folkman, J. (1974). Tumor growth and neovascularization: an experimental model using the rabbit cornea. *Journal of National Cancer Institute*, 52: 413–427.
- Gioia, M., Monaco, S., Van Den Steen, P. E., Sbardella, D., Grasso, G., Marini, S., Overall, C. M., Opdenakker, G., Coletta, M. (2009). The collagen binding domain of gelatinase A modulates degradation of collagen IV by gelatinase B. *Journal of Molecular Biology*, 386: 419–34.
- Gluzman-Poltorak, Z., Cohen, T., Shibuya, M., Neufeld, G. (2001). Vascular endothelial growth factor receptor-1 and neuropilin-2 form complexes. *Journal of Biological Chemistry*, 276: 18688–94.
- Goodwin, A. M. (2007). In vitro assays of angiogenesis for assessment of angiogenic and anti-angiogenic agents. *Microvascular Research*, 74: 172–183.
- Green, W. R. (1986). The uveal tract. In “*Ophthalmic Pathology: An Atlas and Textbook*” W. Spencer (ed.) 1513–1521. Philadelphia. WB Saunders.
- Grossniklaus, H. E., Ling, J. X., Wallace, T. M., Dithmar, S., Lawson, D. H., Cohen, C. Elner, V. M., Elner, S. G., Sternberg, P. (2002). Macrophage and retinal pigment epithelium expression of angiogenic cytokines in choroidal neovascularization. *Molecular Vision*, 8: 119–126.
- Gupta, S., Hastak, K., Afaq, F., Ahmad, N., Muktar, H. (2003). Essential role of caspases in epigallocatechin-3-gallate-mediated inhibition of nuclear factor kappaB and induction of apoptosis. *Oncogene*, 1–16.
- Grossniklaus, H. E., Cingle, K. A., Yoon, Y.D., Ketkar, N., L'Hernault, N., Brown, S. (2000). Correlation of histologic 2-dimensional reconstruction and confocal

- scanning laser microscopic imaging of choroidal neovascularization in eyes with age-related maculopathy. *Archives Ophthalmology*, 118: 625–629.
- Haraguchi, H., Ishikawa, H., Mizutani, K., Tamura, Y., Kinoshita, T. (1998). Antioxidative and superoxide scavenging activities of retrochalcones in *Glycyrrhiza inflata*. *Bioorganic & Medicinal Chemistry*, 6: 339-47.
- Hartwell, D. W., Butterfield, C. E., Frenette, P. S. (1998). Angiogenesis in P- and E-selectin-deficient mice. *Microcirculation*, 5: 173–178.
- Hastak, K., Gupta, S., Ahmad, H., Agarwal, M. K., Agarwal, M. L., Muktar, H. (2003). Role of p53 and NF-kappaB in epigallocatechin-3-gallate-induced apoptosis of LNCaP cell. *Oncogene*, 22: 4851–9.
- Heiduschka, P., Blitgen-Heinecke, P., Tura, A., Kokkinou, D. (2007). Melanin precursor 5,6-dihydroxyindol: protective effects and cytotoxicity on retinal cells *in vitro* and *in vivo*. *Toxicologic Pathology*, 35:1030-8.
- Hoeben, A. L. (2004). Vascular endothelial growth factor and angiogenesis. *Pharmacological Reviews*, 56: 549-80.
- Holekamp, N. M., Noel, B., Olga, V. (2002). Pigment epitheliumderived factor is deficient in the vitreous of patients with choroidal neovascularization due to age-related macular degeneration. *American Journal of Ophthalmology*, 134: 220–227.
- Houck, K. A., Leung, D. W., Rowland, A. M. (1992). Dual regulation of vascular endothelial growth factor bioavailability by genetic and proteolytic mechanisms. *Journal of Biological Chemistry*, 267: 26031–7.
- Hsu, Y. L., Kuo, P. L., Lin, C. C. (2005). Isoliquiritigenin induces apoptosis and cell cycle arrest through p53-dependent pathway in Hep G2 cells. *Life Science*, 77: 279-92.
- Huang, C., Ma, W. Y., Goranson, A., Dong, Z. (1999). Resveratrol suppresses cell transformation and induces apoptosis through a p53-dependent pathway. *Carcinogenesis*, 20: 237-42.
- Hudson, T. S., Hartle, D. K, Hursting, S. D., Nunez, N. P., Wang, T. T., Young, H. A., Arany, P., Green, J. E. (2007). Inhibition of prostate cancer growth by muscadine grape skin extract and resveratrol through distinct mechanisms. *Cancer Research*, 67: 8396–8405.
- Husain, D., Ambati, B., Adamis, A. P., Miller, J. W. (2002). Mechanisms of

- age-related macular degeneration. *Ophthalmology Clinics of North America*, 15: 87–91.
- Ii, T., Satomi, Y., Katoh, D., Shimada, J., Baba, M., Okuyama, T. (2004). Induction of cell cycle arrest and p21(CIP1/WAF1) expression in human lung cancer cells by isoliquiritigenin. *Cancer Letter*, 207: 27-35.
- Ingber, D., Fujita, T., Kishimoto, S., Sudo, K., Kanamaru, T., Brem, H., Folkman, J. (1990). Synthetic analogues of fumagillin that inhibit angiogenesis and suppress tumour growth. *Nature*, 348: 555–557.
- Iruela-Arispe, M. L. (2008). endothelial cell activation. In: “*Angiogenesis: an integrative approach from science to medicine*”. W. A. Figg (ed.). Chapter 3: 35-43.
- Isemura, M., Saeki, K., Kimura, T., Hayakawa, S., Minami, T., Sazuka, M. (2000). Tea catechins and related polyphenols as anti-cancer agents. *Biofactors*, 13: 81–5.
- Jablonski, M. M., Tombran-Tink, J., Mrazek, D. A., Iannaccone, A. (2007). Pigment epithelium-derived factor supports normal development of photoreceptor neurons and opsin expression after retinal pigment epithelium removal. *Journal of Neuroscience*, 20: 7149–7157.
- Jankun, J., Selman, S. H., Swiercz, R., Skrzypczak-Jankun, E. (1997). Why drinking green tea could prevent cancer. *Nature (Lond.)*, 387: 561.
- Janse, E. M., Jeurissen, S. H. (1991). Ontogeny and function of two non-lymphoid cell populations in the chicken embryo. *Immunobiology*, 182: 472–481.
- John, A., Tuszynski, G. (2001). The role of matrix metalloproteinases in tumor angiogenesis and tumor metastasis. *Pathol Oncol Res*, 7: 14–23.
- Joko, J., Mazurek, M. (2004). Transcription factors having impact on vascular endothelial growth factor (VEGF) gene expression in angiogenesis. *Medical Science Monitor*, 10: 89-98.
- Jung, Y. D., Kim, M. S., Shin, B. A. (2001). EGCG, a major component of green tea, inhibits tumour growth by inhibiting VEGF induction in human colon carcinoma cells. *British Journal of Cancer*, 84: 844–50.
- Kang, S. W., Choi, J. S., Choi, Y. J., Bae, J. Y., Li, J., Kim, D. S. (2009). Licorice isoliquiritigenin dampens angiogenic activity via inhibition of MAPK-responsive signaling pathways leading to induction of matrix

- metalloproteinases. *Journal of Nutritional Biochemistry*, 21: 55-65.
- Kanga, S. W., Choia, J.S., Choia, Y.J., Baea, J. Y., Lia, J., Kima, D.S., Kima, J. L., Shina, S. Y., Leeb, Y.G. (2010). Licorice isoliquiritigenin dampens angiogenic activity via inhibition of MAPK-responsive signaling pathways leading to induction of matrix metalloproteinases. *Journal of Nutritional Biochemistry*, 21: 55–65.
- Karakousis, P. C., John, S. K., Behling, K. C., Surace, E. M., Smith, J. E., Hendrickson A. et al. (2001) Localization of pigment epithelium derived factor (PEDF) in developing and adult human ocular tissues. *Molecular Vision*, 7: 154–163.
- Kargozaran, H., Yuan, S. Y., Breslin, J. W., Watson, K. D., Gaudreault, N., Breen, A. (2007). A role for endothelial-derived matrix metalloproteinase-2 in breast cancer cell transmigration across the endothelial-basement membrane barrier. *Clinical Experiment of Metastasis*, 24: 495–5.
- Kato, T., Kure, T., Chang, J. H. (2001). Diminished corneal angiogenesis in gelatinase A-deficient mice. *FEBS Letter*, 508: 187-190.
- Kenyon, B. M., Browne, F., D'Amato, R. J. (1997). Effects of thalidomide and related metabolites in a mouse corneal model of neovascularization. *Experimental Eye Research*, 64: 971–978.
- Keyt, B. A., Berleau, L. T., Nguyen, H. V. (1996). The carboxyl-terminal domain (111-165) of vascular endothelial growth factor is critical for its mitogenic potency. *Journal of Biological Chemistry*, 271: 7788–95.
- Khan, A. A., Dace, D. S., Ryazanov, A. G., Kelly, J., Apte, R. S. (2010). Resveratrol regulates pathologic angiogenesis by a eukaryotic elongation factor-2 kinase-regulated pathway. *American Journal of Pathology*. (Epub ahead of print).
- Kim, B., Tang, Q., Biswas, P. S., Xu, J., Schiffelers, R. M., Xie, F. Y., Ansari, A. M., Scaria, P. V., Woodle, M. C., Lu, P., Rouse, B. T. (2004). Inhibition of ocular angiogenesis by siRNA targeting vascular endothelial growth factor pathway genes: therapeutic strategy for herpetic stromal keratitis. *American Journal of Pathology*, 165: 2177–2185.
- Kim, K. S., Oh, J. S. Kwak, J. S. (1996). Ultrastructure of surgically excised subfoveal neovascular membranes. *Korean Journal of Ophthalmol*, 10: 76–81.

- Kimura, Y., Okuda, H. (2001). Resveratrol isolated from *Polygonum cuspidatum* root prevents tumor growth and metastasis to lung and tumor-induced neovascularization in Lewis lung carcinoma-bearing mice. *Journal of Nutrition*, 131: 1844-9.
- Kisucka, J., Butterfield, C. E., Duda, D. G., Eichenberger, S. C., Saffaripour, S., Ware, J., Ruggeri, Z. M., Jain, R. K., Folkman, J., Wagner, D. D. (2006). Platelets and platelet adhesion support angiogenesis while preventing excessive hemorrhage. *Proceedings of the National Academy of Sciences USA*, 103: 855–860.
- Kobayashi, S., Miyamoto, T., Kimura, I., Kimura, M. (1995). Inhibitory effect of isoliquiritin, a compound in licorice root, on angiogenesis in vivo and tube formation in vitro. *Biological & Pharmaceutical Bulletin*, 18: 1382-6.
- Koh, S. H., Kim, S. H., Kwon, H., Kim, J. G., Kim, J. H., Yang, K. H. (2004). Phosphatidylinositol-3 kinase/Akt and GSK-3 mediated cytoprotective effect of epigallocatechin gallate on oxidative stress-injured neuronal-differentiated N18D3 cells. *Neurotoxicology*, 25: 793-802.
- Korkolopoulou, P., Levidou, G., Saetta, A. A., El-Habr, E., Eftichiadis, C., Demenagas, P., Thymara, I., Xiromeritis, K., Boviatsis, E., Thomas-Tsagli, E., Panayotidis, I., Patsouris, E. (2008). Expression of nuclear factor-kappaB in human astrocytomas: relation to pI kappa Ba, vascular endothelial growth factor, Cox-2, microvascular characteristics, and survival. *Human Pathology*, 39: 1143-52.
- Krzystolik, M. G., Afshari, M. A., Adamis, A. P. (2002). Prevention of experimental choroidal neovascularization with intravitreal anti-vascular endothelial growth factor antibody fragment. *Archives of Ophthalmology*, 120: 338–346.
- Kugler, A. (1999). Matrix metalloproteinases and their inhibitors. *Anticancer Research*, 19: 589–92.
- Kumar, S., Sharma, A., Madan, B., Singhal, V., Ghosh, B. (2007). Isoliquiritigenin inhibits IkappaB kinase activity and ROS generation to block TNF-alpha induced expression of cell adhesion molecules on human endothelial cells. *Biochemistry and Pharmacology*, 73: 1602-12.
- Kusaka, M., Sudo, K., Fujita, T., Marui, S., Itoh, F., Ingber, D., Folkman, J. (1991). Potent anti-angiogenic action of AGM-1470: comparison to the fumagillin parent. *Biochemical and Biophysical Research Communications*, 174:

1070–1076.

- Kvanta, A. (2006) Ocular angiogenesis: the role of growth factors. *Acta Ophthalmologica Scandinavi*, 84, 282–288.
- Kwon, G. T., Cho, H. J., Chung, W. Y., Park, K. K., Moon, A., Park, J. H. (2008). Isoliquiritigenin inhibits migration and invasion of prostate cancer cells: possible mediation by decreased JNK/AP-1 signaling. *Journal of Nutritional Biochemistry*, 20: 663-76.
- Kwon, G. T., Cho, H. J., Chung, W. Y., Park, K. K., Moon, A., Park, J. H. (2009). Isoliquiritigenin inhibits migration and invasion of prostate cancer cells: possible mediation by decreased JNK/AP-1 signaling. *Journal of Nutritional Biochemistry*, 20: 663-76.
- Lai, H. C., Chao, W. T., Chen, Y. T. (2004). Effect of EGCG, a major component of green tea, on the expression of Ets-1, c-Fos, and c-Jun during angiogenesis in vitro. *Cancer Letter*, 213: 181-8.
- Lampugnani, M. G. (1999). Cell migration into a wounded area in vitro. *Methods in Molecular Biology*, 96: 177–182.
- Lamy, S., Gingras, D., and Be'liveau, R. (2002). Green Tea Catechins Inhibit Vascular Endothelial Growth Factor Receptor Phosphorylation. *Cancer research*, 62: 381–385.
- Lee, B., Moon, S. K. (2005). Resveratrol inhibits TNF-alpha-induced proliferation and matrix metalloproteinase expression in human vascular smooth muscle cells. *Journal of Nutrition*, 135: 2767-73.
- Lee, J. H., Canny, M. D., de Erkenez, A. (2005). A therapeutic aptamer inhibits angiogenesis by specifically targeting the heparin binding domain of VEGF165. *Proceedings of the National Academy of Sciences*, 102: 18902–7.
- Lee, P., Wang, C. C., Adamis, A. P. (1998). Ocular neovascularization: an epidemiologic review. *Survey of ophthalmology*, 43: 245–269.
- Leene, W., Duyzings, M. J. M., von Steeg, C. (1973). Lymphoid stem cell identification in the developing thymus and bursa of Fabricius of the chick. *Z. Zellforsch*, 136: 521–533.
- Leibowitz, H. M., Krueger, D. E., Maunder, L. R., (1980). The Framingham Eye Study monograph: An ophthalmological and epidemiological study of cataract, glaucoma, diabetic retinopathy, macular degeneration, and visual acuity in a

- general population of 2631 adults, 1973–1975. *Survey Ophthalmology*, 24: 335–610.
- Li, Y. , Liu, J., Liu, X., Xing, K., Wang, Y., Li, F., Yao, L. (2006). Resveratrol-induced cell inhibition of growth and apoptosis in MCF7 human breast cancer cells are associated with modulation of phosphorylated Akt and caspase-9. *Appl. Biochem. Biotechnol*, 135: 181–192.
- Liang, Y. C., Lin-shiau, S. Y., Chen, C. F., Lin, J. K. (1997). Suppression of extracellular signals and cell proliferation through EGF receptor binding by (-)-epigallocatechin gallate in human A431 epidermoid carcinoma cells. *Journal of Cellular Biochemistry*, 67: 55–65.
- Lin, M. T., Yen, M. L., Lin, C. Y., Kuo, M. L. (2003). Inhibition of vascular endothelial growth factor-induced angiogenesis by resveratrol through interruption of Src-dependent vascular endothelial cadherin tyrosine phosphorylation. *Molecular Pharmacology*, 64: 1029-36.
- Liu, P.L., Tsai, J.R., Charles, A. L (2010). Resveratrol inhibits human lung adenocarcinoma cell metastasis by suppressing heme oxygenase 1-mediated nuclear factor-kappaB pathway and subsequently downregulating expression of matrix metalloproteinases. *Molecular Nutrition and Food*. [Epub ahead of print]
- Maeda-Yamamoto, M., Kawahara, H., Tahara, N., Tsuji, K., Hara, Y., Isemura, M. (1999). Effects of tea polyphenols on the invasion and matrix metalloproteinases activities of human fibrosarcoma HT1080 cells. *Journal of Agricultural and Food Chemistry*, 47: 2350–4.
- Maggiolini, M., Statti, G., Vivacqua, A., Gabriele, S., Rago, V., Loizzo, M. (2002). Estrogenic and antiproliferative activities of isoliquiritigenin in MCF7 breast cancer cells. *Journal of Steroid Biochemistry and Molecular Biology*, 82: 315-22.
- Mahoney, J. M., Waterbury, L. D. (1985). Drug effects on the neovascularization response to silver nitrate cauterization of the rat cornea. *Current Eye Research*, 4: 531-5.
- Makimura, M., Hirasawa, M., Kobayashi, K. (1993). Inhibitory effect of tea catechins on collagenase activity. *Journal of Periodontology*, 64: 630–6.
- Marconcini, L., Marchio, S., Morbidelli, L., Cartocci, E., Albini, A., Ziche, M., Bussolino, F., Oliviero, S. (1999). c-fos-induced growth factor/vascular

- endothelial growth factor D induces angiogenesis in vivo and in vitro. *Proceedings of the National Academy of Sciences*, 96: 9671–9676.
- Mariotti, M., Maier, J. A. M. (2006). Angiogenesis: an overview. In: “*New frontier in angiogenesis*” R. Forough (ed.). 1-30.
- Masuda, M., Suzui, M., Weinstein, I. B. (2001). Effects of epigallocatechin-3-gallate on growth, epidermal growth factor receptor signaling pathways, gene expression and chemosensitivity in human head and neck squamous cell carcinoma cell lines. *Clinical Cancer Research*, 7: 4220–9.
- Masuda, M., Suzui, M., Lim, J. T. E (2003). Epigallocatechin-3-gallate inhibits activation of Her-2/neu and downstream signaling pathways in human head and neck and breast carcinoma cells. *Clinical Cancer Research*, 9:3486–91.
- Matthews, W., Jordan, C. T., Gavin, M., Jenkins, N. A., Copeland, N. G., Lemischka, I. R. (1991). A receptor tyrosine kinase cDNA isolated from a population of enriched primitive hematopoietic cells and exhibiting close genetic linkage to *c-kit*. *Proceedings of National Academy of Sciences. USA*, 88: 9026-30.
- Millauer, B., Wизigmann-Voos, S., Schnürch, H., Martinez ,R., Miller, N. P., Risau, W., Ullrich, A. (1993). High affinity VEGF binding and developmental expression suggest Flk-1 as a major regulator of vasculogenesis and angiogenesis. *Cell*, 72: 835-46.
- Miloso, M., Bertelli, A.A.E., Nicolini, G., Tredici, G (1999). resveratrol-induced activation of the mitogen-activated protein kinases ERK1 and ERK2, in human neuroblastoma SH-SY5Y cells. *Neuroscience Letter*, 264: 141–144.
- Mori, K., Duh, E., Gehlbach, P., Ando, A., Takahashi, K., Pearlman, J. et al. (2001) Pigment epithelium derived factor inhibits retinal and choroidal neovascularization. *Journal of Cellular Physiology*. 188, 253–263.
- Mosmann, T. (1983). Rapid colorimetric assay for cellular growth and survival: application to proliferation and cytotoxicity assays. *Journal of immunological methods*, 65: 55–63.
- Mukhtar, H., Ahmad, N. (1999). Green tea in chemoprevention of cancer. *Society of Toxicology*, 52: 111–7.
- Mukhtar, H., Ahmad, N. (2000). Tea polyphenols: prevention of cancer and optimizing health. *American Journal of Clinical Nutrition*, 71: 1698S-702S.
- Muthukkaruppan V. R., Auerbach, R. (1979). Angiogenesis in the mouse cornea.

- Science*, 205: 1416–1418.
- Nagase, H., Visse, R., Murphy, G. (2006). Structure and function of matrix metalloproteinases and TIMPs. *Cardiovascular Research*, 69: 562–73.
- Neufeld, G., Cohen, T., Gengrinovitch, S., Poltorak, Z. (1999). Vascular endothelial growth factor (VEGF) and its receptors. *FASEB Journal*, 13: 9-22.
- Ng, Y. S., Rohan, R., Sunday, M. E. (2001). Differential expression of VEGF isoforms in mouse during development and in the adult. *Developmental Dynamics*, 220: 112–21.
- Nguyen, M., Shing, Y., Folkman, J. (1994). Quantitation of angiogenesis and antiangiogenesis in the chick embryo chorioallantoic membrane. *Microvascular Research*, 47: 31–40.
- Oak, M. H., El Bedoui, J., Schini-Kerth, V. B. (2005). Antiangiogenic properties of natural polyphenols from red wine and green tea. *Journal of Nutritional Biochemistry*, 16: 1-8.
- Ogata, N., Matsuoka, M., Matsuyama, K., Shima, C., Tajika, A., Nishiyama, T. et al. (2007) Plasma concentration of pigment epitheliumderived factor in patients with diabetic retinopathy. *Journal of Clinical Endocrinology and Metabolism*. 92: 1176–1179.
- Ogata, N., Nishikawa, M., Nishimura, T., Mitsuma, Y. and Matsumura, M. (2002a) Unbalanced vitreous levels of pigment epithelium derived factor and vascular endothelial growthfactor in diabetic retinopathy. *American Journal of Ophthalmology*. 134, 348–353.
- Ogata, N., Wada, M., Otsuji, T., Jo, N., TombranTink, J. and Matsumura, M. (2002b) Expression of pigment epitheliumderived factor in normal adult rat eye and experimental choroidal neovascularization. *Investigation of Ophthalmology and Vision Sciences*, 43, 1168–1175.
- Ohno-Matsui K., Morita I., Tombran-Tink J., Mrazek D., Onodera, M., Uetama T. (2001) Novel mechanism for age related macular degeneration: an equilibrium shift between the angiogenesis factors VEGF and PEDF. *Journal of Cell Physiology*, 189: 323–333.
- Okabe, S., Ochiai, Y., Aida, M. (1999). Mechanistic aspects of green tea as a cancer preventive: effect of components on human stomach cancer cell lines. *Japanese Journal of Cancer Research*, 90: 733–9.

- Oku, N., Matsukawa, M., Yamakawa, S. (2003). Inhibitory effect of green tea polyphenols on membrane-type 1 matrix metalloproteinase, MT1-MMP. *Biological & Pharmaceutical Bulletin*, 26: 1235-8.
- Olofsson, B., Korpelainen, E., Pepper, M. S. (1998). Vascular endothelial growth factor B (VEGF-B) binds to VEGF receptor-1 and regulates plasminogen activator activity in endothelial cells. *Proceedings of National Academy of Sciences USA*, 95: 11709–14.
- O'Reilly, M. S., Holmgren, L., Shing, Y., Chen, C., Rosenthal, R. A., Moses, M., Lane, W. S., Cao, Y., Sage, E. H., Folkman, J. (1994). Angiostatin: a novel angiogenesis inhibitor that mediates the suppression of metastases by a Lewis lung carcinoma. *Cell*, 79: 315–328.
- Ortego, J., Escribano, J., Becerra, S.P., Coca Prados, M. (1996) Gene expression of the neurotrophic pigment epithelium-derived factor in the human ciliary epithelium. Synthesis and secretion into the aqueous humor. *Investigation of Ophthalmology and Vision Sciences*. 37: 2759–2767.
- Pardanaud, L., Yassine, F., Dieterlen-Lievre, F. (1989). Relationship between vasculogenesis, angiogenesis and hematopoiesis during avian ontogeny. *Development*, 105: 473–485.
- Park, A. M., Dong, Z. (2003). Signal transduction pathways: targets for green and black tea polyphenols. *Journal of Biochemistry and Molecular Biology*, 36: 66-77.
- Park, I., Park, K. K., Park, J. H., Chung, W. Y. (2009). Isoliquiritigenin induces G2 and M phase arrest by inducing DNA damage and by inhibiting the metaphase/anaphase transition. *Cancer Letter*, 277: 174-181.
- Park, J. E., Keller, G. A., Ferrara, N (1993). The vascular endothelial growth factor (VEGF) isoforms: differential deposition into the subepithelial extracellular matrix and bioactivity of extracellular matrix-bound VEGF. *Molecular Biology of the Cell*, 4: 1317–26.
- Park, S. K. (2010). Combined cetuximab and genistein treatment shows additive anti-cancer effect on oral squamous cell carcinoma. *Cancer Letter*, 292: 54-63.
- Park, K.W., Morrison, C. M., Sorensen, L.K., Jones, C.A., Rao, Y., Chien, C. B. (2003). Robo4 is a vascular-specific receptor that inhibits endothelial migration. *Developmental Biology*, 261: 251–267.

- Patan, S., Haenni, B., Burri, P. H. (1993). Evidence for intussusceptive capillary growth in the chicken chorio-allantoic membrane (CAM). *Anatomy and Embryology*, 187: 121–130.
- Patan, S., Heanni, B., Burri, P. H. (1996). Implementation of intussusceptive microvascular growth in the chicken chorioallantoic membrane (CAM): Pillar formation by folding of the capillary wall. *Microvascular Research*, 51: 80–98.
- Patan, S., Munn, L. L., Jain, R. K. (1996). Intussusceptive microvascular growth in a human colon adenocarcinoma xenograft: a novel mechanism of tumor angiogenesis. *Microvascular Research*, 51: 260–272.
- Patan, S., Heanni, B., Burri, P. H. (1997). Implementation of intussusceptive microvascular growth in the chicken chorioallantoic membrane (CAM): Pillar formation by capillary fusion. *Microvascular Research*, 53: 33–52.
- Patan, S. (1998). TIE1 and TIE2 receptor tyrosine kinases inversely regulate embryonic angiogenesis by the mechanism of intussusceptive microvascular growth. *Microvascular Research*, 56: 1–21.
- Patricia, L. W. (1998). Ocular neovascularization: an epidemiologic review. *Survey of ophthalmology*, 43:242-249.
- Penfold, P. L., Madigan, M. C., Gillies, M. C. Provis, J. M. (2001). Immunological and aetiological aspects of macular degeneration. *Progress in Retinal and Eye Research*, 20: 385–414.
- Phillips, G. D., Stone, A. M., Jones, B. D., Schultz, J. C., Whitehead, R. A., Knighton, D. R. (1994). Vascular endothelial growth factor (rhVEGF165) stimulates direct angiogenesis in the rabbit cornea. *In Vivo*, 8:961–965.
- Poole, T. C. (1989). Vasculogenesis and angiogenesis: Two distinct morphogenetic mechanisms establish embryonic vascular pattern. *Journal of Experimental Zoology*, 251:224–231.
- Poussier, B., Cordova, A. C., Becquemin, J. P., Sumpio, B. E. (2005). Resveratrol inhibits vascular smooth muscle cell proliferation and induces apoptosis. *Journal of Vascular Surgery*, 42:1190-7.
- Presta, M., Rusnati, M., Belleri, M., Morbidelli, L., Ziche, M., Ribatti, D. (1999). Purine analogue 6-methylmercaptapurine riboside inhibits early and late phases of the angiogenic process. *Cancer Research*, 59: 2417–2424.
- Pulukuri, S. M., Rao, J. S. (2008). Matrix metalloproteinase-1 promotes prostate

- tumor growth and metastasis. *International Journal of Oncology*, 32: 757–65.
- Qiu, G. Stewart, J. M., Satta, S., Freda, R., Lee, S., Guven, D., de Juan, E. Jr., Varner, S. E. (2006). A new model of experimental subretinal neovascularization in the rabbit. *Experimental Eye Research*, 83: 141-152.
- Roskosk, R. (2007). Vascular endothelial growth factor (VEGF) signaling in tumor progression. *Critical Review in Oncology and Hematology*, 62: 179-213.
- Rakoczy, E. P., Yu, M. J., Nusinowitz, S., Chang, B., Heckenlively, J. R. (2006). Mouse models of age-related macular degeneration. *Experimental Eye Research*, 82: 741–752.
- Ribatti, D., Vacca, A., Roncali, L., Dammacco, F. (1996). The chick embryo chorioallantoic membrane as a model for in vivo research on angiogenesis. *International Journal of Developmental Biology*, 40: 1189-97.
- Ribatti, D., Gualandris, A., Bastaki, M., Vacca, A., Iurlaro, M., Roncali, L., Presta, M. (1997). New model for the study of angiogenesis and antiangiogenesis in the chick embryo chorioallantoic membrane: the gelatin sponge/chorioallantoic membrane assay. *Journal of Vascular Research*, 34.
- Ribatti, D., Vacca, A., Roncali, L., Dammacco, F. (2000). The chick embryo chorioallantoic membrane as a model for in vivo research on antiangiogenesis. *Current Pharmaceutical Biotechnology*, 1: 73–82.
- Ribatti, D. Chick embryo chorioallantoic membrane as a useful tool to study angiogenesis. Chapter 5. In: “*International review of cell and molecular biology*”, Volume 270: 182-213.
- Ribatti, D., Nico, B., Vacca, A., Presta, M. (2006). The gelatin sponge–chorioallantoic membrane assay. *Nature protocols*, 1: 85-91.
- Richardson, M., Singh, G. Observations on the use of the avian chorioallantoic membrane (CAM) model in investigations into angiogenesis, *Current Drug Targets Cardiovascular and Haematology Disorder*.3(2003)155–185.
- Rodriguez-Pla, A., Bosch-Gil, J. A., Rossello-Urgell, J., Huguet-Redecilla, P., Stone, J. H., Vilardell-Tarres, M. (2005). Metalloproteinase-2 and -9 in giant cell arteritis: involvement in vascular remodeling. *Circulation*, 112: 264–9.
- Rohan, R. M., Fernandez, A., Udagawa, T., Yuan, J., D’Amato, R. J. (2000). Genetic heterogeneity of angiogenesis in mice. *FASEB Journal*, 14: 871–876.

- Sah, J. F., Balasubramanian, S., Eckert, R. L., Rorke, E. A. (2003). Epigallocatechin-3-gallate inhibits epidermal growth factor receptor signaling pathway: evidence for direct inhibition of ERK 1/2 and AKT kinases. *Journal of Biological Chemistry*, 279: 12755–62.
- Saito, Y., Hasebe-Takenaka, Y., Ueda, T., Nakanishi-Ueda, T., Kosuge, S., Aburada, M. (2007). Effects of green tea fractions on oxygen-induced retinal neovascularization in the neonatal rat. *Journal of Clinical Biochemistry & Nutrition*, 41: 43-9.
- Samolov, B., Kvanta, A., van der Ploeg, I. (2010). Delayed neovascularization in inflammation-induced corneal neovascularization in interleukin-10-deficient mice. *Acta Ophthalmologica*, 88: 251-6.
- Sartippour, M. R., Heber, D., Zhang, L. (2002). Inhibition of fibroblast growth factors by green tea. *International Journal of Oncology*, 21: 487-91.
- Sartippour, M. R., Heber, D., Henning, S. (2004). cDNA microarray analysis of endothelial cells in response to green tea reveals a suppressive phenotype. *International Journal of Oncology*, 25:193-202.
- Schneider, J.K., Gardner, D.K., and Cordero, L. (2008) Use of recombinant human erythropoietin and risk of severe retinopathy in extremely low birth weight infants. *Pharmacotherapy*. 28: 1335–1340.
- Schwesinger, C., Yee, C., Rohan, R. M., Jousseaume, A. M., Fernandez, A., Meyer, T. N. et al. (2001) Intrachoroidal neovascularization in transgenic mice overexpressing vascular endothelial growth factor in the retinal pigment epithelium. *American Journal of Pathology*, 158, 1161–1172.
- Sengupta, S., Toh, S. A., Sellers, L. A. (2004). Modulating angiogenesis: the yin and the yang in ginseng. *Circulation*, 110: 1219-25.
- Sexton, E., Van Themsche, C., LeBlanc, K., Parent, S., Lemoine, P., Asselin, E. (2006). Resveratrol interferes with AKT activity and triggers apoptosis in human uterine cancer cells. *Molecular Cancer*, 5: 45.
- Shen, W. Y., Yu, M. J. T., Barry, C. J., Constable, I. J., Rakoczy, P. E. (1998). Expression of cell adhesion molecules and vascular endothelial growth factor in experimental choroidal neovascularisation in the rat. *British Journal of Ophthalmology*, 82: 1063–1071.
- Shibuya, M., Yamaguchi, S., Yamane, A., Ikeda, T., Tojo, A., Matsushime, H., Sato,

- M (1990). Nucleotide sequence and expression of a novel human receptor-type tyrosine kinase gene (flt) closely related to the fms family. *Oncogene*, 5: 519-24.
- Shing, Y., Folkman, J., Haudenschild, C., Lund, D., Crum, R., Klagsbrun, M. (1985). Angiogenesis is stimulated by a tumor-derived endothelial cell growth factor. *Journal of Cell Biochemistry*, 29: 275–29287.
- Silverman, K. J., Lund, D. P., Zetter, B. R., Lainey, L. L., Shahood, J. A., Freiman, D. G., Folkman, J., Barger, A. C. (1988). Angiogenic activity of adipose tissue. *Biochemical and Biophysical Research Communications*, 153: 347–352.
- Singh, N., Macnamara, E., Rashid, S., Ambati, J., Kontos, C. D., Higgins, E. et al. (2005b) Systemic soluble Tie2 expression inhibits and regresses corneal neovascularization. *Biochemistry and Biophysics Research Community*. 332: 194–199.
- Singh, N., Higgins, E., Amin, S., Jani, P., Richter, E., Patel, A. et al. (2007) Unique homologous siRNA blocks hypoxia-induced VEGF upregulation in human corneal cells and inhibits and regresses murine corneal neovascularization. *Cornea*. 26: 65–72.
- Soker, S., Takashima, S., Miao, H. Q. (1998). Neuropilin-1 is expressed by endothelial and tumor cells as an isoform-specific receptor for vascular endothelial growth factor. *Cell*, 92: 735–45.
- Stacker, S. A., Caesar, C., Baldwin, M. E. (2001). VEGF-D promotes the metastatic spread of tumor cells via the lymphatics. *Nature Medicine*, 7: 186–91.
- Staton, C. A., Stribbling, S. M., Tazzyman, S., Hughes, R., Brown, N. J., and Lewis, C. E. (2004). Current methods for assaying angiogenesis in vitro and in vivo. *International Journal of Experimental Pathology*, 85: 233–248.
- Streilein, J. W., Bradley, D., Sano, Y., Sonoda, Y. (1996). Immunosuppressive properties of tissues obtained from eyes with experimentally manipulated corneas. *Investigative Ophthalmology & Visual Science*, 37: 413-424.
- Streilein, J. W. (2003). Ocular immune privilege: therapeutic opportunities from an experiment of nature. *Nature reviews immunology*, 3: 879–889.
- Sunderkotter, C., Steinbrink, K., Goebeler, M., Bhardwaj, R., Sorg, C. (1994). Macrophages and angiogenesis. *Journal of Leukocyte Biology*, 55: 410–422.
- Suchting, S., Heal, P., Tahtis, K., Stewart, L.M., Bicknell, R. (2005). Soluble Robo4 receptor inhibits in vivo angiogenesis and endothelial cell migration. *FASEB*

- Journal*, 19: 121–123.
- Suri, C., Jones, P. F., Patan, S., Bartunkova, S., Maisonpierre, P. C, Davis. S., Sato, T. N., Yancopoulos, G. D. (1996). Requisite role of Angiopoietin-1, a ligand for the TIE2 receptor during embryonic angiogenesis. *Cell*, 87: 1171–1180.
- Takahashi, H., Shibuya, M. (2005). The vascular endothelial growth factor (VEGF)/VEGF receptor system and its role under physiological and pathological conditions. *Clinical Science*, 109: 227–41.
- Tang, F.Y., Nguyen, N., Meydani, M. (2003). Green tea catechins inhibit VEGF-induced angiogenesis in vitro through suppression of VE-cadherin phosphorylation and inactivation of Akt molecule. *International Journal of Cancer*, 106: 871 - 878.
- Tardy, Y., Resnick, N., Nagel, T., Gimbrone, M. A. Jr., Dewey, C. F. (1997). Shear stress gradients remodel endothelial monolayers in vitro via a cell proliferation-migration-losscycle. *Arterioscler. Arteriosclerosis, thrombosis, and vascular biology*, 17: 3102–3106.
- Tawata, M., Aida, K., Noguchi, T., Ozaki, Y., Kume, S., Sasaki, H. (1992). Anti-platelet action of isoliquiritigenin, an aldose reductase inhibitor in licorice. *European Journal of Pharmacology*, 212: 87-92.
- Taylor, C. M., Weiss, J. B. (1984). The chick vitelline membrane a test system for angiogenesis and antiangiogenesis. *Journal of International Microcirculation Clinical Experiments*, 3: 337.
- Taylor, S., Folkman, J. (1982). Protamine is an inhibitor of angiogenesis. *Nature*, 297: 307–312.
- Terman, B.I., Carrion, M. E., Kovacs, E., Rasmussen, B A., Eddy, R. L., Shows, T. B. (1991). Identification of a new endothelial cell growth factor receptor tyrosine kinase. *Oncogene*, 6: 1677-83.
- Tielsch, J. A. (1995) Vision Problems in the United States: A Report on Blindness and Vision Impairment in Adults Age 40 and Older: Prevent Blindness America. Schaumburg, Prevent Blindness, Inc, 1–20.
- Tosetti, F., Ferrari, N., De Flora, S., Albini, A. (2002). Angioprevention:angiogenesis is a common and key target for cancer chemopreventive agents. *FASEB Journal*, 16:2–14.
- Trompezinski, S., Denis, A., Schmitt, D. (2003). Comparative effects of polyphenols

- from green tea (EGCG) and soybean (genistein) on VEGF and IL-8 release from normal human keratinocytes stimulated with the proinflammatory cytokine TNF α . *Archives of Dermatological Research*, 295: 112-6.
- Tseng, S. H., Lin, S. M., Chen, J. C., Su, Y. H., Huang, H. Y., Chen, C. K. (2004). Resveratrol suppresses the angiogenesis and tumor growth of gliomas in rats. *Clinical Cancer Research*, 10: 2190-202.
- Vingerling, J. R., Klaver, C. C. W., Hofman, A., de Jong, P. T. V. M. (1995). Epidemiology of age-related maculopathy. *Epidemiologic Review*, 17: 347-360.
- Voest, E. E., Kenyon, B. M., O'Reilly, M. S., Truitt, G., D'Amato, R. J., Folkman, J. (1995). Inhibition of angiogenesis in vivo by interleukin 12. *Journal of National Cancer Institute*, 87: 581-586.
- Wang, H. C. (1998). Molecular distinction and angiogenic interaction between embryonic arteries and veins revealed by ephrin-B2 and its receptor Eph-B4. *Cell*, 93: 741-753.
- Ware, J. A., Simons, M. (1997). Angiogenesis in ischemic heart disease. *Nature Medicine*, 3: 158-164.
- Wenk, H. N., Honda, C. N. (2003). Silver nitrate cauterization: characterization of a new model of corneal inflammation and hyperalgesia in rat. *Pain*, 105: 393-401.
- Yamakawa, S., Asai, T., Uchida, T. (2004). (-)-Epigallocatechin gallate inhibits membrane-type 1 matrix metalloproteinase, MT1-MMP, and tumor angiogenesis. *Cancer Letter*, 210: 47-55.
- Yamamoto, S., Aizu, E., Jiang, H., Nakadate, T., Kiyoto, I., Wang, J. C., Kato, R. (1991). The potent anti-tumor-promoting agent isoliquiritigenin. *Carcinogenesis*, 12: 317-23.
- Yarrow, J. C., Perlman, Z. E., Westwood, N. J., Mitchison, T. J. (2004). A high-throughput cell migration assay using scratch wound healing, a comparison of image-based readout methods. *BMC Biotechnology*, 4: 21.
- Yi, X., Ogata, N., Komada, M., Yamamoto, C., Takahashi, K., Omori, K., Uyama, M. (1997). Vascular endothelial growth factor expression in choroidal neovascularisation in rats. *Graefe's archive for clinical and experimental ophthalmology*, 2235: 313-3.
- Yonekura, H., Sakurai, S., Liu, X. (1999). Placenta growth factor and vascular endothelial growth factor B and C expression in microvascular endothelial cells

- and pericytes. Implication in autocrine and paracrine regulation of angiogenesis. *Journal of Biology and Chemistry*, 274: 35172–8.
- Zambarakji, H. J., Nakazawa, T., Donnolly, E. (2006). Dose-dependent effect of Pitavastatin on VEGF and angiogenesis in a mouse model of choroidal neovascularization. *Investigative Ophthalmology & Visual Science*, 47: 2623-2631.
- Zhang, H. M., Keledjian, K. M., Rao, J. N., Zou, T., Liu, L., Marasa, B. S., Wang, S. R., Ru, L., Strauch, E. D., Wang, J. Y. (2006). Induced focal adhesion kinase expression suppresses apoptosis by activating NF-kappaB signaling in intestinal epithelial cells. *American Journal of Physiology*, 290: C1310-20.
- Zhang, H. T., Scott, P. A., Morbidelli, L. (2000). The 121 amino acid isoform of vascular endothelial growth factor is more strongly tumorigenic than other splice variants in vivo. *British Journal of Cancer*, 83: 63–8.
- Zhang, P., Wei, Q., Li, X., Wang, K., Zeng, H., Bu, H., Li, H. (2009). A functional insertion/deletion polymorphism in the promoter region of the NFKB1 gene increases susceptibility for prostate cancer. *Cancer Genetics and Cytogenetics*, 191: 73-7.
- Zhang, T., Yang, D., Fan, Y., Xie, P., Li, H. (2009). Epigallocatechin-3-gallate enhances ischemia/reperfusion-induced apoptosis in human umbilical vein endothelial cells via AKT and MAPK pathways. *Apoptosis*, 14: 1245-1254.
- Zhang, Y. H., Li, Y., Chen, C., Peng, C. W. (2009). Carcinoembryonic antigen level is related to tumor invasion into the serosa of the stomach: study on 166 cases and suggestion for new therapy. *Hepatogastroenterology*, 56: 1750-4.
- Zhang, Z., Ma, J. X., Gao, G., Li, C., Luo, L., Zhang, M., Yang, W., Jiang, A., Kuang, W., Xu, L., Chen, J., Liu, Z. Plasminogen kringle 5 inhibits alkali-burn-induced corneal neovascularization. *Investigation of Ophthalmology and Visual Sciences*. (2005), 46(11):4062-71